

Spring 2008

Acquisition of cardiac control parameters from whole vagus nerve recordings

Marcia A. Pool
Louisiana Tech University

Follow this and additional works at: <https://digitalcommons.latech.edu/dissertations>



Part of the [Biomedical Engineering and Bioengineering Commons](#)

Recommended Citation

Pool, Marcia A., "" (2008). *Dissertation*. 509.
<https://digitalcommons.latech.edu/dissertations/509>

This Dissertation is brought to you for free and open access by the Graduate School at Louisiana Tech Digital Commons. It has been accepted for inclusion in Doctoral Dissertations by an authorized administrator of Louisiana Tech Digital Commons. For more information, please contact digitalcommons@latech.edu.

**ACQUISITION OF CARDIAC CONTROL PARAMETERS FROM WHOLE
VAGUS NERVE RECORDINGS**

by

Marcia A. Pool, B.S.

A Dissertation Presented in Partial Fulfillment
of the Requirements for the Degree
Doctor of Philosophy

COLLEGE OF ENGINEERING AND SCIENCE
LOUISIANA TECH UNIVERSITY

March 2008

UMI Number: 3298936

INFORMATION TO USERS

The quality of this reproduction is dependent upon the quality of the copy submitted. Broken or indistinct print, colored or poor quality illustrations and photographs, print bleed-through, substandard margins, and improper alignment can adversely affect reproduction.

In the unlikely event that the author did not send a complete manuscript and there are missing pages, these will be noted. Also, if unauthorized copyright material had to be removed, a note will indicate the deletion.

UMI[®]

UMI Microform 3298936

Copyright 2008 by ProQuest Information and Learning Company.

All rights reserved. This microform edition is protected against unauthorized copying under Title 17, United States Code.

ProQuest Information and Learning Company
300 North Zeeb Road
P.O. Box 1346
Ann Arbor, MI 48106-1346

LOUISIANA TECH UNIVERSITY

THE GRADUATE SCHOOL

October 16, 2007

Date

We hereby recommend that the dissertation prepared under our supervision by Marcia Pool entitled Acquisition of Cardiac Control Parameters from Whole Vagus Nerve Recordings

be accepted in partial fulfillment of the requirements for the Degree of Doctor of Philosophy in Biomedical Engineering

[Signature]
Supervisor of Dissertation Research
[Signature]
Head of Department
Biomedical Engineering
Department

Recommendation concurred in:
[Signature]
Paul Hood
[Signature]
Raja Kumar

Advisory Committee

Approved:
[Signature]
Director of Graduate Studies

Approved:
[Signature]
Dean of the Graduate School

[Signature]
Dean of the College

ABSTRACT

Heart rate varies continuously depending on the amount of activity being performed or the emotional state of an individual. Both branches of the autonomic nervous system work to alter heart rate depending on the needs of the body. While healthy individuals are capable of altering their heart rate, individuals with certain types of heart disease do not have this ability. For these individuals, cardiac pacemakers are used to alter heart rate. Cardiac pacemakers use sensors to determine the pacing frequency for the heart; however, there is no current optimum sensor. In order to discover a better sensor, this study investigated the use of parasympathetic motor activity via the vagus nerve to predict heart rate.

Vagus nerve activity and EKG signals were recorded simultaneously; two types of recordings were taken: baseline and altered heart rate recordings achieved by performing bi-lateral carotid artery occlusion. Whole vagus nerve discharges were recorded using small silicone cuff electrodes with platinum contacts. Neural activity and EKG signals obtained from these experiments were filtered for frequency content. After filtering, the vagus motor signal was calculated by using a cross correlation technique introduced by Heetderks. The vagus motor activity was integrated between successive R waves taken from the recorded EKG and correlated with instantaneous heart rate. Consistent, high inverse correlations between integrated vagus motor activity and instantaneous heart rate were found in baseline and occlusion recordings. After obtaining

consistent correlations between the integrated vagal motor activity and instantaneous heart rate, a transfer function model was developed using time series analysis methods. The transfer function model whose input was integrated vagus motor activity and whose output was heart rate was capable of predicting heart rate within a 95% confidence interval.

APPROVAL FOR SCHOLARLY DISSEMINATION

The author grants to the Prescott Memorial Library of Louisiana Tech University the right to reproduce, by appropriate methods, upon request, any or all portions of this Dissertation. It is understood that "proper request" consists of the agreement, on the part of the requesting party, that said reproduction is for his personal use and that subsequent reproduction will not occur without written approval of the author of this Dissertation. Further, any portions of the Dissertation used in books, papers, and other works must be appropriately referenced to this Dissertation.

Finally, the author of this Dissertation reserves the right to publish freely, in the literature, at any time, any or all portions of this Dissertation.

Author Marcia A Paul

Date 22 February 2008

DEDICATION

*To my parents
whose love and support
provided me strength to accomplish this pursuit*

TABLE OF CONTENTS

ABSTRACT.....	iii
APPROVAL FOR SCHOLARLY DISSEMINATION	v
DEDICATION.....	vi
TABLE OF CONTENTS.....	vii
LIST OF TABLES.....	x
LIST OF FIGURES	xi
ACKNOWLEDGMENTS	xv
CHAPTER 1: INTRODUCTION	1
1.1 Electrical Conduction System of the Heart.....	1
1.2 Heart Disease	2
1.3 Rate Responsive Pacing.....	4
1.4 Open vs. Closed Loop Control.....	7
1.5 Control Systems of the Heart.....	8
1.6 Heart Rate Variability	10
CHAPTER 2: LITERATURE REVIEW/BACKGROUND.....	12
2.1 Neural Control	12
2.2 Autonomic Nervous System Control.....	16
2.2.1 Use of Sympathetic System for Control	18
2.2.2 Use of Parasympathetic System for Control	20

2.3 Reasons for Focusing on the Parasympathetic System	21
CHAPTER 3: METHODS	26
3.1 Preliminary Work.....	26
3.1.1 Selection of Electrode Implantation Site	26
3.1.2 Differential Recordings.....	27
3.1.3 Electrode Fabrication	27
3.1.4 Surgical Procedure	29
3.1.5 Data Analysis	31
3.2 Final Set of Experiments—Non-Differential.....	31
3.2.1 Electrode Fabrication for Non-Differential Recordings.....	32
3.2.2 Surgical Procedure for Non-Differential Recordings.....	33
3.2.3 Data Analysis for Non-Differential Recordings.....	38
3.2.4 Transfer Function Model of Heart Rate Based on Motor Area	40
CHAPTER 4: RESULTS AND DISCUSSION.....	48
4.1 Preliminary Work.....	48
4.1.1 Selection of Electrode Implantation Site	48
4.1.2 Differential Recordings.....	51
4.2 Final Set of Experiments—Non-Differential.....	60
4.2.1 Transfer Function Model of Heart Rate Based on Motor Area	71
CHAPTER 5: CONCLUSION/FUTURE WORK	90

APPENDIX A: ANIMAL CARE AND USE FORM	93
APPENDIX B: NEUROCAL SIMULATION TO ILLUSTRATE CROSS CORRELATION TECHNIQUE.....	100
APPENDIX C: MATLAB CODE FOR SIGNAL ANALYSIS.....	108
APPENDIX D: SAS CODE AND OUTPUT FOR TRANSFER FUNCTION MODEL.....	114
REFERENCES	137

LIST OF TABLES

Table 1	Types of sensors used for rate adaptive pacing [1].....	6
Table 2	Signal to noise ratio calculated between contacts of different separation distances.....	52
Table 3	Pearson correlation between instantaneous heart rate and integrated neural activity for differential recordings	56
Table 4	Pearson correlations, delay values, and delay correlations for experiment 9	64
Table 5	Pearson correlations, delay values, and delay correlations for experiment 11	65
Table 6	Pearson correlations, delay values, and delay correlations for experiment 13	65
Table 7	Pearson correlations, delay values, and delay correlations for experiment 14	66
Table 8	Forecasted heart rate values, actual heart rate values, and the 95% confidence limits for forecasted values	88

LIST OF FIGURES

Figure 1 The electrical conduction pathway of the heart is shown by the line starting at the SA node and terminating at the ventricles [3].	2
Figure 2 Cardiovascular Disease Deaths vs. Cancer Deaths by Age [4]	3
Figure 3 Trends in Cardiovascular Operations and Procedures [4]	4
Figure 4 Estimated direct and indirect cost of major cardiovascular diseases and stroke in the United States [4]	4
Figure 5 This plot demonstrates how heart rate changes throughout activities [6].	5
Figure 6 Control systems of the heart [1].	9
Figure 7 Change in heart rate due to sympathetic, parasympathetic, and simultaneous sympathetic and parasympathetic stimulation [43]	23
Figure 8 3-D plot of change in heart rate due to sympathetic, parasympathetic, and simultaneous sympathetic and parasympathetic stimulation [43]	23
Figure 9 Capillary tubes and aluminum plate used to make the electrodes, flat clips used to occlude the arteries, and a final electrode consisting of two platinum contacts	29
Figure 10 Schematic of electrode fabrication scaffold and materials.	29
Figure 11 Schematic of the final electrode	33
Figure 12 Mechanical ventilator and CO ₂ monitor used to monitor the animals	35
Figure 13 Analog EKG circuit and the neural amplifiers used	36

Figure 14 Final electrode with proximal lead marked	37
Figure 15 Figure A shows vagus motor activity while Figure B shows the EKG signal	40
Figure 16 A illustrates the continuous signal while B illustrates the result of sample and hold	46
Figure 17 A shows an electrode on the nerve webbing at the heart while B shows the initial electrode placement [63].	49
Figure 18 Final electrode implantation site [64].....	50
Figure 19 Example of raw neural signal obtained	53
Figure 20 Example of digitally filtered neural signal	53
Figure 21 Rectified, averaged neural signal	54
Figure 22 Example of a filtered EKG from Experiment 6.....	55
Figure 23 Integrated right vagus nerve activity (top plot) and instantaneous heart rate (bottom plot).....	57
Figure 24 Integrated left vagus nerve activity (top plot) and instantaneous heart rate (bottom plot).....	58
Figure 25 Histogram of delay values separating motor and sensory activity for a recording from experiment 9	62
Figure 26 Histogram of delay values separating motor and sensory activity for a recording from experiment 13	62
Figure 27 Histogram of delay values separating motor and sensory activity for a recording from experiment 14	63
Figure 28 Baseline correlation values obtained between right vagus nerve motor activity and instantaneous heart rate	68
Figure 29 Scatter plot of integrated right vagus motor activity and instantaneous heart rate from a baseline recording in experiment 14	69
Figure 30 Scatter plot of integrated right vagus motor activity and instantaneous heart rate from an occlusion recording in experiment 14.....	70

Figure 31 Scatter plot of integrated right vagus motor activity and instantaneous heart rate from a baseline recording in experiment 11.....	70
Figure 32 Scatter plot of integrated right vagus motor activity and instantaneous heart rate from an occlusion recording in experiment 11.....	71
Figure 33 Non-continuous integrated motor activity (top) and instantaneous heart rate (bottom).....	73
Figure 34 Continuous, integrated right vagus motor activity (top) and continuous, instantaneous heart rate (bottom).....	74
Figure 35 Averaged, continuous, integrated right vagus motor activity (top) and averaged, instantaneous heart rate (bottom).....	75
Figure 36 The ACF and PACF plots produced by SAS to identify the input variable, area.....	77
Figure 37 ACF and PACF plots of the residuals after estimating a MA(1) model for the input series, area.....	79
Figure 38 Cross correlation plot produced by cross correlating the MA(1) model for area with the output, heart rate.....	81
Figure 39 Transfer function impulse plots [57]......	81
Figure 40 ACF and PACF plot of the residuals after applying the transfer function model.....	84
Figure 41 ACF and PACF plot of the residuals after the AR(2) model was added to the transfer function model.....	87
Figure 42 Actual heart rate values and forecasted values produced by the time series model with 95% confidence intervals marked.....	88
Figure 43 Example illustrating cross correlation technique.....	102
Figure 44 CAPs for each electrode.....	104
Figure 45 Motor activity at distal electrode, proximal electrode, and overall motor activity from both electrodes.....	105

Figure 46 Sensory activity at distal electrode, proximal electrode, and overall sensory activity.....	105
Figure 47 Motor and sensory signals as determined by cross correlation technique.....	106
Figure 48 Motor, sensory, and overall CAP determined from the cross correlation technique.....	106

ACKNOWLEDGMENTS

I would like to thank Dr. Steven A. Jones for providing me with useful feedback on my dissertation research; his suggestions enabled me to compose a more thorough document. In addition to his guidance, Dr. Steven A. Jones along with Dr. Paul N. Hale supported me and guided me throughout the final stages of my time here; without the efforts of Drs. Hale and Jones, this finished product would not have been possible. Also, I would like to thank Dr. Stan Napper for his support throughout this process.

I would also like to thank Dr. Raja Nassar who instilled in me a strong interest in statistics and who also encouraged and guided me in developing the transfer function model for my project. For all the help and instruction he provided regarding the animal protocol, handling, and disposal, I would like to thank Dr. James Spaulding.

I would like to thank Dr. Stan Cronk for his suggestions on editing my dissertation so that I did not have to submit a draft to the English department. For the idea that initiated this project, for the instruction with the animal surgery, for suggestions about data analysis, I would like to thank Dr. Mesut Sahin. For their support, encouragement, and guidance, I would like to thank the members of my committee: Dr. Steven A. Jones, Dr. Paul N. Hale, Dr. Raja Nassar, Dr. Walter Besio, and Dr. Stan Cronk.

I would like to thank the members of my lab, the Neural Sensing and Modulation Lab, for all their support and help. I would like to especially thank my best friend, Kimberlyn Gray, for all her help with completing my experiments, for all the

encouragement throughout the years, and for brainstorming ideas with me about various projects. In addition to my lab, I would also like to thank Ms. Celia Wall for all her help with finding materials, for identifying who I would need to speak to about certain tasks, and for all the good conversations.

Finally, I would like to thank COES for providing me funding through a graduate assistantship. By providing me with opportunities to assist with classes and eventually to teach classes, this assistantship allowed me to realize that I enjoy interacting with students and teaching, something I would not have known otherwise. For allowing me opportunities to foster my classroom instruction skills and for encouraging me in these pursuits, I would like to thank Dr. Roy Schubert, my advisor while I was a graduate assistant.

CHAPTER 1

INTRODUCTION

1.1 Electrical Conduction System of the Heart

The heart consists of two pumps in series: one that pumps blood to the systemic circulation, and one that pumps blood to the pulmonary circulation [1]. In order for the mechanical function of the heart to be accomplished, it has an electrical conduction system that regulates the rhythmicity of the mechanical function. The initiation of the electrical signal in the heart begins in the SinoAtrial node (SA node) located in the upper posterior wall of the right atrium [2]. As the starting point of the electrical signal, the SA node sets the rate of pacing for the heart. From the SA node, the electrical signal depolarizes the atria as it makes its way to the AtrioVentricular node (AV node) located in the connective tissue separating the atria and ventricles. As the atria and ventricles are electrically isolated from each other by the mitral and tricuspid valves, the AV node normally provides the only path of transport of the electrical signal from the atria to ventricles. At the AV node, the electrical signal is delayed due to the nature of the cell composition of the AV node. This allows the blood from the atria adequate time to empty into the ventricles. Next, the electrical signal reaches the bundle of His; there, the signal increases speed due to rapidly conducting Purkinje fibers and travels to the two branches of the bundle of His, the right and left bundle branch. These branches distribute the electrical signal to the myocardium causing the heart to contract from endocardium

(inside) to epicardium (outside) and from apex (point of ventricles) to base. Figure 1 displays the path of electrical conduction in the heart.

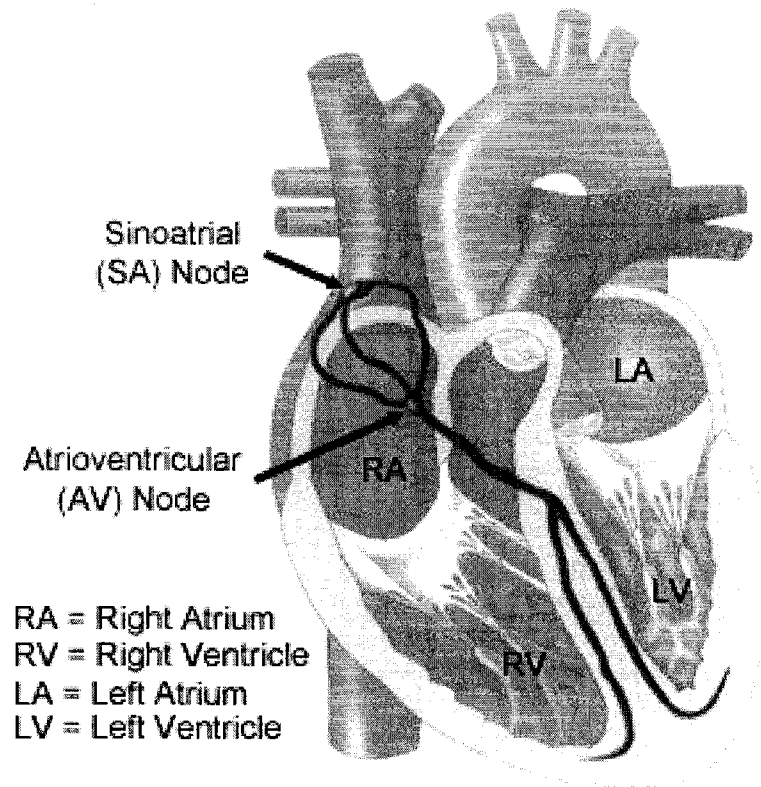


Figure 1 The electrical conduction pathway of the heart is shown by the line starting at the SA node and terminating at the ventricles [3].

1.2 Heart Disease

Cardiovascular disease has been the number one killer in the United States every year since 1900 excluding the year 1918 [4]. Although certain populations may be at a higher risk than others, the most common cause of death across populations is cardiovascular disease [5]. Each day in the United States alone, 2500 people die, an average of one death every 35 seconds [4]. Cardiovascular disease claims more lives each year than all the following: cancer, chronic lower respiratory diseases, accidents,

and diabetes mellitus [4]. Figure 2 compares the number of deaths due to cardiovascular disease and cancer.

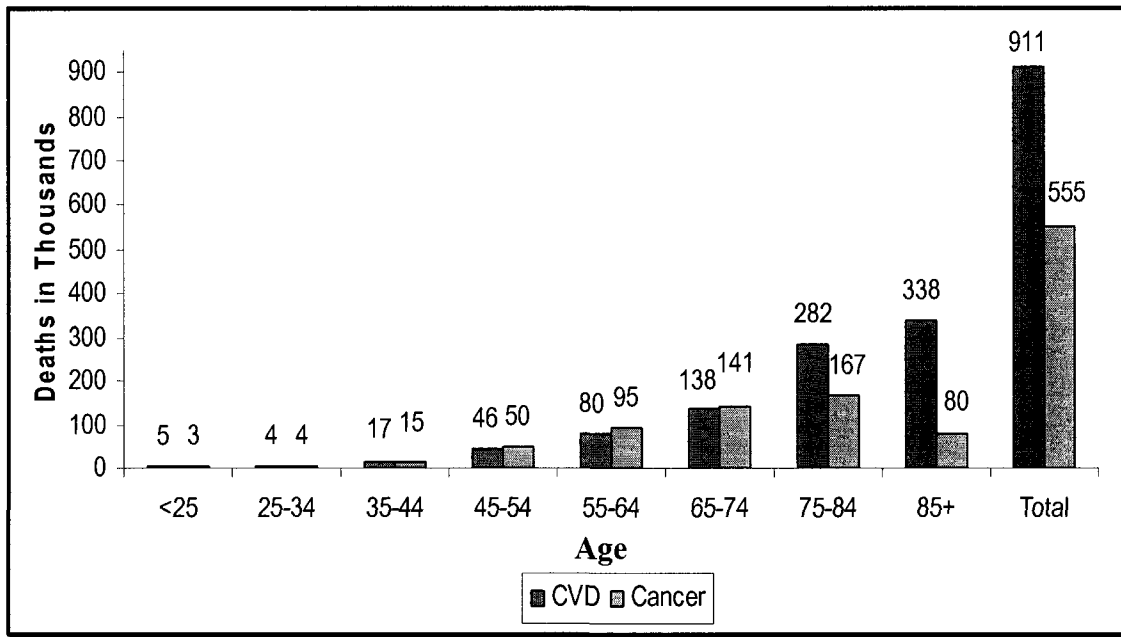


Figure 2 Cardiovascular Disease Deaths vs. Cancer Deaths by Age [4]

One significant subset of cardiovascular diseases is arrhythmias, irregular heart rhythms; in 2003, 197,000 cardiac pacemakers were implanted to assist in correcting heart rhythm [4]. Figure 3 illustrates the trends in cardiovascular procedures; the figure shows a steady increase in the number of pacemaker implants since approximately 1988. Because of the tremendous presence that cardiovascular disease has in health care, it is not difficult to see that the health care cost for these diseases is 212% of the amount spent on all cancers [4]. Figure 4 depicts the estimated billions of dollars spent on subsets of cardiovascular diseases for 2003.

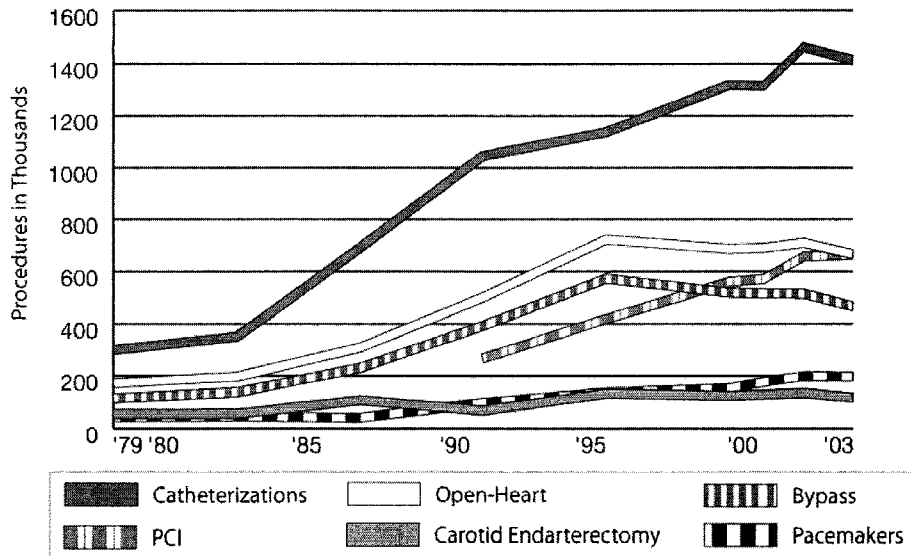


Figure 3 Trends in Cardiovascular Operations and Procedures [4]

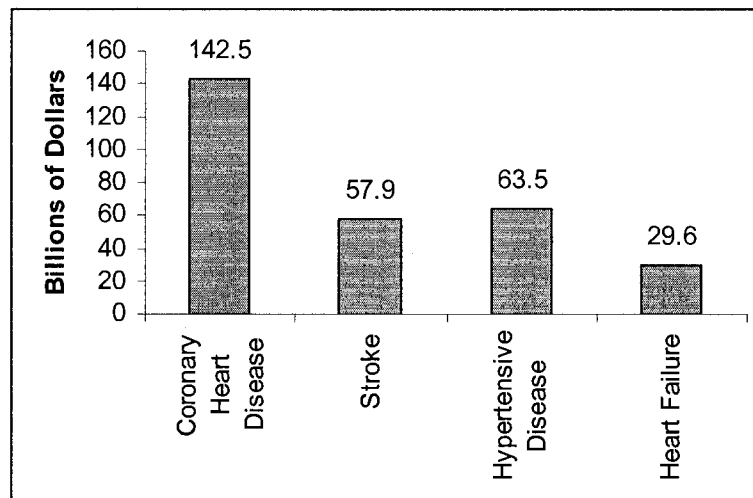


Figure 4 Estimated direct and indirect cost of major cardiovascular diseases and stroke in the United States [4]

1.3 Rate Responsive Pacing

The normal heart rhythm will increase or decrease frequency depending upon the physical needs of the body. Variations in frequency occur naturally during activities such as sleeping, exercise, and emotional situations. During sleep, the heart beats slower.

However, while performing exercise or while expressing strong emotions, the heart rate will increase because the body is requiring more oxygen to maintain functionality.

Figure 5 illustrates the variation in heart rate due to activity. If the SA node is unable to produce change in heart rate necessary for the body, a rate responsive pacemaker is used [6].

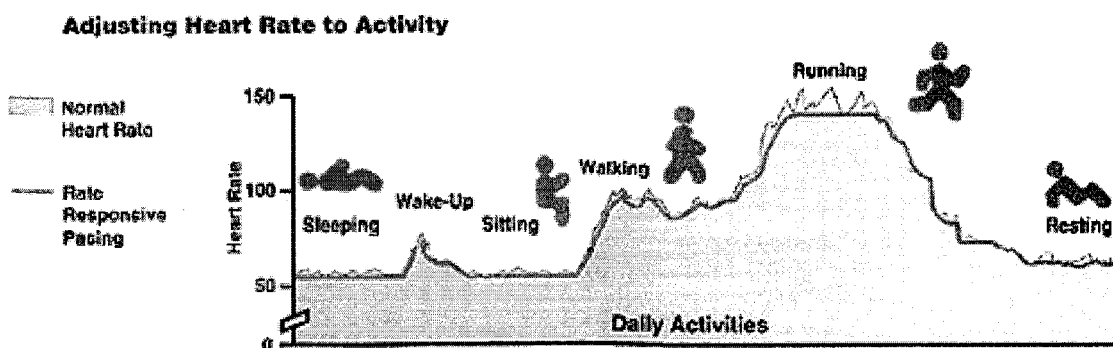


Figure 5 This plot demonstrates how heart rate changes throughout activities [6].

Rate responsive pacemakers function to increase and decrease the frequency of beating according to the body's need. In the case of a stable atrial signal, the pacemaker can use this as a sensor for pacing [1]. However, in at least 50% of pacemaker patients, there is no stable atrial signal so artificial sensors must be used to estimate the appropriate rate of the heart based on the estimated metabolic needs of the body. A rate responsive pacemaker uses several types of sensors to correlate (directly or indirectly) metabolic demand of the body with the pacing rate [1].

Current sensors for cardiac pacemakers are unable to provide emotional and activity heart rate adaptation information with rapid response. One of the most widely used sensors, the activity sensor, does not provide information about emotional

adaptation [1]. A sensor that would provide both emotional and activity adaptation information with a rapid response would be an *improvement on current sensors*.

Table 1 lists several common sensors used for rate adaptive pacing; this plot shows that no sensor has a fast speed of response with closed loop control [1]. While the mixed venous O₂ sensor looks promising, follow-up studies on human implants of the sensor indicate that it has a tendency to deteriorate due to tissue overgrowth [7].

Table 1 Types of sensors used for rate adaptive pacing [1]

Sensor Type	Long Term Stability	Closed Loop Control	Senses Emotions & Stress	Speed of Response
Mixed Venous O₂ Saturation	Yes	Yes	Yes	Slow
QT interval	Yes	No	Yes	Slow
Temperature	Yes	Yes	Little	Slow
Minute Ventilation	Yes	No	Yes	Slow
Activity	Yes	No	No	Fast

Rate responsive pacing provides several benefits to people whose SA node does not function properly [6]. This type of pacing:

- provides an appropriate heart rate for a given activity
- allows patients to perform normal activities more efficiently
- allows patients to participate in moderate exercise
- provides patients with a stronger sense of well-being

Many sensor systems and algorithms have been developed for rate responsive pacing; however, most of these are far from optimal. The optimum system would “bridge the pathological gap between the ANS and the intrinsic rhythm generator” [8]. Efforts are still being made to reach this optimum that would restore sympathetic and parasympathetic stimuli to the pacing of the heart.

1.4 Open vs. Closed Loop Control

As with choosing the appropriate sensor for the cardiac pacemaker, pacemaker designers must also select the type of control: open or closed loop. While closed loop control appears to be the obvious choice, trade-offs sometimes lead to the use of open loop control. Open loop systems offer easier implementation than closed loop systems because the open loop systems do not require a special pacing electrode to be designed [9]. In addition to being more easily implemented, open loop systems do provide reliability with the use of motion-based sensors which are implanted most frequently. However, since the system is “open”, there is no feedback control by which to continuously monitor the effects and needs of the system. This is where closed loop control provides superior performance over open loop systems. Closed loop control can provide physiological feedback so that only the error (the desired rate minus the actual produced rate) is fed into the controller. This allows for a steady state response (the desired rate) to be reached in less time. Therefore, this model more closely resembles the actual cardiovascular control system. Thus, if the appropriate sensor and feedback signal is used, the cardiovascular control system could be reinstated artificially. By using the neural signals that control heart rate, we discover a control system that is an artificial equivalent of the cardiovascular control system.

1.5 Control Systems of the Heart

The cardiac system is one which can quickly and efficiently adapt its performance to changes within the human body. Two methods of regulation are intrinsic pathways and extrinsic pathways [1]. Intrinsic pathways are represented by physical changes to the heart caused by preload (tension of the myocardial fibers before a contraction), afterload (tension on the myocardial fibers after a contraction), and contraction frequency; whereas, extrinsic pathways are due to neural and hormonal changes [1, 10].

Intrinsic pathways excluding the beating of the heart are difficult to measure; however, many of the extrinsic pathways contain measurable variables. Because extrinsic pathways provide measurable variables and because extrinsic pathways are believed to have a more dominant role in cardiac regulation, it is believed that the best option for control of the cardiac system lies in the extrinsic pathways. Figure 6 presents a flow chart of cardiac control influences; solid lines indicate direct proportionality while dashed lines indicate inverse proportionality [1]. For example, the sympathetic activity to the heart is represented as a solid line; the figure shows that as the sympathetic activity increases so does heart rate. The opposite is true of the parasympathetic activity to the heart. As the parasympathetic activity to the heart increases, the heart rate decreases.

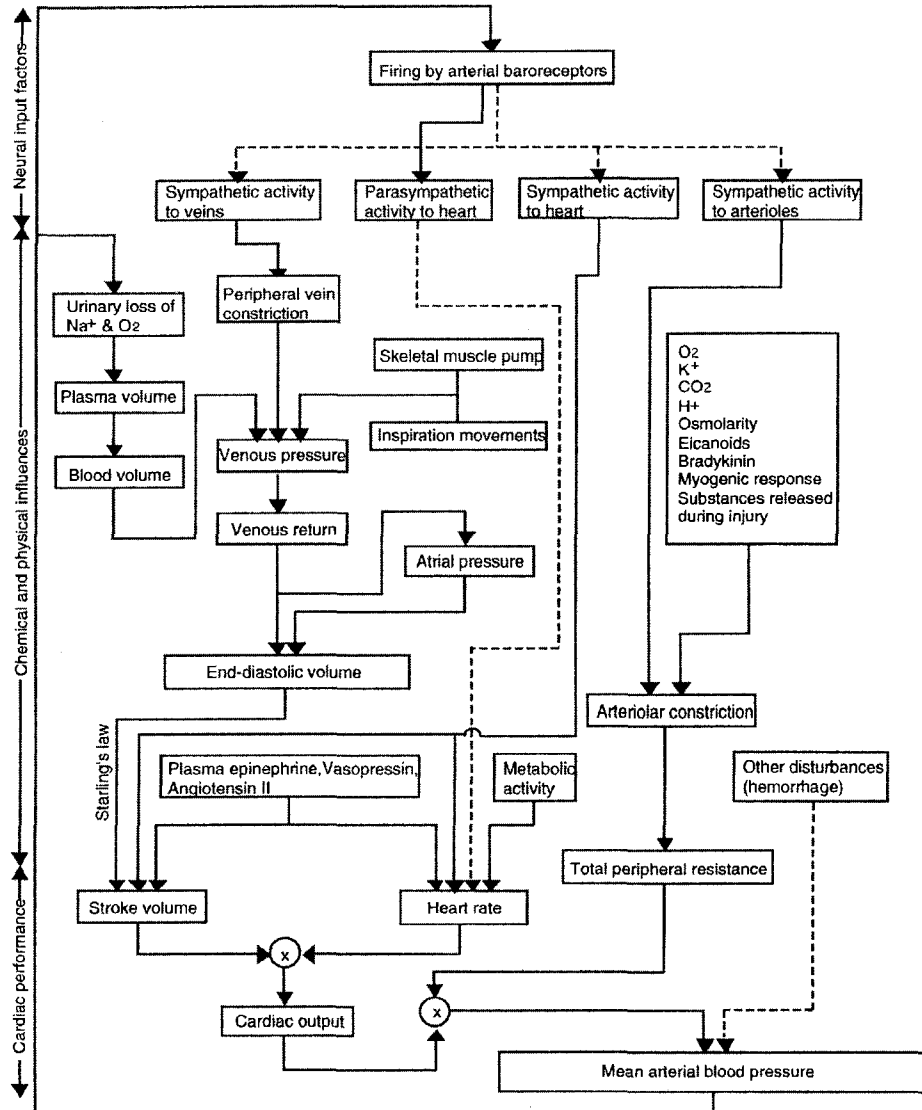


Figure 6 Control systems of the heart [1].

The sympathetic and parasympathetic are both divisions of the Autonomic Nervous System (ANS). The ANS is considered to be a major controlling factor in heart rate regulation [1, 11]. Although the SA node initiates the pulse which produces a heart beat, control of heart rate is determined by a balance of ANS activity along with hormonal and chemical signals; the brain analyzes the signals and transmits control information to the SA node.

1.6 Heart Rate Variability

Although the SA node is considered the “internal pacemaker” of the heart, the SA node is supplied by the ANS, both sympathetic and parasympathetic divisions, whose signals create an increase or decrease in heart rate, respectively. Since heart rate changes with respect to ANS activity, heart rate variability which is the difference in beat to beat heart rate is considered to be an indirect marker of ANS activity [12].

Because heart rate variability is considered a non-invasive marker of ANS activity, much research has been performed, leading to the identification of distinct power spectrums. Two particular distinct regions representative of neurocardiac control in humans are the Low Frequency region (LF), ranging from 0.05-0.12 Hz, and the High Frequency region (HF), ranging from 0.15-0.35 Hz. The low frequency region results from sympathetic activity while the high frequency region results from the parasympathetic activity via the vagus nerve [13-23].

In order to better understand the control systems of the heart, it is important to understand how each division of the ANS affects the cardiac system. While two frequency bands have been identified to represent autonomic activity, there are a few concerns when using the information to assist diseased individuals. Heart rate variability is more prominent in healthy individuals than in individuals whose ANS functions have decreased due to age, disease, or pharmacological blockade [14-16, 24-25]. Healthy individuals do not need assistance in regulating heart rate; however, many individuals with cardiac disease are incapable of regulating their own heart rate. Because heart rate variability is not as prominent in diseased individuals, it may provide an initial approximation to the autonomic activity; but a more in-depth analysis of the autonomic

activity might provide a better understanding of the cardiac control system in diseased individuals.

Bigger et al. explored correlations between time domain and frequency domain measures of heart rate variability. They also investigated how much each distinct frequency band contributed to the total power spectra in a twenty-four hour period. Bigger et al. found the contribution of both the high frequency band (parasympathetic) and the low frequency band (sympathetic) was less than 10% of the total power spectra analyzed in twenty-four hour duration EKGs [26]. Because the contribution of these two important frequency bands to the total power in a twenty-four hour period is very little, changes in the amount of activity in these two bands may not be noticed when analyzing total power [27].

Therefore, due to the lack of heart rate variability in diseased individuals and the small contribution provided by both important frequency bands, this indirect method for analyzing ANS activity is not optimum. A better method to accurately identify ANS activity related to heart rate control would be to directly measure the ANS activity. Direct measurement would provide exact information on the ANS contribution to control of heart rate. In order to directly acquire ANS activity to the heart, electrodes must be placed in or around a nerve. Because of the surgery required to directly acquire ANS signals, an animal model must be used to begin the investigation.

CHAPTER 2

LITERATURE REVIEW/BACKGROUND

2.1 Neural Control

The Autonomic Nervous System (ANS) is responsible for controlling most visceral functions in the body including arterial pressure, body temperature, gastrointestinal secretions, and heart rate. The ANS is characterized by its dynamics and intensity; for instance, the ANS can double the normal heart rate in three to five seconds. The ANS is divided into two sections: the sympathetic nervous system and the parasympathetic nervous system. These two components of the ANS oppose each other. For example, both divisions of the ANS innervate the heart such that the sympathetic system increases the heart rate and the force of contraction of the heart while the parasympathetic system produces the opposite effects by decreasing the heart rate and the force of contraction [28]. ANS activities are carried out automatically; there is no voluntary control involved [29].

The ANS is an output of the Central Nervous System (CNS) with the responsibility of controlling every tissue and organ that the ANS innervates. The hypothalamus and the nucleus of the solitary tract are responsible for initiating ANS signals. The hypothalamus receives sensory information about the status of the body and responds by sending the appropriate ANS and hormonal signals. In addition to the

hypothalamus, the nucleus of the solitary tract also receives sensory information about the status of the body. The nucleus of the solitary tract is capable of initiating a response to some sensory input without the sensory information having to travel to the hypothalamus, thereby acting in a feed forward manner. Once the hypothalamus or nucleus of the solitary tract determines a response to the sensory input, ANS upper motor neurons in the brain send signals to lower motor neurons that innervate specific tissue and organs to accomplish the desired effect [29].

If the parasympathetic motor signals from the ANS via the vagus nerve could be acquired, the signals could be used to better understand the influence of the ANS on heart rate and possibly lead to using the signals as a sensor to control the pacing rhythm of a rate adaptive pacemaker. The idea of using natural signals as a controller for artificial devices is not new. Myoelectric hands and legs which use signals from the body to operate have been designed with some success [30], and sensory receptors of the skin have been found to provide information which can be used to control assistive devices [30].

Neural activity has been correlated with external perturbations of touch, slip, and contact force in experiments with cats and humans [30-31]; from these experiments, a successful sensor was developed to control the hind limbs of a cat [30-32]. Hoffer and Haugland concluded that using neural activity as sensors may be very useful [30-32].

Popović et al. further investigated use of neural signals for muscular control. Multi-electrode recordings were used to design a rule based algorithm which would provide more options than simple rules for an implantable device needing multi-channel Functional Electrical Stimulation (FES). In previous studies, only simple “hand-crafted”

rules such as force transducers were used; however, because improvements in hardware allowed the use of multiple sensors to provide more information for control purposes, a rules-based approach which used an if/then structure was chosen to provide more control options than hand-crafted rules. A chronic cat model was used to prove the efficacy of using multi-electrode recordings to provide input for a rule based algorithm [30, 32].

Neural recordings were taken from the superficial peroneal and tibial sensory nerves in the cat ankle, and EMG signals were also simultaneously recorded from medial gastrocnemius and tibial anterior muscles of the cat ankle. The information from these recordings was analyzed for correlations between neural activity and muscle activity. A rule-based algorithm developed from analyzing the correlation between neural and muscular activity was found to be sufficient to represent the basic structure of the alternation between flexors and extensors in the cat ankle. Therefore, a rule based algorithm which obtained information from neural recordings was capable of triggering stimulation to create flexion and extension in the appropriate time periods in a cat ankle [30, 32].

For nerve recording and stimulation purposes, nerve cuff electrodes have been shown to be safe and effective over time [30]. Recently, nerve cuff electrodes have been used to acquire neural signals to create a visual image. This process is referred to as MINIS – “minimally invasive neural interfacing system” [33]. Coates et al. used nerve cuff electrodes to acquire optic nerve signals. The optic nerve signals were then processed using wavelet theory and analyzed. The information from the analysis was then fed into a trainable neural network that would output what it “saw” in response to a given stimulus [33].

For the MINIS study, twelve stimulus patterns of light were individually delivered to the lateral eye by fiber optic cables; the patterns consisted of 11 different light patterns and one control pattern with no illumination. Six patterns were accurately identified at least 50% of the time for the 329 presentations of each pattern with pattern one being identified correctly 100% for the 329 presentations. The neural network performed well when tested on different data from the same specimen on which it had been trained. However, when testing the neural network on data from a specimen on which it had not been trained, the network did not perform very well; this indicates that the neural network was very specific for each specimen [33].

While the results of the MINIS study indicate that more research is necessary to characterize the neural network's identification of the correct stimulus pattern, the results are encouraging because they indicate progress toward direct use of neural signals acquired by cuff electrodes to predict activity (in this case, vision).

These examples presented here represent only a few of the studies involving investigations into the use of neural signals as a form of control. This field is expanding as new technology offers improvement in signal acquisition and allows for development of smaller electrodes. Also, the use of neural networks allows more information to be gained from recorded signals. The nervous system contains a vast amount of information about the movement of the human body. If this information can be acquired and understood, the neural information can then be used to design prosthetic devices which will more closely mimic the natural movement of the body.

2.2 Autonomic Nervous System Control

Restoration of physiological closed loop control is the optimum goal of rate adaptive pacing. In the pursuit to control heart rate adaptation, many different sensors have been employed, some with closed loop control. However, none of the current sensors provide rapid, closed loop response that is capable of adjusting to emotional stress in addition to physical activity [1, 34]. Closed loop control is preferable to open loop control because the feedback information allows for a regulated adjustment of heart rate based on metabolic need. One possible source for rate adaptation which would provide fast, closed loop control, as well as information to adapt to emotional and physical stress levels, is the autonomic nervous system.

The concept of using the ANS to control rate adaptive pacing is not new. Because the ANS is intact and properly functioning in patients with heart disease and because the ANS is a control pathway for heart rate, evaluating ANS activity can provide valuable information on heart rate control. Schaldach et al. investigated the use of indirect measures of ANS activity on the heart to control a rate adaptive pacemaker. Direct measurement of ANS activity was not practical at the time of this study; so, intracardiac impedance was used as an indirect measurement of ANS activity, mainly sympathetic [11].

A 4 kHz square wave with a constant current of 40 μA was injected via the pacing electrode already present in the ventricle to measure intracardiac impedance. Signal processing was performed to improve the quality of the impedance signal which contained information about the contractility of the heart. Because the contractility of the heart is affected by the sympathetic nervous system, the impedance signal contained

indirect measurements of ANS activity, although mainly sympathetic. An algorithm was developed to extract the ANS information from the impedance signal; the algorithm was easily adaptable for different patients. For each patient, the algorithm was calibrated to the individual's impedance signal and physiological requirements [11].

A clinical study of 234 patients was performed to determine the effectiveness of this type of rate adaptive pacemaker. The performance of the rate adaptive pacemaker that employed indirect ANS measurements to adjust heart rate was evaluated by analyzing heart rate trends for a twenty-four hour period as well as heart rate response to exercise. Successful pacing was achieved by 93% of single chamber systems and by 96% of dual chamber systems; however, the pacemaker failed in patients with high beat to beat variability or with low signal dynamic range. Of particular interest is the performance of the ANS based pacemaker to emotional and mental stress: the ANS based pacemaker was capable of providing correct rate adaptation in emotional and mental stress situations as well as during exercise [11].

However, because the ANS based pacemaker relied on indirect measurements of ANS activity, anything that affected the contractility of the heart would affect the rate of pacing supplied by the ANS based pacemaker. Drugs that modify the flux of Ca^{2+} through cells would alter the response of the ANS based pacemaker because contractility of the heart is changed by changing the flux of Ca^{2+} . For instance, the use of digitalis results in an increase in the ANS based pacemaker's pacing rate which is in contrast to the effect of digitalis on the intrinsic sinus rate [11]. However, if the ANS information was acquired directly from the nerves innervating the heart, one could conclude that the effects of change in contractility due to drugs would not affect the output of a pacemaker

because the direct neural recordings used as input to the pacemaker would still provide heart rate control info from the CNS.

2.2.1 Use of Sympathetic System for Control

While one group in the previous section analyzed indirect measurements of total ANS activity to study heart rate, most studies have analyzed either the sympathetic or the parasympathetic division of the ANS to investigate heart rate control. Mabuchi et al. investigated the use of sympathetic neural signals to regulate heart rate. However, this study did not use the cardiac nerves; instead, skin sympathetic nerve activity was recorded from the median nerve using microneurograph techniques. The number of sympathetic nerve pulses was counted, and an algorithm was developed to alter the positive pressure, the vacuum pressure, and the pumping rate of an artificial heart system based on the number of nerve pulses. The investigators noted that if sympathetic nerve signals were used to regulate heart rate, a better location for acquiring the signals would be from the cardiac sympathetic nerves, although this approach would be much more invasive [35-36].

Ikeda et al. investigated the use of using the cardiac sympathetic nerve activity to predict heart rate. For this study, one of the left cardiac sympathetic nerves of each rabbit was exposed from the fatty tissue by a median thoracotomy. The cardiac sympathetic nerve was cut and platinum electrodes were attached to it to record the activity. Two sets of sympathetic nerve activity and heart rate were recorded in each experiment. The first set of data was used to develop a transfer function representing heart rate based on sympathetic nerve activity. The second set of data was to validate the transfer function

developed; the data from the second set was not used in the development of the model so the prediction was not biased [34].

The transfer function approximated a first order, low pass filter with a delay whose corner frequency was 0.024 ± 0.013 Hz and whose time delay was 0.98 ± 0.09 s. The transfer function closely approximated heart rate for the second set of data when the previous history of neural activity was known; this indicates that the heart rate is dependent on previous neural activity as well as instantaneous neural activity. To determine the accuracy of the prediction, correlation coefficients were calculated between the predicted and recorded heart rate; the correlation coefficients ranged from 0.80 to 0.98. From this information, the transfer function was determined to have successfully predicted heart rate [34, 37].

The results of this study were encouraging; however, Ikeda et al. noted a few possible problems which would prevent direct clinical application of these experiments. First, only the sympathetic nerve activity was recorded; this does not account for the vagal activity which has been shown to have a significant effect on heart rate. Due to the sympathetic and vagal interactions, a complex model may be more accurate. Second, in this study, the range of heart rates was less than what may occur naturally; therefore, some nonlinear components which were not considered in this linear model may exist. Third, the type of electrode used for this study is not capable of chronic use; an electrode which can record chronically would be important for clinical applications. However, though a few problems were noted with this study, the fact that the transfer function accurately predicted heart rate makes this method seem particularly interesting [34].

2.2.2 Use of Parasympathetic System for Control

Yambe et al. performed a study in which vagal nerve measurements were recorded in goats [38-39]. Yambe et al. have investigated possibilities for a total artificial heart [40-41]. The goal of this project was to determine if vagus nerve signals could be used to design an artificial heart system.

Four healthy adult goats were used for this chronic study. Internal electrodes were used to continuously monitor the EKG, and catheters were used to monitor arterial blood pressure and left atrial pressure in the goats. Recordings from the left vagus nerve were taken using invasive, bipolar, stainless steel electrodes; the electrodes were connected to connective tissue to insure stability for the chronic experiment. After the surgery to insert the electrodes was completed, each animal was moved to a cage [38-39].

Neural recordings as well as hemodynamic parameters were recorded in awake animals. A baseline recording was taken in addition to recordings during altered hemodynamic states. To alter the hemodynamic properties of the animal, drugs including methotrexate and nitroglycerin were used in the awake condition. Time series recordings were acquired by a computer using an A-D converter [38-39].

Vagal nerve activity was recorded; however, the signal was contaminated at times due to movement of the animal. In the time series data acquired, burst discharges of the vagus were synchronized with respiration. After drugs were introduced to increase blood pressure, the vagus nerve showed increased activity. This was followed by a decrease in heart rate and a decreased ascending aortic flow. These results were obtained in all four goats, lending evidence to the possibility of using vagal nerve recordings for an artificial heart control algorithm [38-39]. Although these results indicate a possibility of vagal

control, more information about the vagus activity and its affect on heart rate must be investigated so that a model can be developed that will accurately represent the relationship between the vagus activity and heart rate as was illustrated between the sympathetic activity and heart rate in the study in the previous section.

2.3 Reasons for Focusing on the Parasympathetic System

If only one division of the ANS were used to determine the pacing rate of the heart, which system would be best, the sympathetic or the parasympathetic? Studies have been performed to investigate use of both sympathetic and parasympathetic activity, though studies which have investigated sympathetic control of heart rate predominate the literature. However, arbitrary use of one division may not be sufficient to reproduce heart rate control information due to complex interactions between the parasympathetic and sympathetic divisions.

Levy et al. investigated the interactions between the parasympathetic and sympathetic divisions by performing stimulation experiments. The experiment consisted of three stimulation levels for sympathetic and parasympathetic divisions; the three levels were low, intermediate, and high stimulation values. The high stimulation value for the parasympathetic (vagus) nerve was determined to be the highest vagal stimulation which did not produce a second or third degree block, and the high stimulation value for the sympathetic nerve was determined to be the stimulation which increased the heart rate to 80% of maximum level. The intermediate level of both divisions was set to half the maximum stimulation for each division, respectively; while, the low stimulation was

considered to be no measurable stimulation. All possible combinations of the three levels and two divisions were performed randomly [42].

Results of the stimulation experiments revealed an expected result and one that was not expected. The result of stimulating the sympathetic system alone at the high stimulation level of 4 Hz increased the heart rate from a control of 182 beats/min to 260 beats/min; this is expected because the sympathetic system acts as an accelerator to increase heart rate. When the vagus nerve was stimulated alone at the highest level of 8 Hz, the heart rate decreased from a control value of 170 beats/min to 100 beats/min; this too was expected because the parasympathetic division acts as a brake to slow the heart rate. However, when both parasympathetic and sympathetic divisions were simultaneously stimulated, the outcome was not an algebraic summation of the individual responses seen from the parasympathetic and sympathetic divisions; the result showed almost no appreciable difference from parasympathetic stimulation alone [42-43].

Simultaneous stimulation at the high level of the parasympathetic (8 Hz) and the sympathetic (4 Hz) was performed to determine the interaction between the divisions. The result of the simultaneous stimulation was a decrease of heart rate from a control value of 190 beats/min to 120 beats/min. Simultaneous stimulation which caused the heart rate to decrease by 70 beats/min was very similar to the parasympathetic high level stimulation which also caused the heart rate to decrease by 70 beats/min. Figures 7 and 8 show the results of these stimulations. The attenuation of sympathetic activity by the parasympathetic stimulation was seen throughout all combinations of stimulations performed for these experiments [42-44].

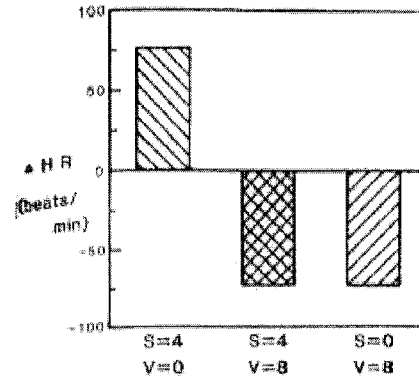


Figure 7 Change in heart rate due to sympathetic, parasympathetic, and simultaneous sympathetic and parasympathetic stimulation [43]

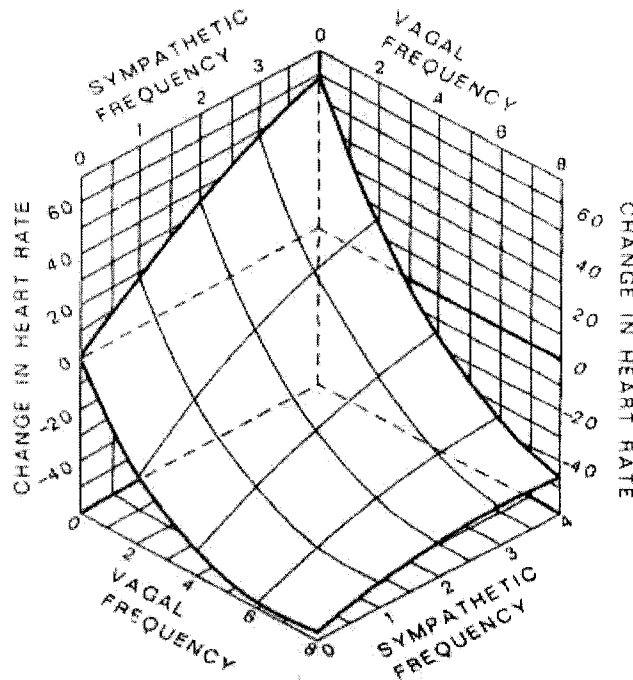


Figure 8 3-D plot of change in heart rate due to sympathetic, parasympathetic, and simultaneous sympathetic and parasympathetic stimulation [43]

In addition to being the dominant controller of the system, the parasympathetic system is much faster than the sympathetic system in response time. In experiments which investigated the modulation of heart rate, the sympathetic system produced a small

gain and a phase delay; whereas, the parasympathetic system produced a high gain with no phase delay [45]. As a comparison between the systems, the sympathetic influence on cardiac control is in the order of magnitude of seconds (10^0); whereas, the parasympathetic effects are in the order of magnitude of milliseconds (10^{-3}) [46]. From this, one can conclude that the dominance and kinetics of the parasympathetic system make it a very important component to examine in the control of heart rate.

Levy et al. also confirmed previous investigations which noted the potential for beat-to-beat control by the vagus due to its rapid kinetics. Levy found that the sympathetic system with its “sluggish” kinetics is not a suitable control [47]. Again, stimulation experiments were used to investigate the kinetics of the parasympathetic and sympathetic divisions. The effects on heart rate due to sympathetic stimulation were gradual and decayed slowly; while the effects due to parasympathetic stimulation were rapid and decayed quickly. These studies indicated that the sympathetic division is too slow to contribute to beat-to-beat regulation of heart rate [47].

Besides investigating kinetics and dominance of each division, location has also been investigated. More specifically, which side (right or left) has a greater effect on heart rate? Levy et al. performed stimulation experiments to confirm previous findings which noted that the right side controls the SA node while the left side produced a greater effect on the AV node. The results showed that right sympathetic stimulation produced a higher increase in heart rate (SA node) when compared to left sympathetic stimulation. Also, right vagal stimulation produced a larger decrease in heart rate when compared to left vagal stimulation. Therefore, it was concluded that the nerves on the right side, both

sympathetic and parasympathetic, exert more control on the SA node which sets the pacing rate of the heart [48].

Because experiments indicated that the parasympathetic division of the ANS is dominant and has kinetics which would allow for beat-to-beat control of heart rate, the parasympathetic division was chosen to investigate neural heart rate control for this project. After deciding on a division of the ANS to investigate, the location to investigate was determined from the literature review which indicated that the right side produces a greater effect on the SA node. So, for this project, the right vagus nerve was chosen as the source of information on neural control of heart rate.

CHAPTER 3

METHODS

3.1 Preliminary Work

3.1.1 Selection of Electrode Implantation Site

Necropsies of several different animal species were performed to determine the best electrode implantation site; one dog and several rats were examined. The necropsies were performed on animals that had been humanely euthanized after being used in other research projects. For each necropsy, the animal was surgically opened to expose the thoracic cavity so that the heart could be located. Dissection through connective tissue and isolation of nerves and nerve branches was performed to trace the paths of nerves, specifically the vagus nerve, that terminated at the sinoatrial node of the heart. After the necropsy was performed, all animals necropsied were properly disposed according to the Louisiana Tech Institutional Animal Care and Use Committee (IACUC).

In addition to the several necropsies performed, one surgery was performed on a goat to access the vagus nerve around the cardiac plexus. For this procedure, which had been approved by the IACUC, the animal was anesthetized using xylazine and ketamine, mechanically ventilated, and monitored throughout the surgery for depth of anesthesia and vital signs. A midline incision was made to expose the sternum which was then surgically opened to expose the heart. Tracing of the vagus nerve was performed to

follow it to the cardiac plexus region. Unfortunately, this is all that was could be accomplished because the animal died during the procedure. After the death of the animal, dissection to isolate nerves and trace the nerves to the heart was performed. The animal was then properly disposed according to the procedures established by the IACUC.

3.1.2 Differential Recordings

A set of differential neural recordings was also performed; the recordings were the difference between the proximal and distal contact. For differential recordings, Sprague-Dawley rats were used; the IACUC approved the protocol for these experiments. A sample IACUC experiment form is shown in Appendix A. Cuff electrodes were designed to acquire the vagus nerve signal; two different configurations were used: an electrode with 5 platinum contacts and an electrode with 2 platinum contacts.

3.1.3 Electrode Fabrication

The electrodes were fabricated using platinum foil (thickness = 0.025mm, purity = 99.95%) from Goodfellow Cambridge Limited (England), Teflon coated stainless steel wire from A-M Systems, Inc., and a two-component mixture silicone elastomer from Silicone Technology/Nusil Technology (MED-4211). Small sections of platinum foil (width ~1mm) were cut and welded onto the end of a Teflon coated stainless steel wire whose end had been stripped of Teflon. A Dual Power 125 Stored Energy Power Supply resistance welder from Standard Resistance Welder Company was used to connect the stainless steel wire and the platinum contacts. The strength of the weld between the platinum and wire was manually checked to ensure that the weld would hold under slight tension. Next, the silicone elastomer was mixed; the silicone elastomer mixture is a 10:1

mixture of part A to part B. The correct amounts of the silicone elastomer were measured, thoroughly mixed, and set aside while the electrode aluminum scaffold was prepared. An aluminum plate with a raised section in the center was used to prepare the cuff electrode; the raised section in the center of the scaffold created a tunnel through the center of the final electrode which is where the nerve was placed during the experiments. Before the scaffold was used to mold the electrode, the aluminum scaffold was first sprayed with a dry film silicone lubricant (LPS Dry Film Silicone Lubricant) to allow easy removal of the finished electrode. A glass capillary tube, shown in Figure 9, was then placed on the elevated line of the scaffold. Silicone elastomer was poured over each end of the capillary tube, and the whole scaffold was heated to secure the capillary tube in place.

After the capillary tube was secured, platinum contacts were placed between the elevated line of the scaffold and the capillary tube. Once the contacts were arranged in the desired location, silicone elastomer mixture was poured over the whole configuration, and the entire scaffold was heated to mold the electrode. An illustration of the electrode is shown in Figure 10. After the electrode had been molded and after the scaffold cooled, a razor blade was used to remove the electrode from the scaffold and to trim the edges of the molded electrode. The platinum contacts of the molded electrode were manually checked to identify if any silicone were present; if there was silicone on the contact, the silicone was removed from the contacted using a surgical scalpel blade.

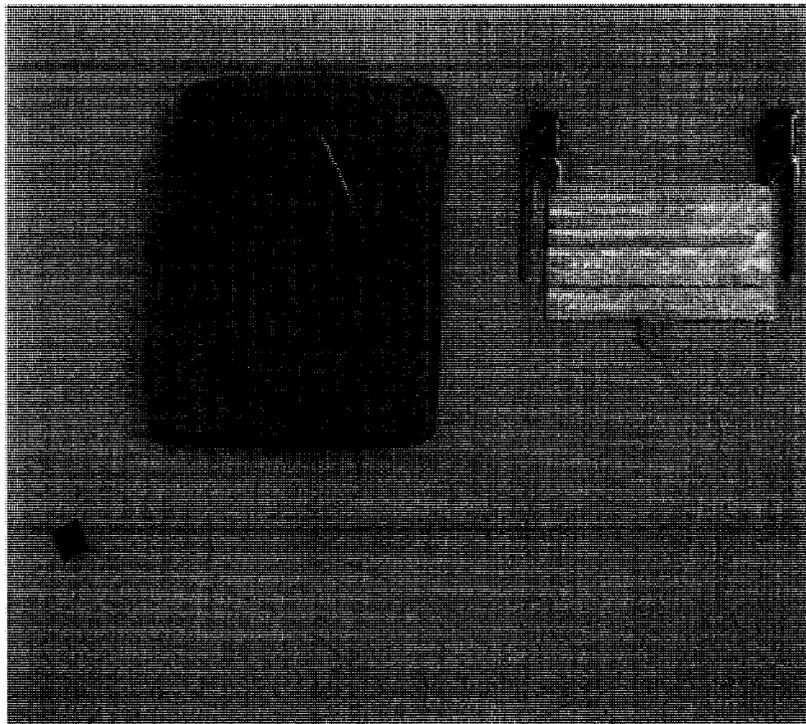


Figure 9 Capillary tubes and aluminum plate used to make the electrodes, flat clips used to occlude the arteries, and a final electrode consisting of two platinum contacts

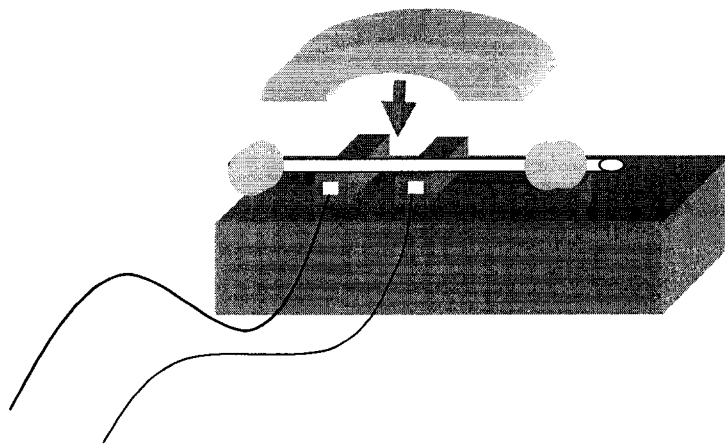


Figure 10 Schematic of electrode fabrication scaffold and materials.

3.1.4 Surgical Procedure

After the fabrication of the electrodes was completed, they were used in animal experiments. To anesthetize the animal, IntraPeritoneal injections (IP) of either

Nembutal or Xylazine and Ketamine were used. Once the animal was under proper sedation, the animal was moved to a heated surgical table. Surface EKG electrodes were placed on the right arm, left leg, and left arm to acquire the EKG signal. EKG signals acquired through the surface electrodes were first analog processed to amplify the signal and filter the noise before being taken into the computer. A tracheotomy was performed so that the animal could be mechanically ventilated; the tubing used for the tracheotomy was PE 205.

After the animal had been mechanically ventilated, the surgery continued with further dissection into the neck. Isolation of the right and left vagus nerves was performed; in these experiments, either the right or the left vagus nerve was used depending on which was easier to access. After isolating the nerve, the electrode was placed under the nerve so that the nerve sat in the tunnel of the electrode; saline was then poured on the nerve and electrode combo to remove any blood and to hydrate the nerve. The nerve electrode configuration was then dried using a cotton-tipped applicator. To secure the electrode from the in vivo environment, Kwik-Sil™ (World Precision Instruments) was used; Kwik-Sil™ was applied to the top of the electrode so that the nerve was isolated. The electrode contact wires were then connected to the analog neural amplifiers. All signals, neural and EKG, were acquired into a computer using a National Instruments E Series DAQ board. Sampling rate for acquisition was 100K Samples/s.

To elicit a change in heart rate, two methods were used: respiratory occlusion and injection of nitroglycerin. Respiratory occlusion was performed by turning off the mechanical ventilator without opening any of the tubing to ambient air; the longest respiratory occlusion was 30s. Attempts were made to inject nitroglycerin into the vein

in the tail of the rat and into a vein of the leg; none of these attempts were considered successful. Upon completion of the experiment, the animal was humanely euthanized using an IntraCardiac (IC) injection of potassium chloride (KCL).

3.1.5 Data Analysis

To analyze the data acquired during the experiments, MathWorks' MATLAB and MATLAB's Signal Processing Toolbox were used. The neural signals were digitally filtered using a Hamming window with a passband of 400 Hz to 7 kHz and order of 1000; the passband for filtering the signals was determined from the power spectrum of the neural signals. A Hamming window with a passband from 1 Hz to 100 Hz and filter order of 500 was used to filter the EKG signal. After the EKG was filtered, R waves were manually selected and the sample index of the R wave was saved such that the instantaneous heart rate could be calculated throughout the file by using the R-R interval. To get the instantaneous heart rate per minute, the following formula was used

$$HR_{\text{min}} = \frac{1}{RR_{\text{interval}}} \times Fs \times 60$$

where HR_{min} is heart rate in beats/min, RR_{interval} is the number of samples indexes between each successive R wave, and Fs is the sampling rate in Samples/s.

3.2 Final Set of Experiments—Non-Differential

A set of non-differential neural recordings was also performed to acquire information about the motor neural signal in the vagus nerve. For these non-differential recordings, four Sprague-Dawley rats ranging from 200-430 g were used. The IACUC approved the protocol for these experiments. Cuff electrodes were fabricated to acquire

the vagus nerve signal; each electrode used in this set of experiments consisted of two platinum contacts.

3.2.1 Electrode Fabrication for Non-Differential Recordings

Electrodes were fabricated in the same manner as described Section 3.1.3: platinum foil of the same dimensions described earlier was used for contacts, Teflon coated stainless steel wire was welded to the contacts, and silicone elastomer was used to mold the electrode. In this set of experiments, electrode contact number was non-varied; electrodes consisted of two platinum contacts of ~1mm width and ~1mm separation between the contacts. An illustration of the final electrode is shown in Figure 11. While much care was used to ensure that the measurements were 1mm, the distance may not have been exactly 1mm because some contact movement was witnessed as the silicone elastomer was poured over the scaffold used to mold the electrode. However, the movement did not greatly displace the contacts; the contacts were almost or exactly 1 mm apart as measured on the electrodes used for the experiments.

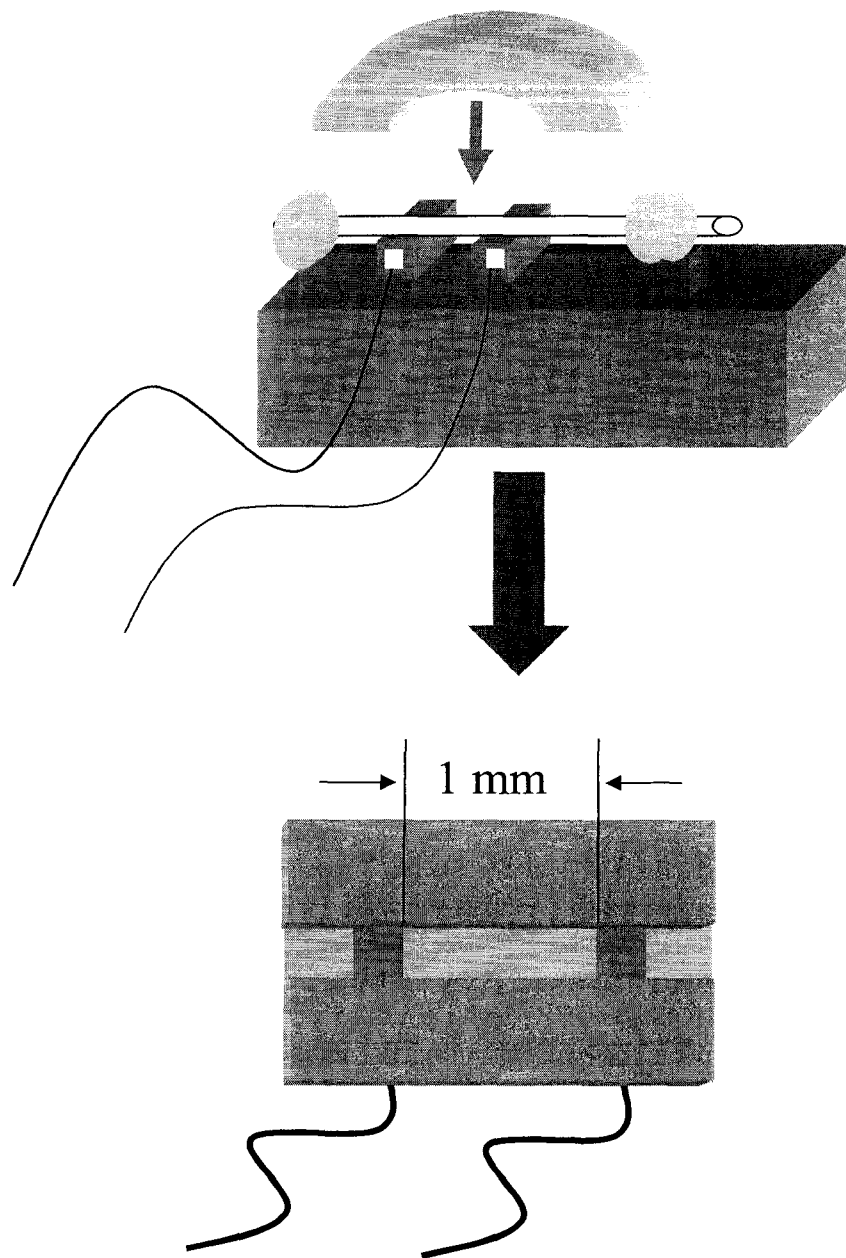


Figure 11 Schematic of the final electrode

3.2.2 Surgical Procedure for Non-Differential Recordings

To anesthetize the animals, IntraPeritoneal injections (IP) of Xylazine (12 mg/kg) and Ketamine (80 mg/kg) were used. Once the animal was under proper sedation, the animal was moved to a heated surgical table. Surface EKG electrodes were placed on the

right arm, left leg, and left arm to acquire the EKG signal. EKG signals acquired through the surface electrodes were first analog processed to amplify the signal and filter noise before being taken into the computer. In addition to an analog EKG filter, a 60 Hz notch filter was designed and added into the analog circuit.

A tracheotomy was performed so that the animal could be mechanically ventilated; the tubing used for the tracheotomy was PE 205. The ventilator and the CO₂ monitor used during the experiments are shown in Figure 12. After the animal had been mechanically ventilated, further dissection into the neck was performed until the right vagus nerve, right carotid artery, and left carotid artery were isolated. During the experiment, distilled water or saline was used to keep the tissues in the animal hydrated. After isolating the nerve, the electrode was placed under the nerve so that the nerve sat in the tunnel of the electrode; saline was then poured on the nerve and electrode combination to remove any blood and hydrate the nerve. The nerve electrode configuration was then dried using a cotton-tipped applicator. To secure the electrode from the in vivo environment, Kwik-Cast™ (World Precision Instruments) was used; Kwik-Cast™ was applied to the top of the electrode so that it provided isolation for the nerve.

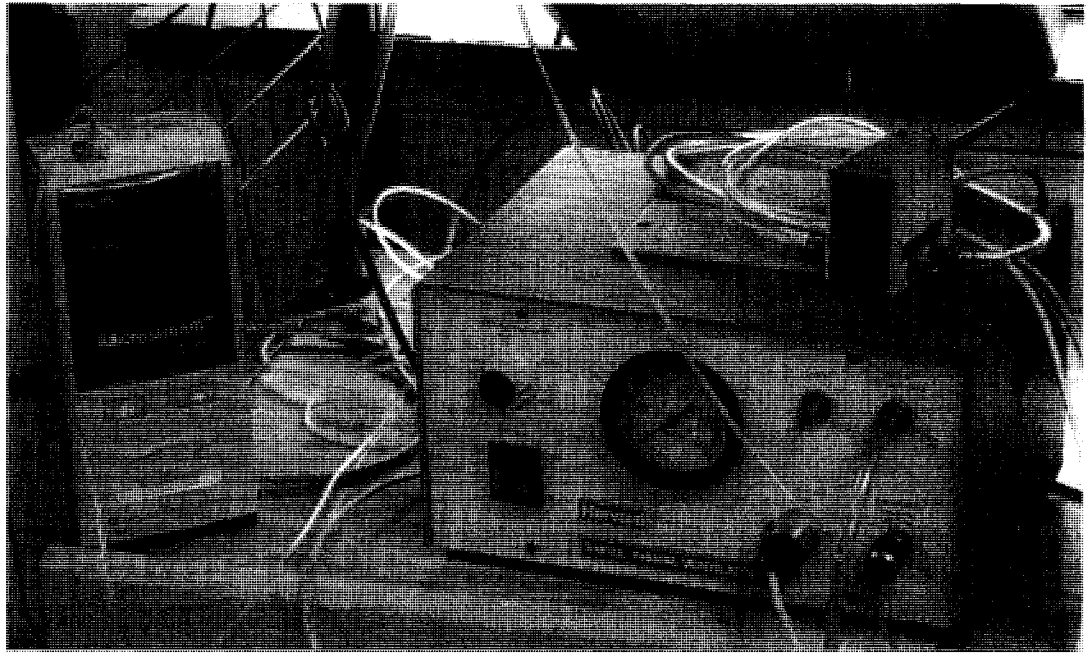


Figure 12 Mechanical ventilator and CO₂ monitor used to monitor the animals

Each contact wire was connected to a neural amplifier with each amplifier having a bandpass filter from 90 Hz to 13 kHz which was grounded to the animal so that each contact produced a signal, as opposed to the previous differential recordings where the difference of the contacts was taken into the computer. The neural amplifiers and the EKG circuit are shown in Figure 13. All signals, two neural and one EKG, were acquired into a computer using a National Instruments E Series DAQ board. The sampling rate for acquisition of neural and EKG signals was 65K Samples/s; this sampling rate was different from the previous sampling rate of 100K Samples/s used in differential recordings because a different DAQ board whose maximum sampling of 200 Samples/s was used for this set of experiments.

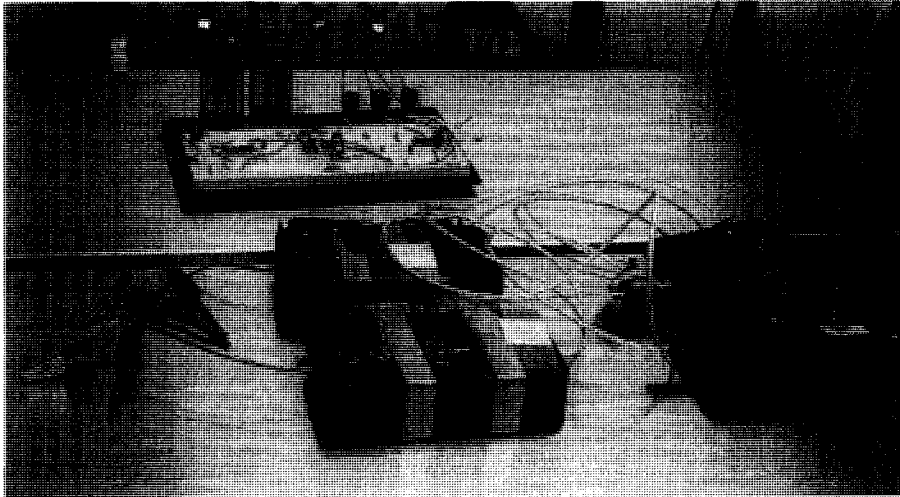


Figure 13 Analog EKG circuit and the neural amplifiers used

One of the final electrodes used for the non-differential experiments is shown in Figure 14. The wire connected to the first contact is marked by a piece of black tape around the wire; the contact lead was marked so that the proximal contact and distal contact could be distinguished for recording purposes. After the electrode was implanted, a baseline recording of neural and EKG signals was taken. After the baseline recordings were taken, recordings of the neural and EKG signals were taken while inducing heart rate change. To elicit a change in heart rate, bilateral carotid occlusion was performed [49-54]. Flat, smooth clips were used to manually occlude both right and left carotid arteries. Occlusions were performed at 20 s, 25 s, 30 s, and 60 s intervals. The procedure for an occlusion recording was as follows. Manual occlusion of both arteries coincided with onset of recording. Recording continued throughout the occlusion and for at least 20 s after the occlusion was removed. At least three minutes of recovery for the animal was allowed between occlusion recordings; more time was allowed for recovery if the animal had not stabilized.

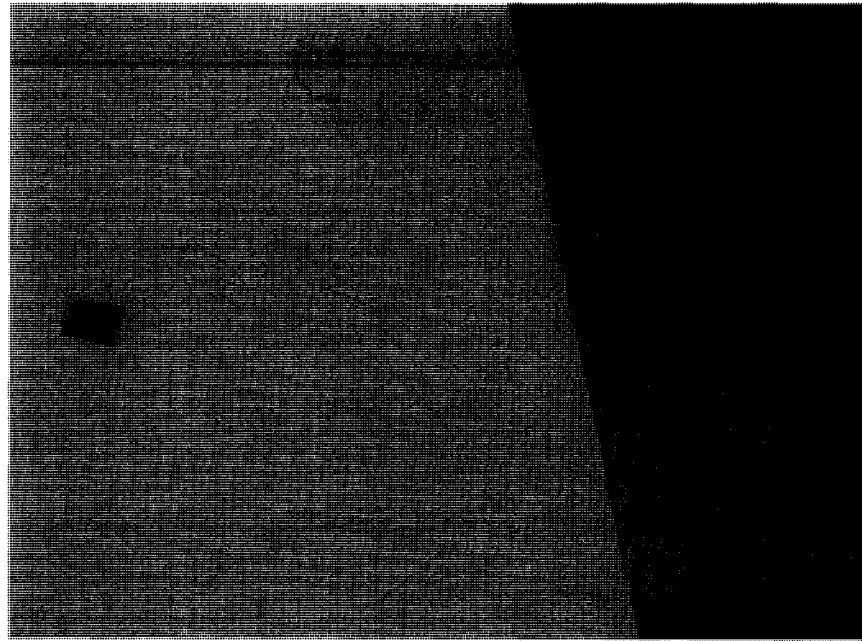


Figure 14 Final electrode with proximal lead marked

Carbon dioxide, depth of anesthesia, and the animal's breathing were monitored throughout the experiment to insure that the animal was comfortable and under proper sedation. Not all occlusion times were used for each experiment. For experiments 9 and 11, 20 s, 25 s, and 30 s occlusion times were used; each occlusion was performed twice during the experiment. For experiment 13, 20 s, 25 s, 30 s, and 60s occlusion times were used; each occlusion was performed twice during the experiment. For experiment 14, 20 s and 30 s occlusion times were used; each occlusion was performed three times during the experiment. In addition to the baseline and occlusion recordings, after all occlusion recordings had been taken, two additional recordings were taken for each experiment. These two recordings were (1) a recording after the right vagus nerve had been cut distal to the electrode thereby eliminating sensory traffic and (2) a recording after the right vagus nerve had been cut distal and proximal to the electrode so that the nerve was no longer connected to the rest of the animal's body, thereby showing the thermal noise

present. Finally, upon completion of the experiment, the animal was humanely euthanized using an IntraCardiac (IC) injection of potassium chloride (KCL).

3.2.3 Data Analysis for Non-Differential Recordings

To analyze the data acquired during the experiments, MathWorks' MATLAB and MATLAB's Signal Processing Toolbox were used. The two neural signals were digitally filtered using a Hamming window with a passband of 1 kHz to 5 kHz and order of 1000; the passband for filtering the signals was determined from the power spectrum of the neural signals. After the neural signals were filtered, the motor signal delay was calculated. A sliding window cross correlation was used to find the delay between the neural signal recorded by the proximal contact and the neural signal recorded by the distal contact [55-56]. A Neurocal simulation to illustrate this technique is outlined in Appendix B. The proximally recorded neural signal was channel 1 and the distally recorded signal was channel 2; the sliding window cross correlation held channel 1 steady while shifting channel 2 forward and backward to find the greatest correlation between the two signals. Therefore, due to channel 1 being the proximal recording and channel 2 being the distal recording, a positive lag with high correlation was sought to identify the motor signal. After the positive lag with the highest correlation value was determined, this lag value was used to calculate the motor signal by shifting the distal recording forward by the number of lags and subtracting the two neural channels. For more details, see the MATLAB code in Appendix C. The motor signal obtained was then smoothed by averaging it over 10 ms intervals.

Before calculating heart rate, the EKG signal was filtered using a Hamming window with a passband from 0.3 Hz to 100 Hz and filter order of 500. After the EKG was filtered, R

waves were manually selected and the sample index of the R wave was saved such that the instantaneous heart rate could be calculated throughout the file by using the R-R interval. To get the instantaneous heart rate per minute, the following formula was used where HR_min is heart rate in beats/min, $RR_{interval}$ is the number of samples indexes between each successive R wave, and F_s is the sampling rate in Samples/s.

$$HR_min = \frac{1}{RR_{interval}} \times F_s \times 60$$

Once the heart rate and vagal motor signal were calculated, the area of the motor signal between successive R waves could be obtained by integrating the motor activity. Since the sample index of the R waves was saved, it was used to identify the indexes between which the motor signal was integrated. Figure 15 shows an example of an integrated motor file that was integrated between successive R waves. Sample index values from each R wave obtained during calculation of instantaneous heart rate were saved, and those indexes were used to integrate motor activity from one sample after an R wave to the sample index of the next R wave. The section of integrated motor activity is marked by the arrows in the figure; the sections marked by the arrows show two integrated regions. After the integration of the motor signal between R waves, an area file of the integrated sections between R waves was generated whose length was the same as the heart rate file. Finally, the correlation coefficient between the heart rate and area of motor activity directly preceding each heart beat was calculated.

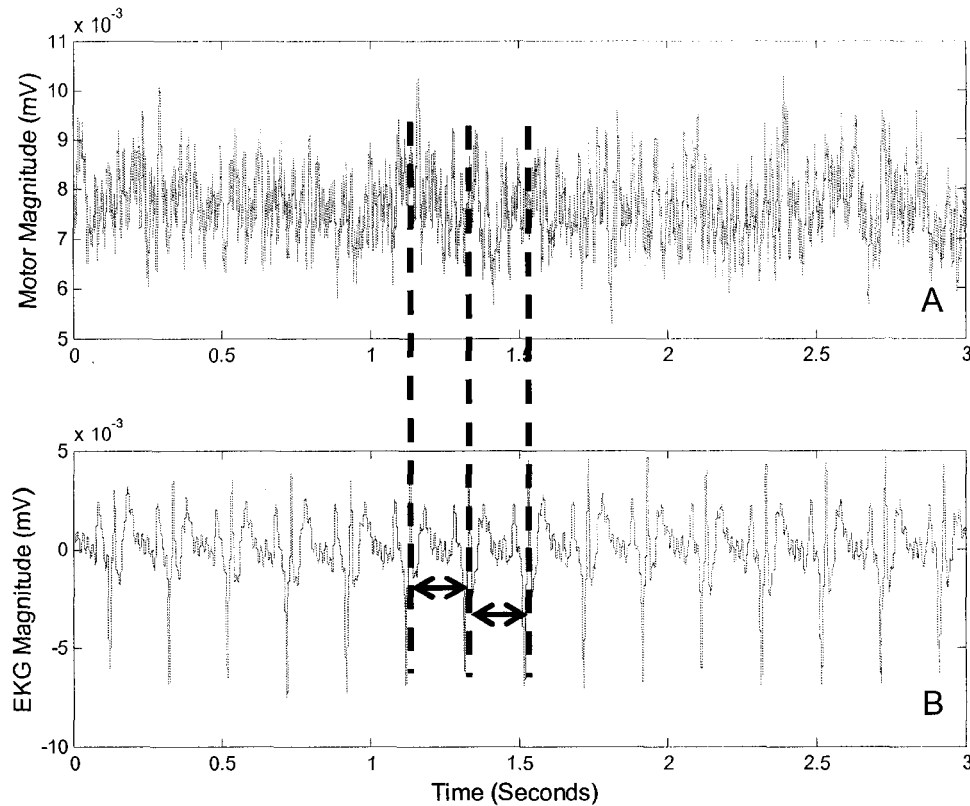


Figure 15 Figure A shows vagus motor activity while Figure B shows the EKG signal

3.2.4 Transfer Function Model of Heart Rate Based on Motor Area

Transfer functions relate an output series to one or more input series. Therefore, a transfer function model will quantify the relationship between the output, heart rate, and the input, motor area. In a single input, single output linear system, the output series, y , and the input series, x , are related as follows:

$$y_t = \nu(B)x_t + n_t$$

where $\nu(B)$ is the transfer function and n_t is the noise series of the system which is independent of the input series. For a causal system where $\nu(B) = \sum_{j=0}^{\infty} \nu_j B^j$ and B is

the backshift operator such that $B^j x_t = x_{(t-j)}$, the single input, single output, linear system model becomes

$$y_t = v_0 x_t + v_1 x_{(t-1)} + v_2 x_{(t-2)} + \dots + n_t$$

or

$$y_t = v_0 x_t + v_1 B x_t + v_2 B^2 x_t + \dots + n_t$$

or

$$y_t = v(B) x_t + n_t$$

The transfer function, $v(B)$, is represented in the rational form as

$$v(B) = \frac{\omega_s(B) B^b}{\delta_r(B)}$$

where $\omega_s(B) = \omega_0 - \omega_1 B - \dots - \omega_s B^s$, $\delta_r(B) = 1 - \delta_1 B - \dots - \delta_r B^r$, and b is the time lag before an input impulse produces and output response [57].

A transfer function model is analogous to an AutoRegressive, Moving Average (ARMA) model. An ARMA model $\phi_q(B) Z_t = \theta_q(B) a_t$ can be rewritten as

$$Z_t = \frac{\theta_q(B)}{\phi_q(B)} a_t$$

where $\theta_q(B)$ is the moving average term, $\phi_q(B)$ is the autoregressive term, and a_t is the white noise term. From this, it can be seen that the numerator term of the rational transfer function is representative of the moving average process, and the denominator term on the rational transfer function is representative of the autoregressive process. The difference between the ARMA and the transfer function is that the ARMA terms are for a white noise series whereas the transfer function terms are for a specified input series [57].

Beginning with the general rational transfer function, a specific transfer function relating heart rate and motor activity was designed using a three step process: identification, estimation and diagnostic checking, and forecasting. The identification

stage involves pre-whitening the input series, transforming the output series by the pre-whitened model of the input series, performing a cross correlation between the pre-whitened input series and the filtered output series, and identifying a preliminary estimate of a transfer function. However, before pre-whitening can be performed, the series must be stationary; if the series is not stationary, differencing of the series must be performed to stabilize the series [57].

Direct cross correlation between the input series and the output series often provides misleading information about the relationship between the two series due to autocorrelation. To avoid this, pre-whitening is performed. Pre-whitening is the process of fitting an AutoRegressive, Integrated, Moving Average (ARIMA) model to the input series. To determine a model for the input series, the patterns of the AutoCorrelation Function (ACF) and Partial AutoCorrelation Function (PACF) for the input series are analyzed and compared to established typical patterns; the pattern of each will indicate a type (autoregressive or moving average) and an order of a possible model.

The autocorrelation function, ρ_k , is related to the covariance, γ_k , as shown below where k is the lag number, Z_t is the time series process, μ is the mean of the process, and γ_0 is the covariance at lag zero.

$$\gamma_k = \text{Cov}(Z_t, Z_{t+k}) = E(Z_t - \mu)(Z_{t+k} - \mu)$$

$$\rho_k = \frac{\gamma_k}{\gamma_0}$$

For a stationary process, the ACF is an even function; therefore, the ACF is typically only plotted for nonnegative lags. The PACF is used to investigate the correlation

between different values in a series after the linear dependence of each subsequent value has been removed as shown below [57].

$$\text{Corr}(Z_t, Z_{t+k} \mid Z_{t+1}, \dots, Z_{t+k-1})$$

A sufficient model for the input series is one which reduces the residuals to white noise. Once this model is determined, the input series is filtered with the model, and the output series is also filtered by the same model. Next, the filtered input series is cross correlated with the filtered output series. From the result of the cross correlation plot, an initial estimation of the type of transfer function (number of numerator and denominator parameters to expect as well as the delay value) can be obtained by comparing the cross correlation plot to known theoretical patterns [57].

After identifying an initial estimation for the type of transfer function, the transfer function parameters must be estimated. The transfer function model $y_t = \nu(B)x_t + n_t$ can also be written as

$$y_t = \frac{\omega(B)}{\delta(B)} x_{(t-b)} + \frac{\theta(B)}{\phi(B)} a_t$$

where y_t is the output series, $\omega(B)$ is the numerator parameter of the rational transfer function $\nu(B)$, $\delta(B)$ is the denominator parameter of the rational transfer function $\nu(B)$, $x_{(t-b)}$ is the input series, $\theta(B)$ is the moving average term of the noise model, n_t , $\Phi(B)$ is the autoregressive term of the noise model, n_t , and a_t is a white noise term.

From this re-written version, the noise term (second term) is easily seen as an ARMA model. The parameters of the transfer function model which must be estimated are ω , δ , θ , and Φ . SAS, a statistical analysis software program, will estimate the parameters ω and δ for the initial estimation of the transfer function; diagnostic checking

of the residuals will determine if the estimated transfer function is adequate or if a noise term must be added. If residuals of the transfer function indicate that the transfer function alone is not adequate, an ARMA noise model based on transfer function residual analysis is added to create the full model. After adding the ARMA model, diagnostic checking of the residuals of the full transfer function model is performed. If analysis of the residuals indicates only white noise and no pattern, then the full model is considered adequate [57].

After the full transfer function model has been designed, the next check of the model is to forecast values and compare forecasted values against actual values. To do this, input values with known output values are used, but the model is given only the input values. The model then returns output values (forecasted values) for the given input values. If the model is sufficient, the forecasted values will be within a determined statistical confidence limit, typically 95%, of the actual values. If the model is sufficient, then it can be used to predict output values when given an input series [57].

To design a transfer function model relating motor activity and heart rate, a baseline recording and an occlusion recording, each consisting of 80 consecutive heart beats from experiments 9, 11, 13, and 14, were selected for a total of eight motor area and eight heart rate files. One key requirement of time series analysis is that data must be equidistant samples; that is, the sampling interval between data points must be constant [57]. Because the increments between each area and heart rate data point were not the same due to changes in heart rate (the distance between the points would be shorter as heart rate increased, while the distance between the points would be longer as heart rate decreased), each heart rate file and area file was made continuous. There are several

methods presented in the literature for transforming non-equidistant sampled data into equidistant sampled data. After examining the different methods, the sample and hold method was chosen for this data because 1) it is robust, 2) it correctly estimates the variance of the original data, 3) it is recommended for high data densities, and 4) it does not produce false peaks seen in other re-sampling methods [58-62].

Once the sample and hold method had been chosen to transform the data, the method was applied as follows. The sample index values of the R waves had been previously saved; therefore these values were used to transform the area and heart rate into continuous files. To make these files continuous, the area and heart rate files were made equal to the length from the first R wave's sample index to the last R wave's sample index. Once the area and heart rate files consisted of all sample points between the first R wave's sample index and the last R wave's sample index (see Figure 16A), a custom MATLAB m-file was run to make all values before a heart beat equal to those of the previous heart beat (see Figure 16B). Figure 16A illustrates the non-continuous signal which could not be used for time series analysis; only the non-zero data points were available. The zeros were added to show that sample points existed between data points. Also, notice that the number of sample points (zeros) between non-zero values varies; this represents the non-constant increment between data points. Figure 16B illustrates how the non-continuous signal, which did not attach values to sample points between data points, was transformed into a continuous signal that could be used in time series modeling.

1 0 0 2 0 0 0 0 3 0 0 0 4 0 0 0 0 5	A
1 1 1 2 2 2 2 2 3 3 3 3 4 4 4 4 4 5	B

Figure 16 A illustrates the continuous signal while B illustrates the result of sample and hold

After all the area and heart rate files were transformed into a continuous form, the file of the shortest length was determined; then, the length of all files was made equal to the length of the shortest file. Once all the files were the same length, all eight heart rate files were averaged to make one array of heart rate values, and all eight area files were averaged to make one array of area values. The length of each of these two arrays, heart rate and area, was over 1,000,000 points. To make this more manageable, it was determined that 91 points would be used to design the model and 10 points would be used to validate the model through forecasting. To select these 101 points, a custom MATLAB m-file was run which used a “for” loop structure to select 101 points at specified intervals from the total length of over 1,000,000; the m-file selected points at equal intervals so that time series analysis could be used.

After the 101 point array of heart rate data and the 101 point array of area data were determined, SAS was used to design a transfer function model of heart rate based on motor area. After loading the heart rate and area data into SAS, the first step was to pre-whiten the input series; this was performed by fitting a model to the independent variable, area. Next, the dependent variable, heart rate, was filtered by the model fitted to the independent variable; then, the filtered independent and dependent variables were cross correlated. To determine the structure of the transfer function (numerator, denominator, and lags), the cross correlation plot was examined and compared with plots from

documented transfer functions models [57]. Once the appropriate model was identified, the transfer function model was estimated using SAS. The AutoCorrelation Function (ACF) and Partial AutoCorrelation Function (PACF) plots produced by SAS, after estimating the transfer function, were examined to determine if the model was adequate, demonstrated by the residuals being white noise, or if a modification was needed. The residual analysis indicated that a noise term was needed. Therefore, the form of the final transfer function model was $y_t = \nu(B)x_t + n_t$ where y_t is the output, $\nu(B)$ is the rational transfer function, x_t is the input, and n_t is the noise model.

After the appropriate model had been identified, validation of the model was performed. SAS was used to forecast ten future points based on given motor area values. Before designing the model, the area and heart rate were both input into SAS for a total of 91 points. However, for SAS to forecast the heart rate values for points 92-101, only the area values for points 92-101 were necessary; this was accomplished by inputting the area values for points 92-101 and inserting a single decimal point to represent a missing value for each heart rate for points 92-101. SAS generated the forecasted values for points 92-101 in addition to predicting all of the heart rates from input area values 1-91, assigned a 95% confidence limit to those values, and returned the residual, the numerical amount between the forecasted value and the actual value. For more detail on the SAS code used or the SAS output, see Appendix D.

CHAPTER 4

RESULTS AND DISCUSSION

4.1 Preliminary Work

4.1.1 Selection of Electrode Implantation Site

The first electrode implantation site was the cardiac branches of the vagus nerve as shown in Figure 17B. During the necropsies, dissection of the cardiac plexus region was performed. To get to the level of the vagal cardiac innervations, much delicate dissection was required. On the heart, the nerves were very small and formed a web looking much like a spider web. This can partially be seen in Figure 17A which shows a bundle of small nerves running through a cuff electrode. If this bundle of nerves were held with tweezers and not forced together in the electrode, one could see the webbing of nerves.

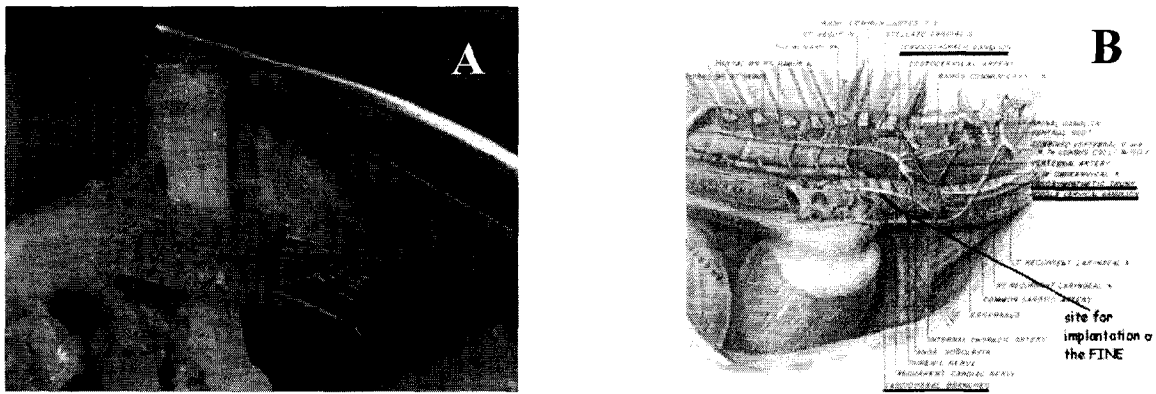


Figure 17 A shows an electrode on the nerve webbing at the heart while B shows the initial electrode placement [63].

After this location was examined more thoroughly, this location was determined not to be feasible due to the difficulty in electrode implantation and the invasiveness required in implanting the electrode at this level. This procedure would be too invasive for human experimentation unless heart transplantation were being performed. For the experiments performed in this study, this location was also determined to be too invasive with the life of the animal being in question while dissection to this level was performed. In addition to the depth of dissection required for this location, much time was needed to carefully dissect down to this level without severing any of the small nerves. Considering the time requirement and invasiveness of the procedure, this location was ruled out as an electrode implantation site.

Once this initial location was discounted, another location along the vagus nerve was sought. A location more proximal to the cardiac plexus was determined to be an easily accessible, much less invasive location. The location determined to be useful for these experiments was the common carotid artery level of the vagus nerve. Because a tracheotomy was performed for these experiments, the common carotid artery location would already be partially dissected. With a little further dissection, this location could

be exposed more easily than a more distal location. The vagus nerve runs along the carotid artery, and the two are enclosed in a sheath. This common carotid artery level of the vagus nerve was the section used to record data for all experiments in this project.

Figure 18 illustrates the electrode implantation site used for the experiments performed in this project.

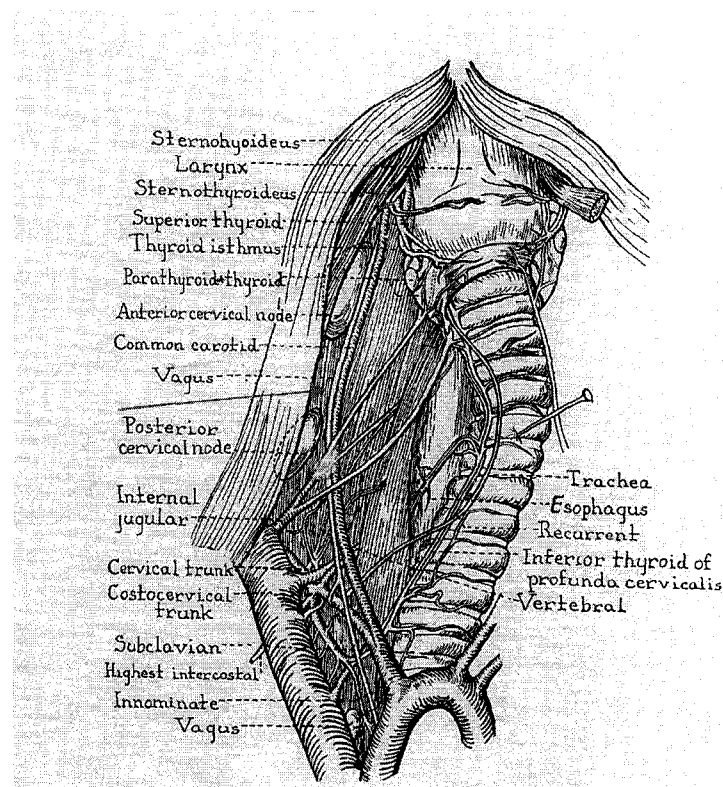


Figure 18 Final electrode implantation site [64]

Once the location for electrode implantation had been decided, the vagus nerve, right or left, had to be determined. For the differential recordings and for the procedures used to perfect the dissection of the nerve, either the right or left vagus nerve was used depending on which was available. From the literature, it is shown that the right vagus nerve is the main controller of the SA node [48]. However, during the preliminary

experiments, the right vagus nerve was not always available due to damage caused by the surgery; in such a case, the left vagus nerve was used instead. The left vagus nerve also affects the heart but primarily affects the AV node therefore recording from the left vagus nerve also returns information about the heart [48]. Although either the right or left vagus nerve was used during the differential recordings, only the right vagus nerve was used for non-differential experiments 9-14 which produced the data used to design the transfer function model.

4.1.2 Differential Recordings

Differential recordings were initially performed to determine if a high correlation between heart rate and whole nerve recordings could be obtained. For these recordings, three methods were used to alter heart rate: respiratory occlusion, nitroglycerin injection, and carotid artery occlusion. Nitroglycerin injection never elicited a change in heart rate. This is believed to be due to insufficient cannulation of a vein; different veins in the leg were used to attempt access for injection. However, either the vein collapsed or the nitroglycerin spilled out instead of continuing up the vein. Also, this method for heart rate alteration required more time than the other two methods because dissection to the veins in the leg and cannulation of the vein had to be performed. Therefore, nitroglycerin was eliminated as a repeatable method of alteration of heart rate.

In one experiment in which an electrode with five platinum contacts was used, the signal to noise ratio achieved by using different contacts for recording was calculated. The results of this experiment are shown in Table 2. The signal to noise ratio for all combinations of contacts tried was approximately the same; therefore, it was determined that larger separation of contacts was not important for these recordings.

Table 2 Signal to noise ratio calculated between contacts of different separation distances

Signal to Noise Ratio between Different Contacts		
Experiment 3		
Contacts		Average
1, 2		1.23
2, 4		1.23
2, 5		1.22
4, 1		1.24

For the differential recordings, an example of a raw nerve signal is shown in Figure 19. The raw signal shows contamination by the EKG signal which is seen as the long, slender spikes in the signal; three such contaminations are marked in Figure 19 by arrows. For the nerve signals to be of use in this study, the nerve signals were processed for frequency content using a Hamming window; the filtered nerve signal is shown in Figure 20. The filtered nerve signal is not contaminated with the EKG signal. After the neural signal was filtered, the signal was rectified and a 10 ms moving average window was used to smooth the signal and improve quality. Figure 21 shows the rectified, averaged nerve signal. Figures 19-21 show data from the same section of the same neural signal; this allows one to observe the change that each stage of the neural signal processing produced.

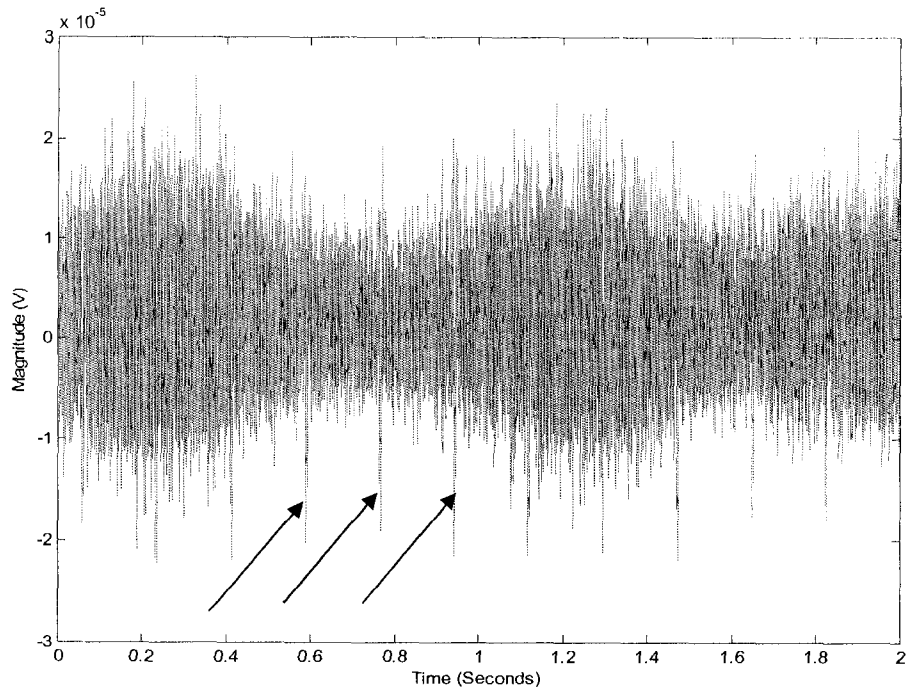


Figure 19 Example of raw neural signal obtained

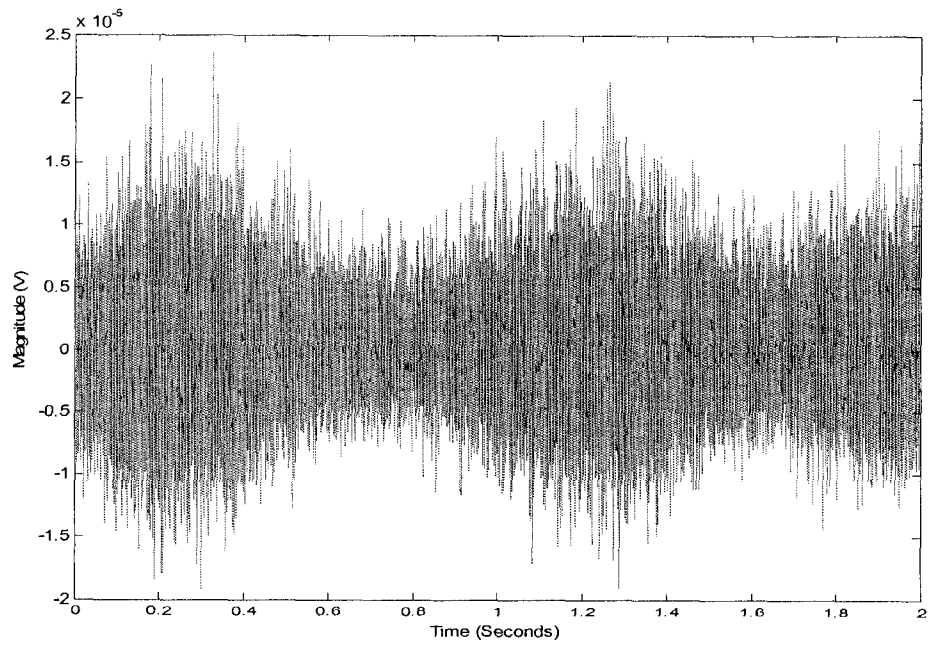


Figure 20 Example of digitally filtered neural signal

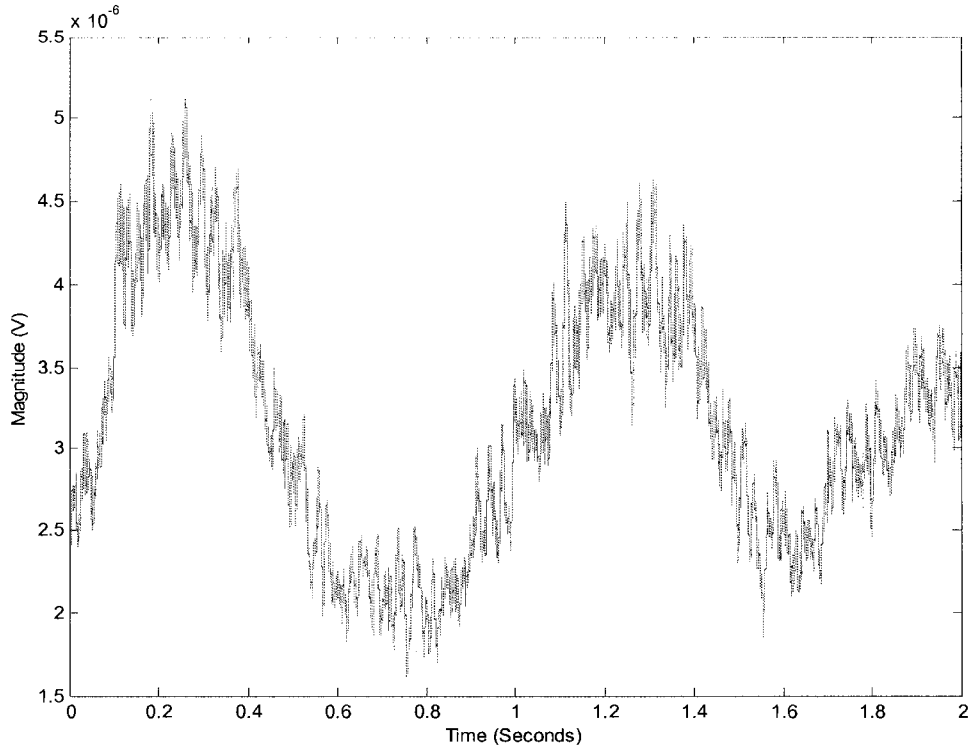


Figure 21 Rectified, averaged neural signal

The acquired analog EKG signal was processed for frequency content to isolate the frequency range required for the EKG signal and therefore eliminate the noise contamination in the signal. The filtered EKG signal is shown in Figure 22; an example of the R waves which were manually chosen to calculate instantaneous heart rate can be seen clearly in this figure. The baseline wandering due the respiratory cycle of the animal has been removed from Figure 22; this allows for the signal to be centered around zero.

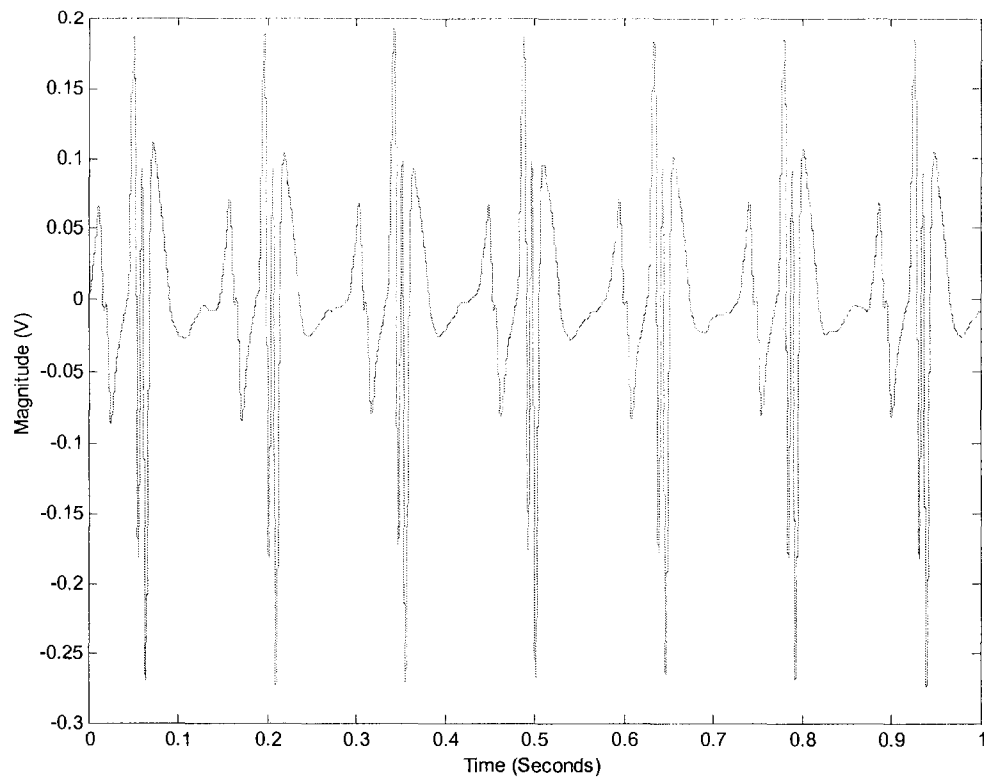


Figure 22 Example of a filtered EKG

After the instantaneous heart rate had been calculated and the neural signal had been smoothed and rectified, the neural activity was integrated between R waves to produce a matrix of integrated neural activity. The length of the integrated neural activity and the instantaneous heart rate was equal. Then, a correlation was performed between the integrated neural activity and the instantaneous heart rate to determine how the two were related. In several experiments, differential recordings were made on the right and the left vagus nerves. For each of these right and left recordings, correlation was performed separately between the instantaneous heart rate and integrated neural signal. Table 3 shows the Pearson correlation values (R values) obtained from different data sets in different differential experiments.

Table 3 Pearson correlation between instantaneous heart rate and integrated neural activity for differential recordings

Experiment	Data Set	Neural and HR Pearson correlation
1	baseline 2	-0.31
1	occlusion 2	-0.60
1	baseline 3	-0.29
1	occlusion 3	-0.76
1	baseline 4	-0.35
1	occlusion 4	-0.94
3	nitroglycerin 1	-0.37
3	nitroglycerin 2	-0.68
3	nitroglycerin 3	-0.56
3	occlusion 1	-0.06
3	occlusion 3	-0.87
8	occlusion 1 right	-0.33
8	occlusion 1 left	-0.41
8	occlusion 2 right	-0.17
8	occlusion 2 left	-0.25
8	occlusion 3 right	-0.05
8	occlusion 3 left	-0.15
8	occlusion 5 right	0.02
8	occlusion 5 left	-0.21
8	occlusion 7 right	-0.63
8	occlusion 7 left	-0.83
8	occlusion 8 right	-0.48
8	occlusion 8 left	-0.61
	AVERAGE	-0.43

Correlation values obtained from the right vagus nerve were consistently lower than the correlations obtained from the left vagus nerve. Table 3 provides the actual correlation values obtained. Figure 23 shows integrated right vagus nerve activity on the top plot and instantaneous heart rate on the bottom plot; by visually analyzing the two plots, one can see that the two plots do not show much inverse correlation. Figure 24

shows the integrated left vagus nerve activity on the top plot and the instantaneous heart rate on the bottom plot; again, by analyzing these two plots, it appears that little correlation exists between the two.

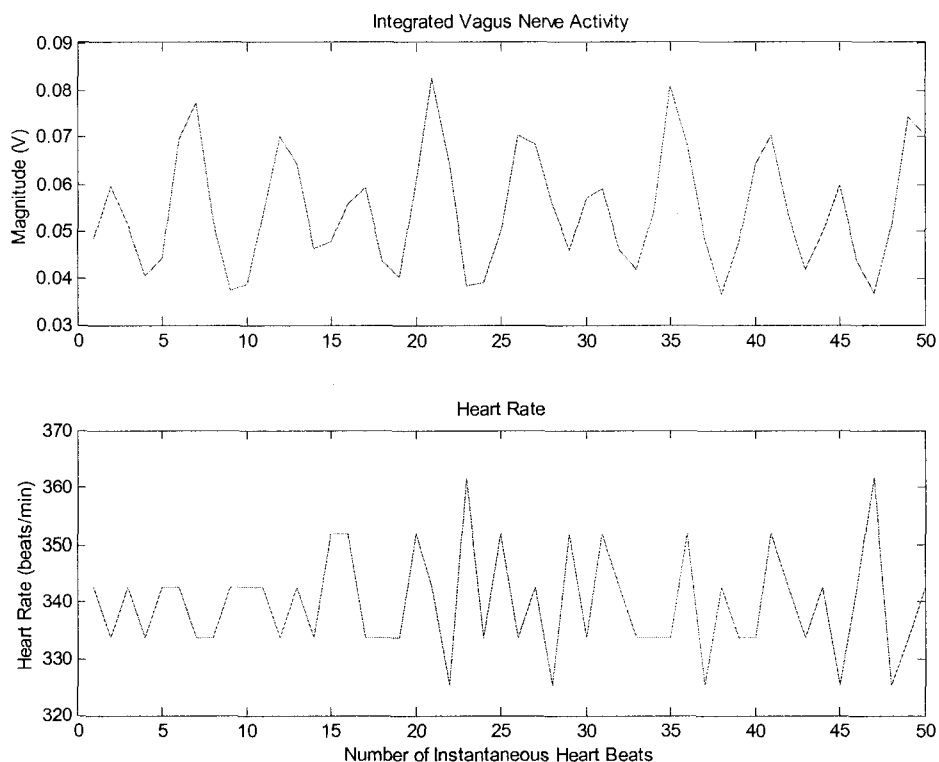


Figure 23 Integrated right vagus nerve activity (top plot) and instantaneous heart rate (bottom plot)

Higher correlations were obtained from the left vagus nerve than from the right vagus nerve, although not significantly higher. This is somewhat unexpected because the right vagus nerve predominately innervates the SA node which is the “internal pacemaker” of the heart while the left vagus nerve also innervates the SA node but has a stronger effect on the AV node of the heart [48]. All recordings were whole nerve recordings containing both sensory and motor activity; therefore, the correlation values may have been influenced by other neural information. The vagus nerve innervates many

organs in the body and carries sensory and motor signals for these organs; therefore there is a possibility that signals to or from other organs may have contaminated the correlation values. Alternatively, the neural signal could have been stronger in the left nerve; even though the left vagus nerve primarily controls the AV node, it does innervate the SA node. Regardless of the reason for the slightly higher inverse correlation seen in the left vagus nerve, the correlations obtained were inconsistent and frequently not high (<-0.50) inverse correlations.

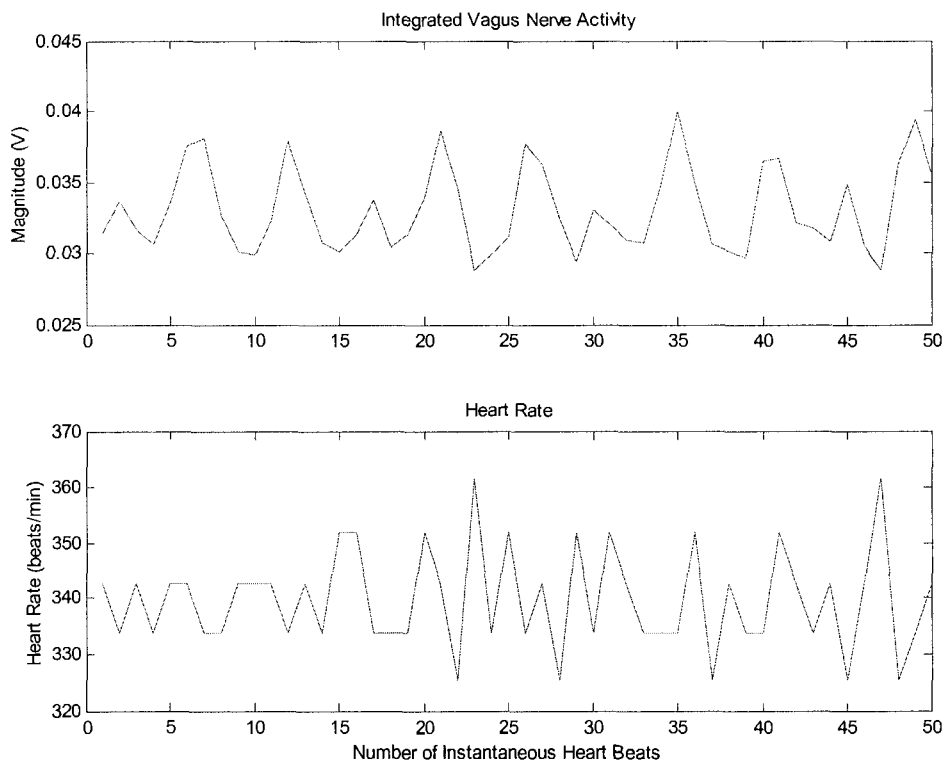


Figure 24 Integrated left vagus nerve activity (top plot) and instantaneous heart rate (bottom plot)

Although most correlations obtained were not high, high inverse correlations were obtained for a few files with the highest being -0.94 ; however, many files returned very

low inverse correlations with the lowest being -0.05. In one instance, a very small positive correlation, 0.02, was returned. The mean of correlations obtained from differential recordings obtained across experiments and across data sets was -0.43. The magnitude of correlations obtained from these recordings varied greatly; a consistent pattern was not seen. However, with the exception of one file that returned a small, positive correlation of 0.02, all other files returned an inverse correlation which indicated that the neural activity was indeed parasympathetic activity.

An inverse correlation is desired because as the heart rate goes up, the parasympathetic activity should withdraw or decrease. The opposite should occur for a decrease in heart rate, i.e. as the heart rate slows down, the parasympathetic activity should increase. This inverse correlation is due to the nature of the parasympathetic system, a part of the autonomic nervous system which consists of the both the sympathetic system and the parasympathetic system. The sympathetic system is the section that is responsible for the fight or flight response while the parasympathetic system is responsible for returning the body to the previous, natural state. Therefore, since an inverse correlation indicates an opposing relationship between the two variables being compared, an inverse correlation is desired to reveal the nature of the parasympathetic activity to heart rate. Since the recordings are from the vagus nerve, either right or left, parasympathetic activity is expected to be seen because the vagus nerve is a parasympathetic nerve which innervates the heart as well as many other organs.

While inverse correlations were obtained with consistency, the magnitude of these correlations varied greatly. These correlations were not easily repeatable and consistent; therefore it was determined that this method of recording would not be useful in

developing a model of heart rate based on neural activity. Before attempting to develop a model for heart rate, repeatable and consistent correlation values from recordings were desired so that the model would be based on an accurate occurrence and not on a chance occurrence of high inverse correlation. After performing several differential recording experiments without observing a repeatable and consistent correlation, it was determined that this would not be the best method to acquire data that would be used to develop a model for heart rate.

Another method which would produce repeatable, consistent recordings was sought. To obtain such recordings, it was determined that the vagal motor signal would be used. The vagus nerve is a mixed nerve consisting of sensory and motor fibers; therefore to obtain the motor signal, a new method of recording was required. Upon the determination to use the vagal motor signal, which contains control information from the brain transmitted through the vagus nerve, a non-differential recording set up was implemented so that the motor signal could be extracted from whole nerve recordings.

4.2 Final Set of Experiments—Non-Differential

Non-differential recordings were performed to determine if a high correlation between heart rate and vagus motor activity could be obtained. For the non-differential recordings, two neural signals from the right vagus nerve and an EKG signal were recorded. The neural and EKG signals were processed for frequency content as in the differential recording, and the instantaneous heart rate was calculated from the manually selected R waves. Because the two neural signals were recorded with respect to ground instead of differentially, directional information could be extracted from the signals by using a cross correlation method introduced by Heetderks [55-56]. The cross correlation

method allowed for the extraction of the vagal motor signal which was then averaged. The averaged motor signal was integrated between successive R waves to form an array of integrated motor activity which was the same length as the instantaneous heart rate array. A Pearson correlation test between the integrated motor activity and the instantaneous heart rate was performed to determine how the two were related.

Figures 25-27 display histograms of the cross correlation results; “A” in all these figures represents a baseline recording while “B” represents an occlusion recording. The occurrences represented in these histograms have a correlation value greater than or equal to 0.5; occurrences with correlation values less than 0.5 are not shown. Histograms allow for sensory and motor activity to be viewed easily; for these histograms, the motor activity is on the positive horizontal axis while the sensory information is on the negative horizontal axis. While each histogram is calculated from a different occlusion time and a different experiment, the trend is the same throughout the figures; there is a withdrawal of parasympathetic motor activity (represented on the positive horizontal axis) during occlusion recordings. This is expected because bi-lateral carotid artery occlusion has been shown to elevate heart rate which would require a withdrawal of parasympathetic activity [49-54].

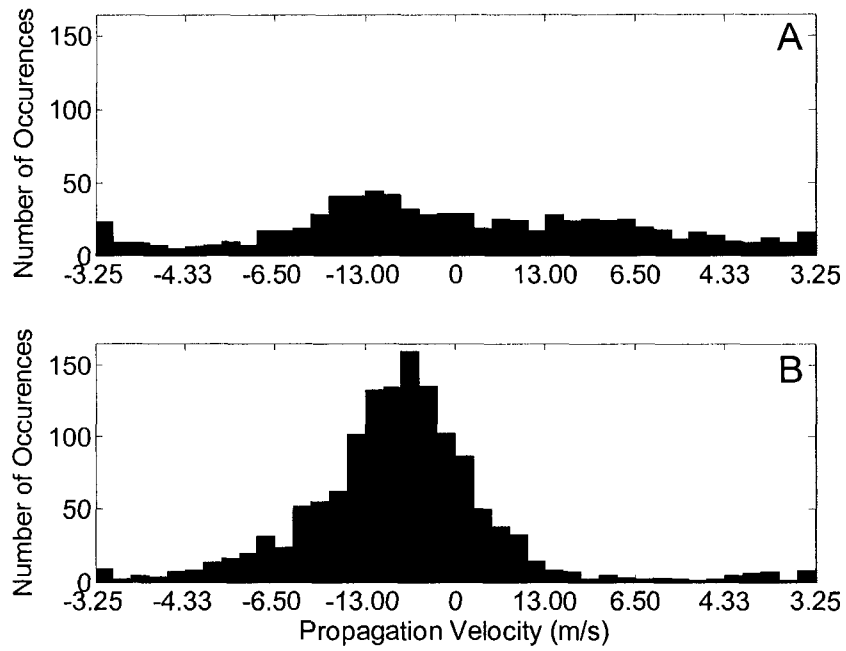


Figure 25 Histogram of delay values separating motor and sensory activity for a recording from experiment 9

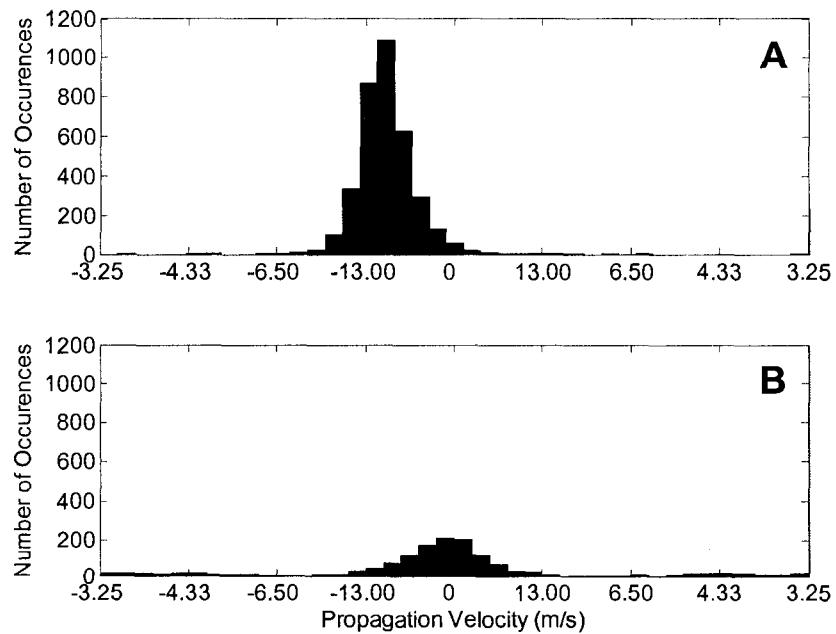


Figure 26 Histogram of delay values separating motor and sensory activity for a recording from experiment 13

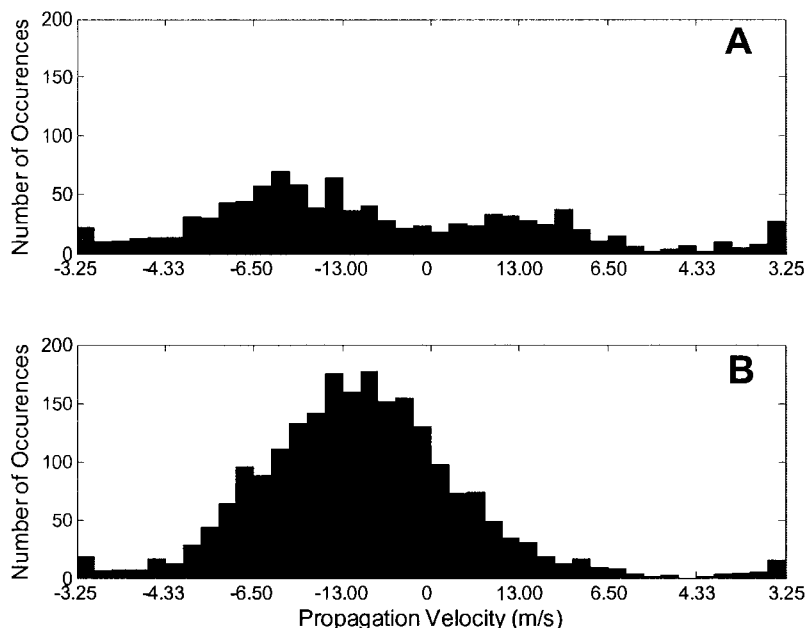


Figure 27 Histogram of delay values separating motor and sensory activity for a recording from experiment 14

Consistent, high inverse correlations were obtained between vagal motor activity and instantaneous heart rate. Tables 4-7 show the results of the correlation test for different data sets in different experiments. More than one baseline correlation value is shown because several baseline recordings were taken for each experiment before any occlusion was attempted. Baseline recordings were free of the noise due to movement that was present in the occlusion recordings; therefore, for baseline recordings, correlation between instantaneous heart rate and vagal motor activity was performed on longer sections of the baseline recordings than on most occlusion recordings.

While the length (number of heart beats) of the occlusion recordings in Tables 4-7 is generally shorter than those for baseline recordings, there are a few files which are nearly as long as the baseline recordings. Most occlusion recordings had to be segmented and correlation analysis performed on each section of the recording because extreme

noise was present in portions of the file. The extreme noise seen was due to the occlusion which generally induced movement in the animal or to the removal of the occlusion clips; this can be seen by looking at the occlusion recordings on a time scale so that one can see when the occlusion was removed. However, even though the occlusion recordings were generally shorter than the baseline recordings, a consistency of correlation values was seen.

In Tables 4-7, the Pearson correlations obtained between the integrated right vagus nerve activity and the instantaneous heart rate for experiments 9-14 are shown in the “Motor and HR correlation” column. In addition to the correlation values, the table also shows the delay value determined by the cross correlation method for each data set, the value of the correlation between the proximal and distal contact at that delay value, the number of heart beats in the data set, the mean value of the heart rate for the data set, and the standard deviation of the heart rate for the data set. Finally, the mean and standard deviation across different data sets for the delay value and correlation are shown at the bottom of the table.

Table 4 Pearson correlations, delay values, and delay correlations for experiment 9

Data Set	Delay for sensory/ch2 (samples)	Delay correlation	Motor and HR correlation	# Heart Beats	Mean HR	STD HR
Baseline	2	0.927	-0.90	103	208.87	8.54
Baseline	1	0.931	-0.62	102	208.54	36.28
Occlusion 20s	2	0.914	-0.74	28	219.57	28.69
Occlusion 20s	3	0.9951	-0.82	60	260.36	37.01
Occlusion 25s	4	0.96978	-0.75	37	284.85	360.89
Occlusion 25s	5	0.9913	-0.87	39	260.04	86.75
Occlusion 30s	1	0.9644	-0.71	40	224.34	33.54
Occlusion 30s	4	0.8604	-0.86	80	238.38	50.67
MEAN	2.75		-0.78			
STD	1.49		0.10			

Table 5 Pearson correlations, delay values, and delay correlations for experiment 11

Data Set	Delay for sensory/ch2 (samples)	Delay correlation	Motor and HR correlation	# Heart Beats	Mean HR	STD HR
Baseline	2	0.8962	-0.92	207	299.69	20.33
Baseline	2	0.8668	-0.80	183	290.94	8.48
Baseline	3	0.9073	-0.74	253	293.10	8.15
Baseline	5	0.8469	-0.73	144	290.73	8.28
Occlusion 20s	4	0.8402	-0.80	209	308.32	10.58
Occlusion 25s	1	0.9331	-0.86	164	307.039	13.56
Occlusion 30s	4	0.8557	-0.58	309	303.52	21.31
Occlusion 20s	2	0.9731	-0.64	68	304.71	10.18
Occlusion 25s	4	0.9018	-0.43	167	297.73	7.81
MEAN	3.00		-0.72			
STD	1.32		0.15			

Table 6 Pearson correlations, delay values, and delay correlations for experiment 13

Data Set	Delay for sensory/ch2 (samples)	Delay correlation	Motor and HR correlation	# Heart Beats	Mean HR	STD HR
Baseline	1	0.872	-0.56	54	217.41	8.11
Baseline	1	0.9106	-0.46	114	203.03	4.69
Occlusion 20s	1	0.8434	-0.66	68	207.83	5.27
Occlusion 20s	1	0.9192	-0.41	112	190.41	4.36
Occlusion 25s	1	0.7312	-0.26	135	203.90	5.49
Occlusion 60s	1	0.8714	-0.75	38	198.42	5.28
Occlusion 60s	2	0.8871	-0.83	117	196.88	5.31
Occlusion 60s	1	0.8612	-0.89	40	204.83	6.14
MEAN	1.13		-0.60			
STD	0.35		0.22			

Table 7 Pearson correlations, delay values, and delay correlations for experiment 14

Data Set	Delay for sensory/ch2 (samples)	Delay correlation	Motor and HR correlation	# Heart Beats	Mean HR	STD HR
Baseline	1	0.8635	-0.80	154	222.01	10.60
Baseline	2	0.8415	-0.70	101	219.37	8.14
Occlusion 20s	1	0.871	-0.81	267	252.15	41.84
Occlusion 20s	4	0.9413	-0.82	210	188.59	23.10
Occlusion 20s	4	0.9232	-0.66	65	198.44	7.64
Occlusion 30s	4	0.8963	-0.77	251	220.21	27.77
Occlusion 30s	4	0.8761	-0.91	237	205.57	16.03
Occlusion 30s	5	0.8717	-0.86	99	207.99	15.54
MEAN	3.13		-0.79			
STD	1.55		0.08			

The “Delay correlation” column refers to the correlation obtained between the proximal and distal neural signals at the given delay value shown in “Delay for sensory/ch2”. The delay with the highest correlation value was used to calculate the vagal motor activity for each set of data. Different delay values which had the highest correlation between the proximal and distal contacts were seen in different experiments as well as in different data sets of the same experiment. If different delay values were seen only in different experiments, one reason could be that slight variations in electrode separation in different electrodes used for each experiment caused the change in delay values. However, this does not explain separate delay values in the same experiment in which all recordings were taken with the same electrode. Also, the electrode used in experiment 13 was used again for experiment 14, and different delay values were seen between experiment 13 and 14.

So, something other than electrode variations had to be responsible for different delay values. Another possible reason for different delay values in the same experiment could be changes in neural activity. Slight changes in propagation velocity of neural

signals would change the delay value. In addition, if more neural traffic, either sensory or motor, were present in some recordings, the alignment of the proximal and distal signals as determined by the cross correlation method may have been affected by the extra neural traffic. The cross correlation method returns the delay value and the correlation between the proximal and distal neural signals at that delay value; if more neural traffic were present, the highest correlation between the two neural signals might have been slightly different than if less neural activity were involved in the correlation determination. Although different delay values were seen, all delay values which were used to determine motor activity were between one sample delay and five sample delays; with a sampling rate of 65,000 Samples/s, one sample delay corresponds to 15.385 μ s, and a five-sample delay corresponds to 76.923 μ s. So, the delay values, while not exactly the same throughout recordings, were not extremely different.

The delay values used to determine motor activity in experiment 13 were remarkably steady throughout the experiment as compared to the other experiments. With the exception of one file, all delay values used to determine motor activity for experiment 13 were one sample delay. Experiment 13 was performed in the same manner as the other experiments; therefore, there is no apparent reason as to why the delay values for this particular experiment were steady.

Figure 28 shows the correlation values which were obtained between baseline instantaneous heart rate and baseline vagal motor activity. The information in this plot is also presented in Tables 4-7; however, this plot allows for correlation values from baseline recordings across experiments to be shown together. The baseline correlation values in Figure 28 are all close except for experiment 13; this is most likely due to poor

connection between the electrode contacts and the nerve. The poor connection was not noticed until later in the experiment, at which time the electrode was repositioned and a note made in the surgical records. However, for the files recorded after the repositioning of the electrode, the correlation values were higher, as expected from previous experiments. Therefore, the lower correlation values in some files of experiment 13 were most likely due to poor connection between the electrode contacts and the nerve.

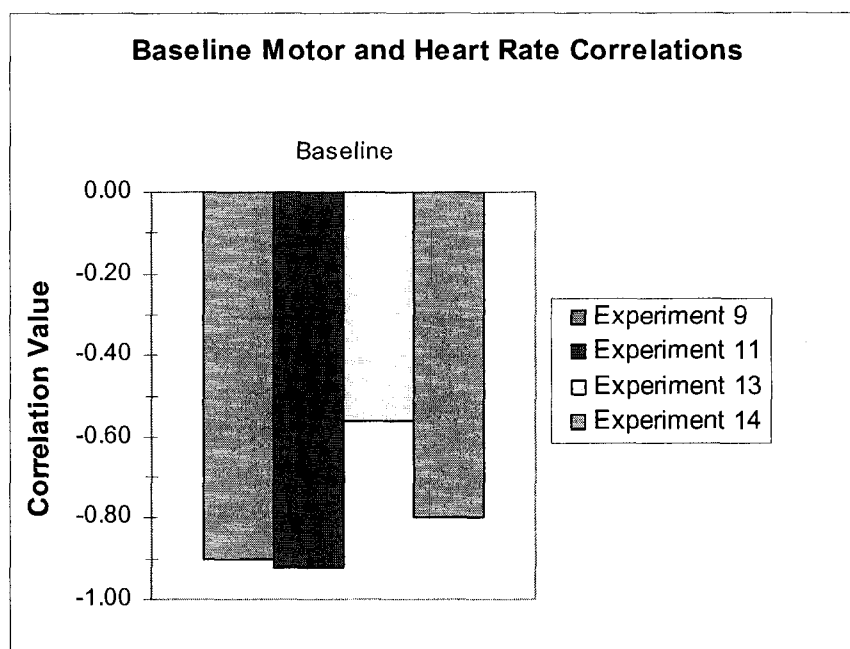


Figure 28 Baseline correlation values obtained between right vagus nerve motor activity and instantaneous heart rate

Figures 29-32 show scatter plots of integrated vagal motor activity versus instantaneous heart rate; scatter plots are useful to analyze how one variable affects another. From the scatter plots, a linear relationship between integrated vagal motor activity and instantaneous heart rate is suggested. These scatter plots include data from different experiments and include baseline and occlusion recordings as noted in the figure

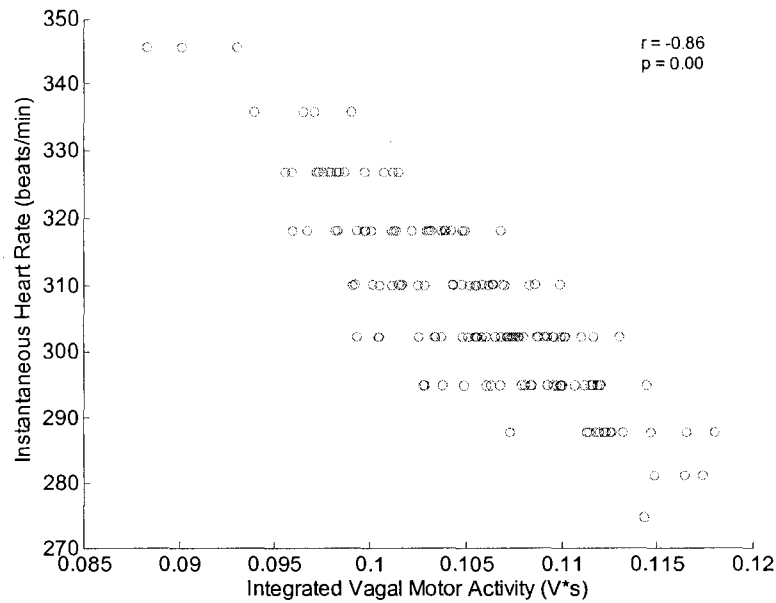


Figure 32 Scatter plot of integrated right vagus motor activity and instantaneous heart rate from an occlusion recording in experiment 11

4.2.1 Transfer Function Model of Heart Rate Based on Motor Area

After successfully establishing a consistent, high, inverse correlation between the vagal motor area and heart rate during the non-differential recordings, a transfer function model was designed to determine the relationship between vagal motor area and heart rate using time series analysis. For the model to be a better representation of the overall relationship between vagal motor area and heart rate, a model that incorporated different experiments was developed; two sets of data from each non-differential experiment that contained 80 consecutive heart beats were used. A baseline recording and an occlusion recording were selected from each experiment to incorporate different types of recordings. Eighty consecutive heart beats were selected to give a typical length of data

from which to design a model; with a average heart rate of 4 beats/s for the animal, eighty consecutive heart beats corresponds to approximately 20s.

One key requirement of time series analysis is that the time interval between points be constant. This constant time interval was not the case of the eighty data points of heart rate and area selected to design the model; the changing time interval is due to changing heart rate. As the heart rate increased, the time interval between beats would be shorter while the time interval between beats would be longer as heart rate decreased. Since the time interval was not constant between these selected data points, the data could not be used to design a time series model.

In order for these selected points to be used to design a time series model, the time interval between the points had to be constant. To make the time interval between the points constant, each series of eighty heart beats and eighty area points was transformed into the length of the original signal. Figure 33 shows one plot of the eighty selected heart rate and area data points. Figure 34 shows the plot of the eighty selected heart rate and area data points that have been changed into a continuous form; i.e., the sample value of the first selected heart rate is sample one in the continuous form, and the sample value of the last selected heart rate is the last sample value in the continuous form. Once the data was transformed into constant time interval data, the design of the model continued.

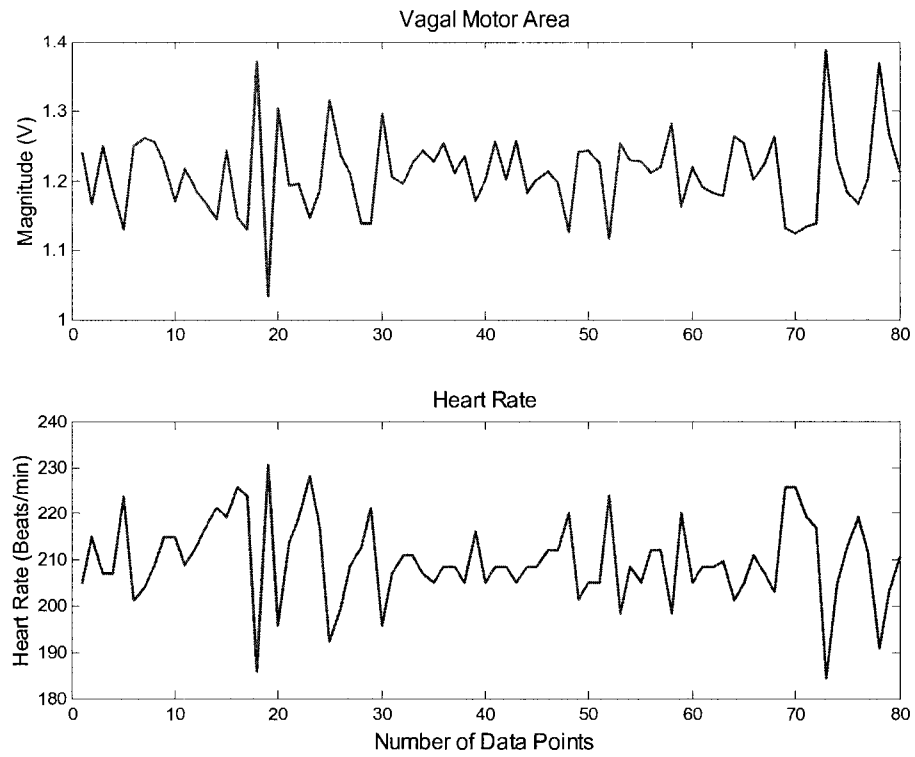


Figure 33 Non-continuous integrated motor activity (top) and instantaneous heart rate (bottom)

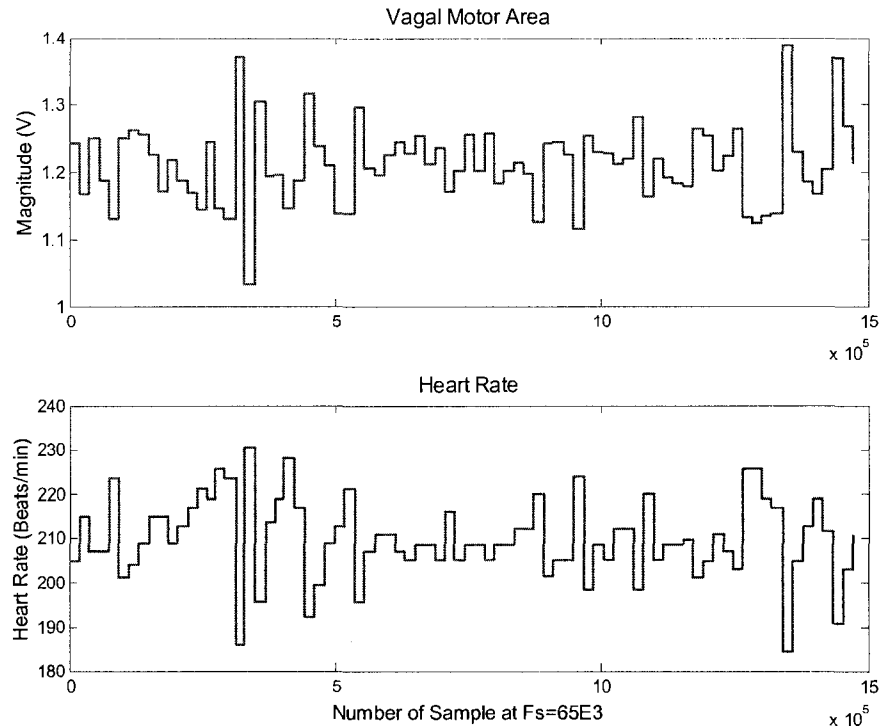


Figure 34 Continuous, integrated right vagus motor activity (top) and continuous, instantaneous heart rate (bottom)

After each series chosen from the non-differential recordings was transformed into a constant time interval series, each set of series (heart rate and area) was averaged across experiments to form one series of heart rate and one series of area. Averaging across experiments was performed to acquire a better representation of each signal, heart rate and area, so that the model would not be influenced too strongly by one experiment versus another. One hundred one points at equal intervals were selected from the averaged data to be used to design the transfer function model.

The averaged data was plotted and examined for stationarity, trends, and seasonality. From the plots, both series were determined to be stationary in the mean (little change over time) so that differencing was not required. No trends or seasonality

were seen in the plots. Figure 35 displays the plots of area and heart rate that were examined.

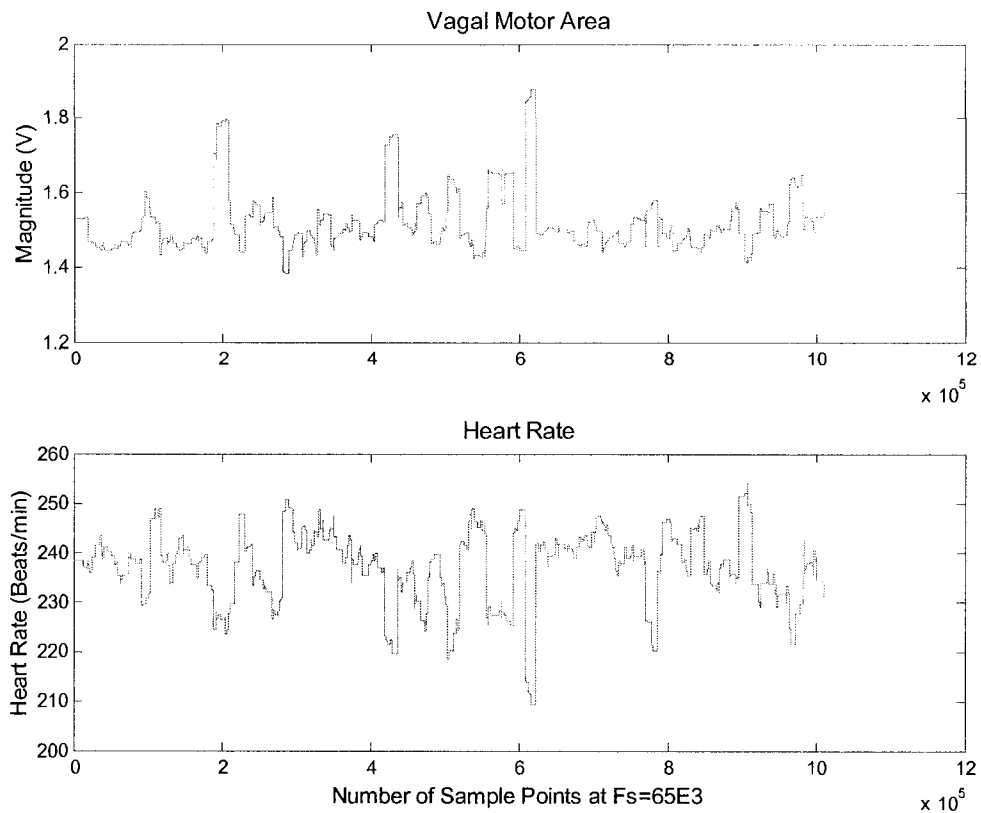


Figure 35 Averaged, continuous, integrated right vagus motor activity (top) and averaged, instantaneous heart rate (bottom)

After examination of the heart rate and area data was completed, time series analysis was used to develop a transfer function of form

$$y_t = v(B)x_t + n_t \quad \text{Equation 1}$$

where y_t is the output series, x_t is the input series, $v(B)$ is the transfer function, and n_t is the noise series that is independent of the input series x_t [57]. The first step in identification of a transfer function model was to pre-whiten the input series, that is, to

develop a model for the input series using SAS. Examination of the AutoCorrelation Function (ACF) and the Partial AutoCorrelation Function (PACF) plots for the input series, area, indicated that the series can be modeled as a first order Moving Average process, (MA(1)). Figure 36 shows the output of the ACF and PACF for the input series, area. The ACF (see section 3.2.4) of the input series became insignificant (“cuts off”) after lag 1 on the ACF plot, i.e. the value was less than two standard errors which mark the 95% confidence interval in the SAS program, and the PACF decayed (“tailed off”) with alternating spikes indicating that the MA(1) parameter θ_1 was less than zero. An autocorrelation check for white noise was performed on the input series; the results of this check strongly rejected the hypothesis that the input series was white noise with $p = 0.0011$ for the first six autocorrelations and $p = 0.0006$ for the next six autocorrelations. The typical form of a MA(1) process is shown in Equations 2 and 3 where a_t is a zero mean white noise process with constant variance, θ_1 is the first order moving average parameter, B is the backshift operator (see section 3.2.4), t is sample time, and μ is the mean of the Z_t .

$$\dot{Z}_t = Z_t - \mu \quad \text{Equation 2}$$

$$\dot{Z}_t = a_t - \theta_1 a_{t-1} = (1 - \theta_1 B)a_t \quad \text{Equation 3}$$

Name of Variable = AREAL																									
Mean of Working Series		1.522581																							
Standard Deviation		0.084701																							
Number of Observations		101																							
Autocorrelations																									
Lag	Covariance	Correlation	-1	9	8	7	6	5	4	3	2	1	0	1	2	3	4	5	6	7	8	9	1		
0	0.0071742	1.00000]]	
1	0.0030587	0.42635]]
2	-0.0000828	-.01154]]
3	0.00028889	0.04027]]
4	0.00054393	0.07582]]
5	0.0010612	0.14792]]
6	-0.0002754	-.03839]]
7	-0.0015990	-.22288]]
8	-0.0004241	-.05912]]
9	-0.0000120	-.00168]]
10	-0.0001967	-.02742]]
11	-0.0005479	-.07637]]
12	-0.0015599	-.21743]]
13	-0.0006780	-.09451]]
14	0.00073566	0.10254]]
15	0.00019675	0.02742]]

"." marks two standard errors

Partial Autocorrelations																								
Lag	Correlation	-1	9	8	7	6	5	4	3	2	1	0	1	2	3	4	5	6	7	8	9	1		
1	0.42635]]
2	-0.23626]]
3	0.19038]]
4	-0.04334]]
5	0.18707]]
6	-0.26295]]
7	-0.05269]]
8	0.05771]]
9	-0.07317]]
10	0.02965]]
11	-0.08637]]
12	-0.13230]]
13	0.05352]]
14	0.07589]]
15	-0.04748]]

Figure 36 The ACF and PACF plots produced by SAS to identify the input variable, area.

Since the ACF and PACF of the input series indicated a MA(1), a MA(1) was estimated for the input series. The moving average parameter and the mean of the series were determined by conditional least squares estimation to be significant with t values of -8.86 and 127.26, respectively. After estimating a MA(1), an autocorrelation check of the

residuals, ACF plot of the residuals, and PACF plot of the residuals was examined to determine if the estimated MA(1) model was adequate. The autocorrelation check of the residuals showed that the model was adequate and that the residuals were not significant at $\alpha = 0.05$. In addition to the autocorrelation check, the ACF and PACF plots of the residuals also indicated that the MA(1) model of the input series was adequate because there was no pattern in the ACF or PACF plots. Figure 37 shows the ACF and PACF plot of the residuals of the estimated MA(1) process; the ACF and PACF are not significant within two standard errors. There is an ACF and PACF value at lag 7 that is slightly larger than two standard errors. But, because there is only one significant value, because the value is not highly significant in either plot, and because all other parameters of model adequacy indicate that the model is adequate, the estimated MA(1) model was determined to be appropriate. The estimated MA(1) model is shown below where 1.5226 is the estimated mean, and -0.66595 is the value of θ_1 . B is the backshift operator where $B^j x_t = x_{t-j}$ (see section 3.2.4), and a_t is a zero mean white noise process. The value of θ_1 is negative as indicated during the identification stage by the alternating positive and negative values of the PACF of the input series, area.

$$Area_t = 1.5226 + (1 - (-0.66595B))a_t \quad \text{Equation 4}$$

$$Area_t = 1.5226 + (1 + 0.66595B)a_t \quad \text{Equation 5}$$

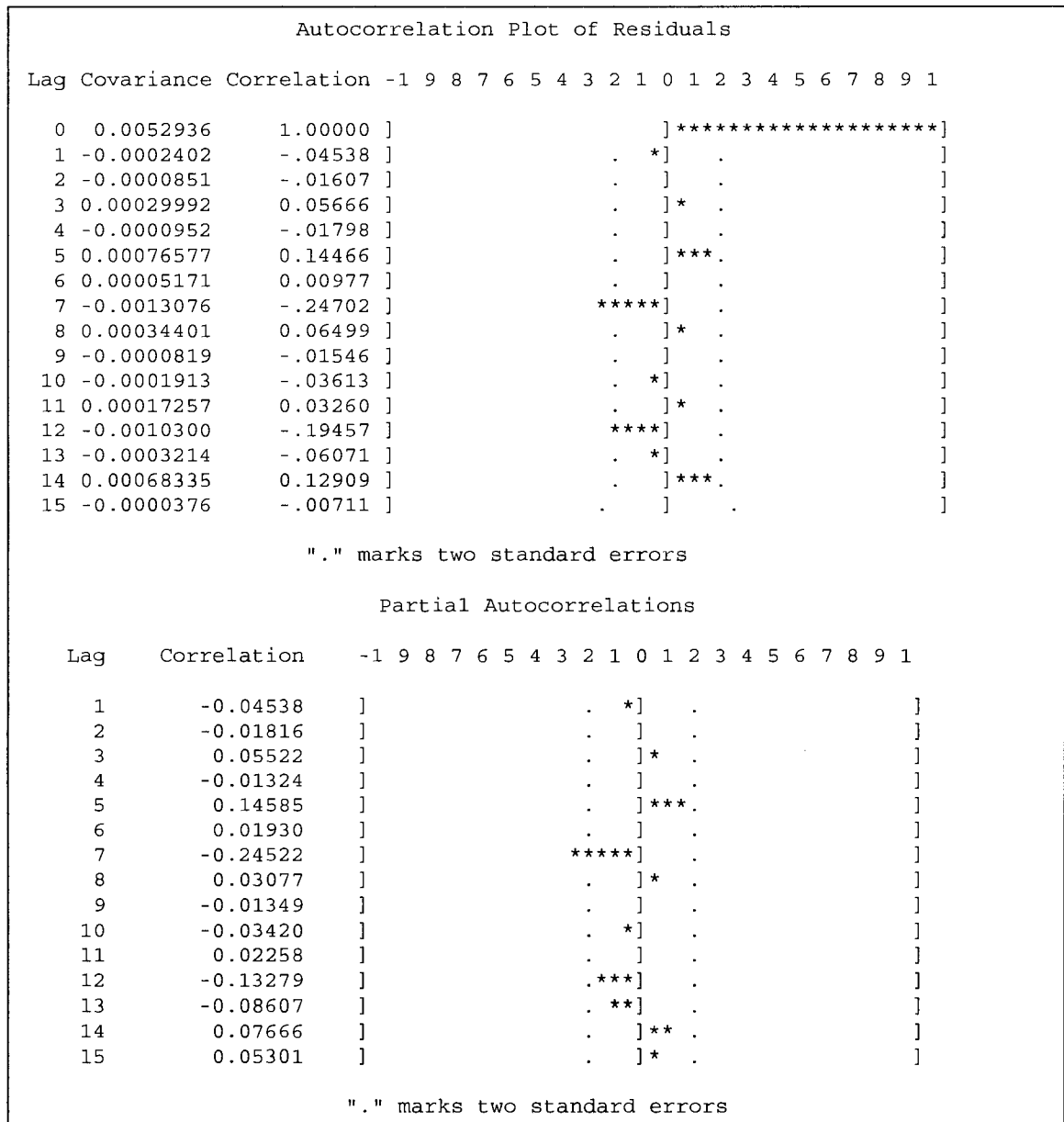


Figure 37 ACF and PACF plots of the residuals after estimating a MA(1) model for the input series, area

The number of lags, fifteen, was chosen to keep the bias of the autocovariance function small; generally, for a given number of observations, n , the number of lags, k , is chosen such that $k \leq (n / 4)$ to keep the bias small [57]. Since the number of observations

used to design the model was ninety-one, the number of lags should be equal to or less than twenty-two; fifteen lags falls within the range of the number of allowable lags.

After pre-whitening the input series, identification of the impulse response function and transfer function commenced. SAS was used to first transform the output series, heart rate, with the pre-whitening model developed for the input series, area; then, SAS was used to cross correlate the transformed input series, area, with the transformed output series, heart rate. A cross correlation plot was produced from this procedure; Figure 38 shows the cross correlation obtained. The cross correlation plot shows a high peak at lag zero with all the other lag correlation being insignificant; this indicates that the location of the weighting variable is at lag zero. This cross correlation pattern was compared to typical impulse response functions presented in [57]. Figure 39 shows several typical impulse response patterns which were used to identify the form of the transfer function for this data. From the comparison, a transfer function of the form in Equation 6 was determined to be the closest fit to the cross correlation pattern obtained. In Equation 6, ω_0 is the numerator term of the rational transfer function $\nu(B)$, and x_t is the input series with t indicating time.

$$\nu(B)x_t = \omega_0 x_{t-2}$$

Equation 6

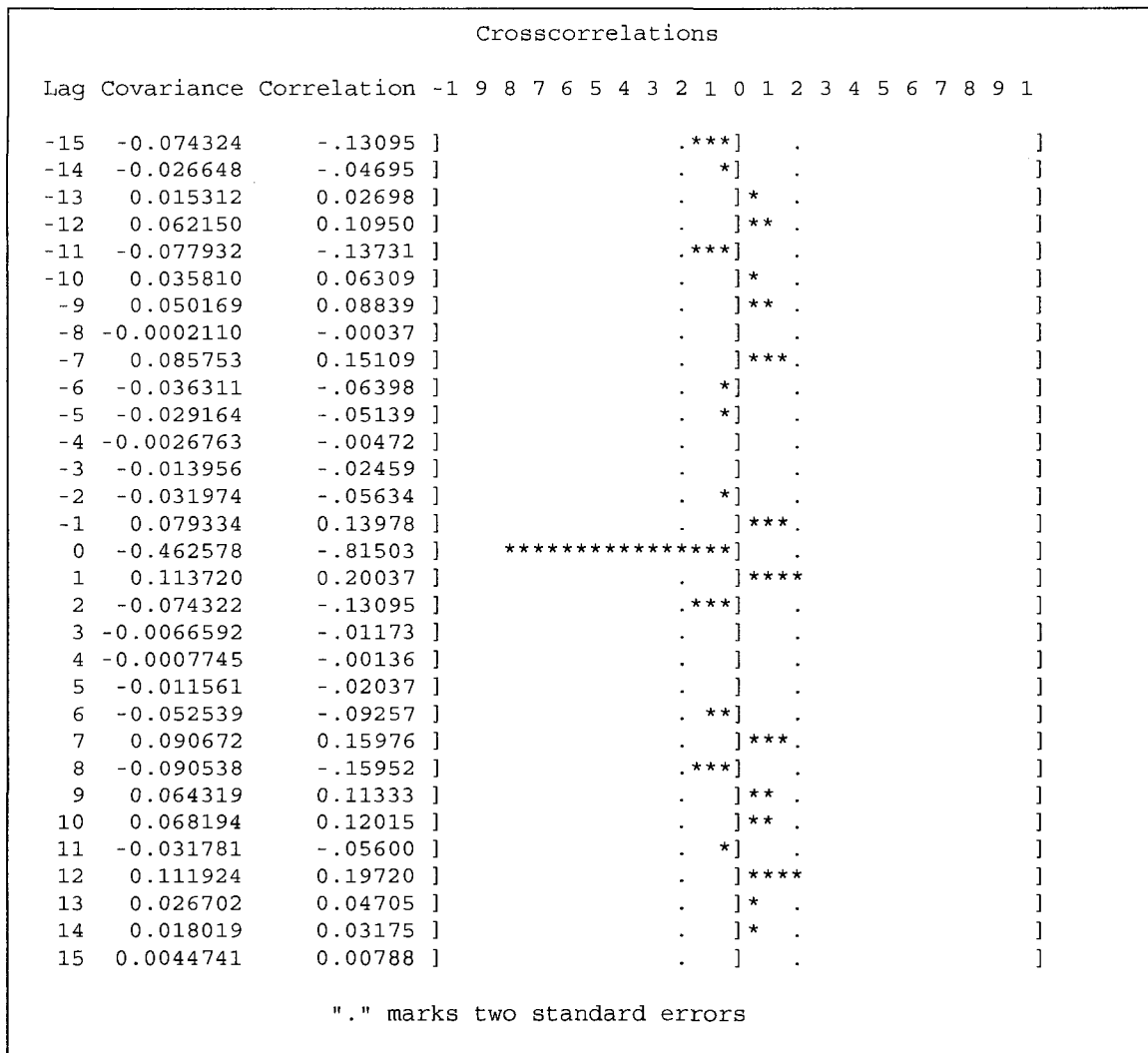


Figure 38 Cross correlation plot produced by cross correlating the MA(1) model for area with the output, heart rate

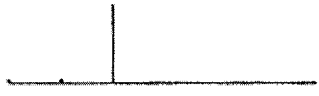
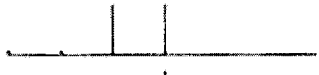
(b, r, s)	Transfer function	Typical impulse weights
$(2, 0, 0)$	$\nu(B)x_t = \omega_0 x_{t-2}$	
$(2, 0, 1)$	$\nu(B)x_t = (\omega_0 - \omega_1 B)x_{t-2}$	
$(2, 0, 2)$	$\nu(B)x_t = (\omega_0 - \omega_1 B - \omega_2 B^2)x_{t-2}$	

Figure 39 Transfer function impulse plots [57].

This transfer function form was determined to be the best fit because the cross correlation pattern contained a finite number of impulse response weights (one) and because the impulse response weight was on only one side of the zero axis. From the information on the cross correlation pattern, the transfer function form was altered to fit the specific conditions of this situation. The transfer function form specifically altered for this problem was determined to contain only one impulse weight, ω_0 , at lag zero; this is represented by the Equation 7. In Equation 7, ω_0 is the numerator term of the rational transfer function $\nu(B)$, and x_t is the input series with t indicating time

$$\nu(B)x_t = \omega_0 x_t \quad \text{Equation 7}$$

The only significant correlation was at lag zero; therefore the only impulse weight was at lag zero. Since there was only one impulse response weight at lag zero, the right hand side of the typical form transfer function was altered to read $\omega_0 x_t$ (meaning that the weight is at lag zero) instead of $\omega_0 x_{t-2}$ which denotes an impulse response weight at the second lag.

In addition to the cross correlation plot, SAS returned a cross correlation check between series. This check is counter to the hypothesis that there is not a cross correlation between series; this hypothesis was strongly rejected ($p < 0.0001$) indicating that there was indeed a cross correlation between series. A cross correlation between series is useful because the cross correlation function measures the strength and direction (based on positive and negative lags) of the relationship between the input and output series [57].

After determining a possible form for the transfer function for this model of heart rate based on vagal motor area, the transfer function chosen was estimated using SAS.

An autocorrelation of white noise check indicated that the residuals were not white noise and that the model was not adequate. Therefore, the ACF and PACF plot of residuals was examined to identify the noise model; Figure 40 displays these plots. The ACF plot of the residuals tailed off while the PACF plot of the residuals cut off after lag two; this pattern indicated a second order AutoRegressive process, AR(2). The typical form of an AR(2) process is shown in Equations 8 and 9 where a_t is a zero mean white noise process, ϕ_1 is the first order parameter, and ϕ_2 is the second order parameter.

$$(1 - \phi_1 B - \phi_2 B^2) \dot{Z}_t = a_t \quad \text{Equation 8}$$

or

$$\dot{Z}_t = \phi_1 \dot{Z}_{t-1} + \phi_2 \dot{Z}_{t-2} + a_t \quad \text{Equation 9}$$

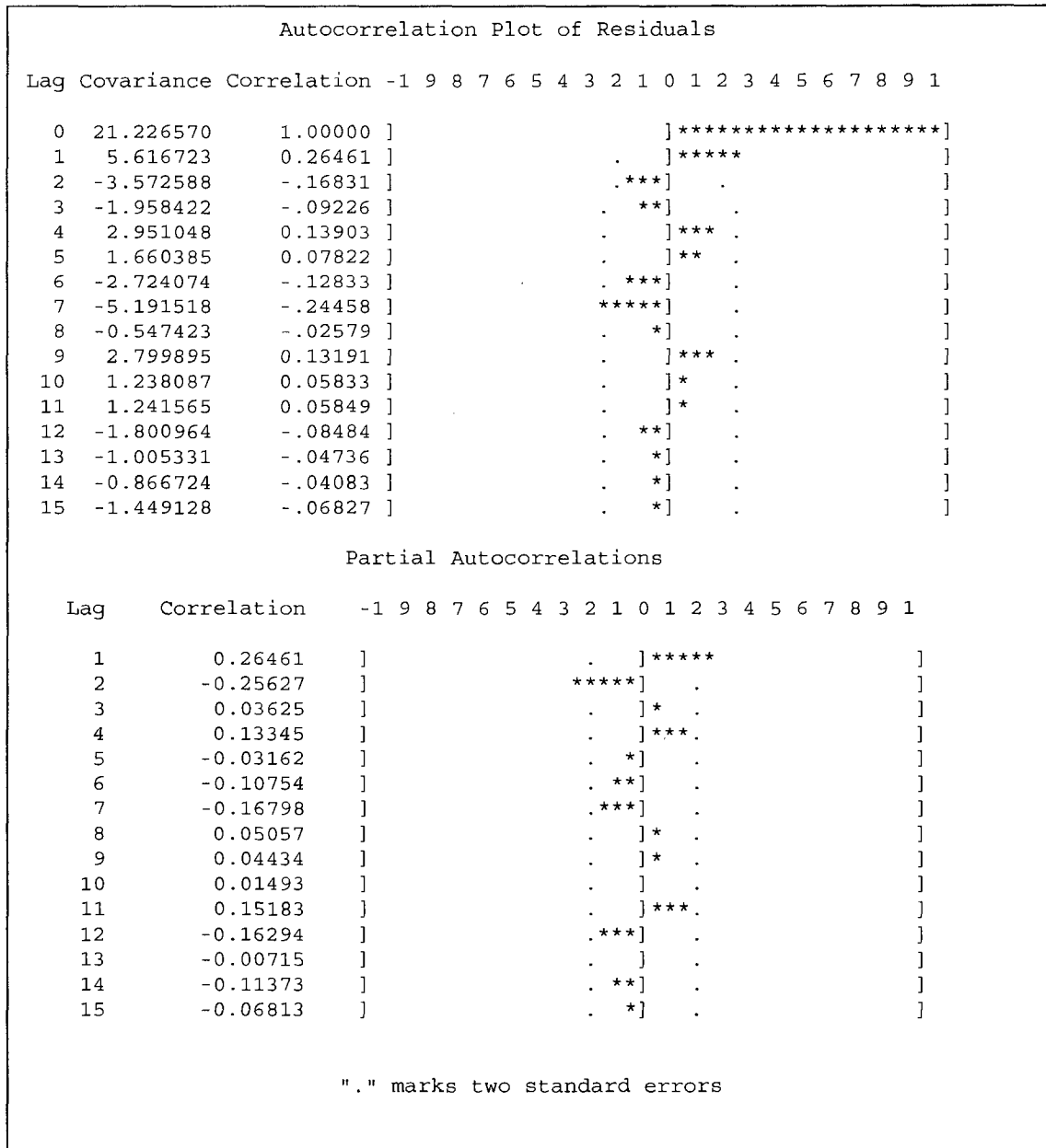


Figure 40 ACF and PACF plot of the residuals after applying the transfer function model

Since the ACF and PACF plots of the residuals indicated an AR(2), an AR(2) model was added to the transfer function model to account for the inadequacies in the transfer function model alone. The AR(2) model estimated using SAS is given below in Equation 10 and 11 where 355.9442 is the mean of the heart rate, $\phi_1=0.40129$, and $\phi_2=-$

0.30897. B is the backshift operator where $B^j x_t = x_{t-j}$, and a_t is a zero mean white noise process. Equation 11 represents another form of Equation 10 where

$\dot{HR} = HeartRate - \mu$; μ is the mean of the heart rate.

$$HeartRate = 355.9442 + \frac{1}{1 - 0.40129B + 0.30897B^2} a_t \quad \text{Equation 10}$$

or

$$\dot{HR} - \phi_1 \dot{HR}_{t-1} + \phi_2 \dot{HR}_{t-2} = a_t \quad \text{Equation 11}$$

After adding the AR(2) model to the transfer function model, the final model becomes Equation 12.

$$HeartRate = \omega_0 x_t + 355.9442 + \frac{1}{1 - \phi_1 B + \phi_2 B^2} a_t \quad \text{Equation 12}$$

When all the parameter values in the final model are added, the final model becomes Equation 13 or 14.

$$HeartRate = -78.2341area_t + 355.9442 + \frac{1}{1 - 0.40129B + 0.30897B^2} a_t \quad \text{Equation 13}$$

or

$$\dot{HR} - \phi_1 \dot{HR}_{t-1} + \phi_2 \dot{HR}_{t-2} = -78.2341area_t + a_t \quad \text{Equation 14}$$

Conditional least squares method was used to estimate the values of all the parameters in the final model. All parameters, the mean of heart rate, ϕ_1 , ϕ_2 , and ω_0 were determined to be significant at $\alpha = 0.05$. An autocorrelation check of residuals of

the final model revealed that the residuals were white noise and that the model was adequate. In addition to the autocorrelation check of residuals, the ACF and PACF plots of the residuals were examined to determine if any were significant. The ACF and PACF plots shown in Figure 41 indicate that the final model is adequate because all the ACF and PACF correlations are not significant. Finally, a cross correlation check of the residuals with the input series, area, was performed; the residuals were proven to be white noise and not correlated with the input series. After all these checks were performed, the final model heart rate based on vagal motor area was considered to be adequate. For more details on the SAS model, see Appendix D.

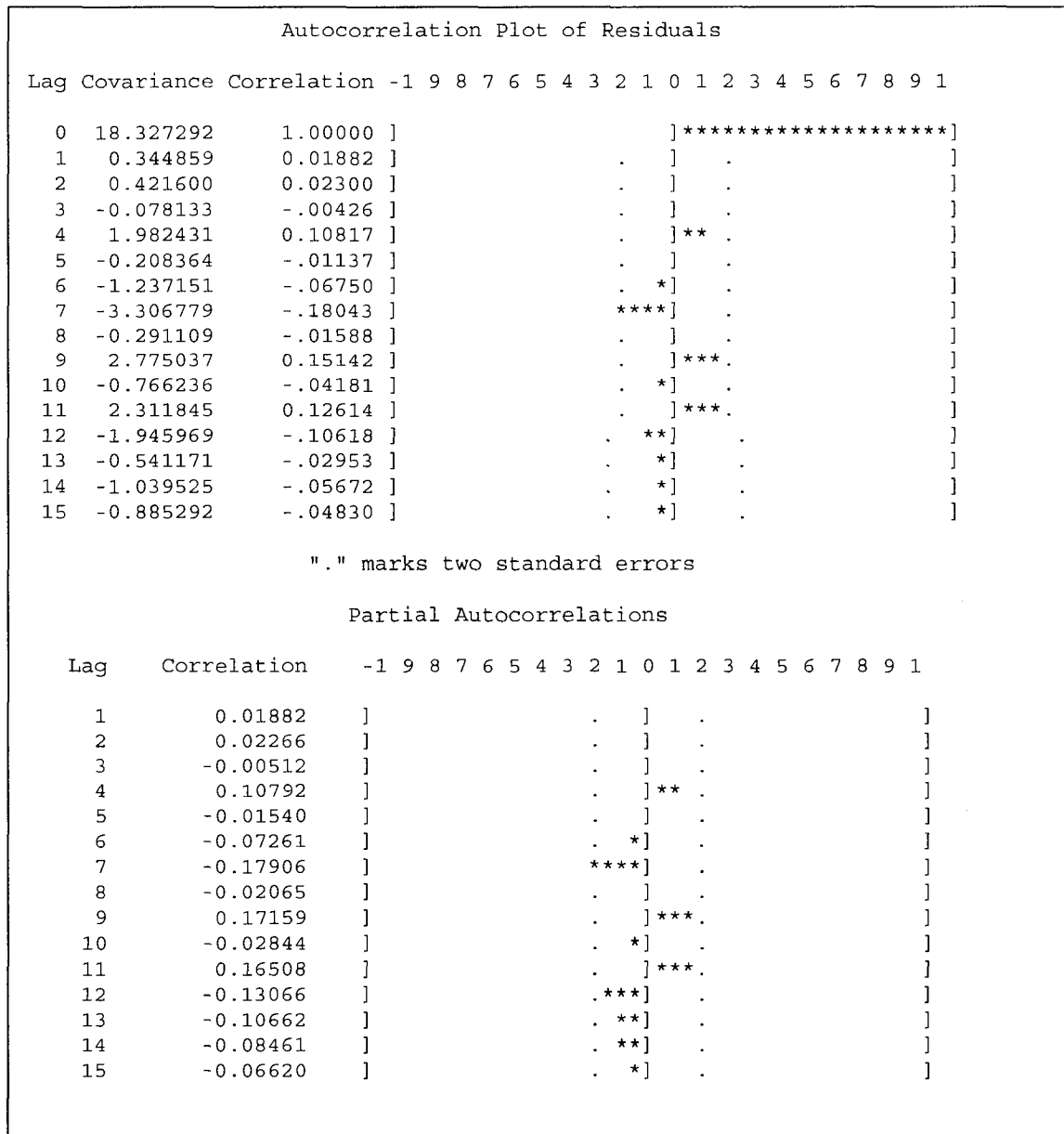


Figure 41 ACF and PACF plot of the residuals after the AR(2) model was added to the transfer function model

To validate the final model, the final model was used to forecast ten heart rate values, whose actual values were already known, based on only the input vagal motor area. SAS was used to perform the forecasting. The final model successfully predicted all ten heart rate values within a 95% confidence interval. Figure 42 shows the plot of actual and forecasted values along with upper and lower lines indicating a 95%

confidence interval. Table 8 shows the exact values of the actual heart rate, forecasted heart rate, and upper and lower 95% confidence interval.

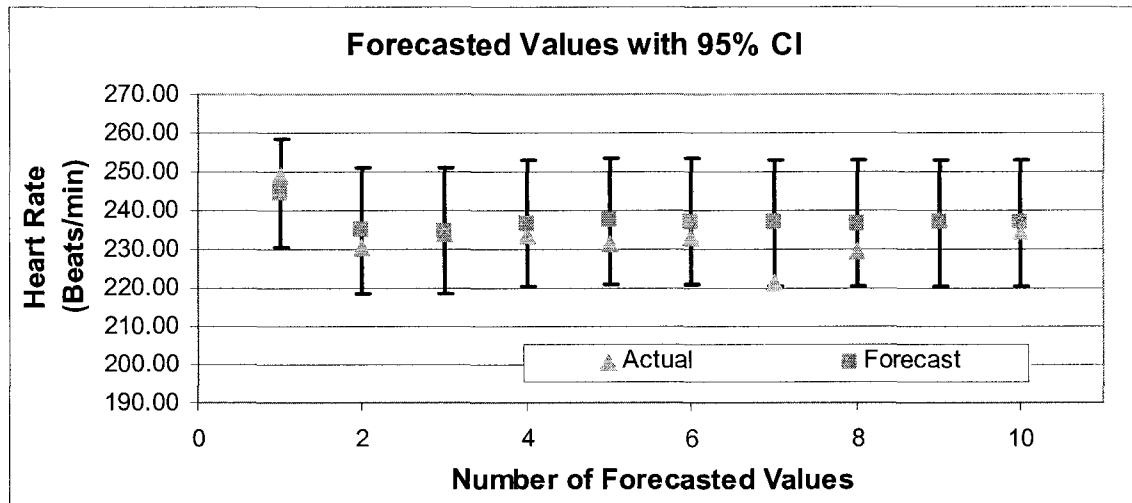


Figure 42 Actual heart rate values and forecasted values produced by the time series model with 95% confidence intervals marked

Table 8 Forecasted heart rate values, actual heart rate values, and the 95% confidence limits for forecasted values

Actual	Forecast	95% CL	
248.96	244.65	230.69	258.61
230.29	234.84	218.67	251.01
233.89	234.73	218.51	250.94
233.43	236.60	220.31	252.89
231.34	237.38	221.09	253.67
233.14	237.12	220.83	253.42
221.42	236.77	220.48	253.07
229.49	236.71	220.42	253.01
237.74	236.80	220.50	253.09
234.43	236.85	220.55	253.15

Forecasting was the last tool used to test the adequacy of the final model developed using time series analysis. While all the tests indicated that the final model was adequate, forecasting proved that the model could accurately predict the heart rate

with only the vagal motor area as an input. Also, the final model developed was a model with zero lags; this indicates that no previous information is needed to predict heart rate. However, to make the model more accurate, the AR(2) model of the residuals that was added to the transfer function model does require the heart rate information from two previous heart beats. So, while the heart rate can be predicted on a beat to beat basis given the vagal motor activity immediately preceding the R wave of that heart beat, the heart rate is more accurately predicted if the two previous heart beats are known.

CHAPTER 5

CONCLUSIONS/FUTURE WORK

Whole vagus nerve recordings at the carotid artery level can be obtained by using silicone cuff electrodes. If the proximal and distal contact leads of a two contact electrode are both used as inputs to an amplifier, a differential recording is achieved. Simultaneously recording of whole nerve signals and EKG allows for a Pearson correlation to be performed between integrated neural activity and instantaneous heart rate. When the neural signal acquired from a distal recording is integrated between successive R waves of the simultaneously recorded EKG (based on the sample index of each R wave), an array of integrated neural activity is obtained equal to the length of the instantaneous heart rate array. When a Pearson correlation is calculated between the integrated neural activity array and instantaneous heart array, inconsistent Pearson correlations are returned across experiments. These inconsistent correlations indicate that a better method is required to analyze the relationship between neural activity and instantaneous heart rate.

If each contact of a two contact electrode is recorded with respect to ground (a non-differential set up), two neural signals can be recorded: one from the proximal contact and one from the distal contact. From these two signals, the neural motor signal can be extracted using a cross correlation technique introduced by Heetderks [55]. The neural motor signal can be integrated as in the differential recordings between successive

R waves to produce an array of integrated, motor activity which is equal in length to the instantaneous heart rate array. Consistent, high, inverse correlations are returned when a Pearson correlation is calculated between integrated, motor activity and instantaneous heart rate. These consistent correlations suggest a relationship exists between integrated, motor activity and instantaneous heart rate.

To quantify the relationship between integrated, motor activity and instantaneous heart rate, a transfer function model was developed using time series analysis methods. The transfer function model is theoretically adequate based on diagnostic checking and residual analysis. In addition to being theoretically adequate, the transfer function model is considered practically adequate because the actual heart rate values were within the 95% confidence interval of the forecasted values calculated by the transfer function model.

The final model is useful because it not only accurately predicts heart rate but also predicts heart rate on a beat to beat basis when given the integrated motor activity. In addition to providing beat-to-beat updates, this model provides closed loop control because the heart rate predicted by the model adjusts based on integrated neural activity.

For future research endeavors, additional acute and chronic experiments should be performed to validate the transfer function designed here or to determine how different the transfer function varies with different subjects. Also, recording data where the change in heart rate is greater than that seen here in the data used to develop the transfer function model (~ 40 beats/min) would be useful in determining if the relationship between integrated, motor activity and instantaneous heart rate is linear across a larger range. Finally, to further improve signal quality in the non-differential experiments, a tri-

polar electrode could be used. This would allow for two differential signals to be obtained from the whole nerve; the differential signals would provide better signal to noise ratio and possibly increase correlation value due to less noise.

APPENDIX A

ANIMAL CARE AND USE FORM

Mesut Sahin
Louisiana Tech University
College of Engineering and Science
Campus Box # 10

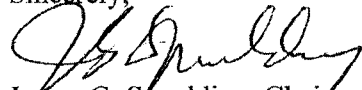
Dear Dr. Sahin,

An expedited review by the Louisiana Tech University's Institutional Animal Care and Use Committee (IACUC) has been carried out on your proposed experimental protocol entitled:

Extraction of the Neural Control Information for the Whole Heart from the ANS.

I have approved the protocol as the designated reviewer in consultation with Dr. Green the veterinarian on the IACUC. The proposed procedures were found to provide reasonable and adequate safeguards for the comfort of the animals and the safety of the researchers. Failure to follow the protocol as approved may result in the termination of research. The full IACUC will confirm the approval by a pole vote that is currently being conducted. You will receive written notification if the full committee requests modification or does not approve. If you have any questions please call me at 257-4573 or via e-mail at jgspauld@latech.edu.

Sincerely,



James G. Spaulding, Chair
Louisiana Tech University IACUC

ANIMAL USE INFORMATION

In order to use vertebrate animals in research or instruction at Louisiana Tech University, you must have the approval of the Institutional Animal Care and Use Committee. Please complete this questionnaire. If the animals are to be housed in the Animal Care Facility, please review your needs with the Facility Director, Dr. James Spaulding, in order to schedule facility use and to prepare a budget. After obtaining the signature of the Facility Director, send the form to Dr. Les Guice, Vice President for Research and Development. If you will not be housing animals, send the form directly to Dr. Guice. He will convene a meeting of the IACUC. Your proposal will be reviewed. You will receive notice of approval or recommendations for changes required for approval.

Project Title _____ **Proposal Number**

Project Director _____

Telephone _____

Email _____ **Performance Period**

Granting Agency _____ **Date Due**

- I. Information for the Animal Care Committee**
 - A. Description of the proposed experiment or laboratory exercise. Attach relevant pages from grant proposal or laboratory exercise. Include literature review and citations:**

 - B. Statement supporting the need to use animals in the proposed research or laboratory exercise:**

 - C. Brief description of the methods used on the animals. Include specific steps taken to minimize pain and suffering.**

D. Does the research require surgery? yes no
If yes, what anesthetic will be used, in what dosage? If this is not the anesthetic used normally, justify its use.

E. Will animals be killed at the conclusion of the research? yes no
If yes, describe the method of euthanasia to be used?

If no, what will be done with the animals?

F. Are pathogens or hazardous substances associated with this research?
yes no
If yes, explain precautions to be taken to prevent spreading to other animals and personnel.

If no university animal care facilities are required, skip to section IV. If animals are to be housed at Louisiana Tech, you must meet with the Animal Facility Director, Dr. James Spaulding (318-257-4573), to complete sections II and III.

II. Animals and Facilities Required:

A. Species and strain required: _____

B. Commercial supplier: _____

C. Number of animals required and length of time in facility:

1. Initial number _____ ; Age/Size: Initial _____ ; Maximum _____

2. Type of housing required: _____

3. Maximum number of animals in the facility at any time: _____

4. Date of initiation is _____ ; Date of termination is _____

PLEASE NOTE! If the above dates change, please notify the Facility

Director. Every effort will be made to schedule your changes. The sooner you request a schedule modification, the more likely it can be accommodated.

D. Date of Grant Notification or date when funds will be committed: _____

E. Special requirements: If any of the following apply, please explain in the space provided.

1. Veterinary care

2. Work or storage space

3. Surgical space

4. Access to the facility other than weekdays 8am-5pm.

5. Do you want the facility personnel to perform any procedure other than feeding, watering, and cleaning the cages of your animals? If so, please describe the procedure in detail and estimate the number of hours per day required. You may attach an additional sheet.

III. Costs: To complete this section you must meet with the Animal Facility Director (318-257-4573)

A. Total number of animals to be housed _____

B. Number of days each animal will be housed _____

C. Number of Animal Days (A X B) _____

D. Cost for 1 animal/day _____ X animal days _____

E. List Special Services Requested of facility personnel:

Cost/hour _____ X Hours needed _____ = _____

**F. Cost of Animals (if supplied by Tech, see cost sheet)
Species, Sex, and Age of Animals**

Cost per animal(see cost sheet) _____ X number needed _____ = _____

G. Special supplies (list with price)

Total cost of special supplies = _____

H. Special equipment needed (list)

Total cost of special equipment = _____

I. Total to be paid Animal Facilities Account = _____

Enter the above costs in the appropriate section of your grant proposal or indicate the source of your funds.

IV. Information on personnel working directly with the animals.

	Name	Where trained	Tetanus	Immunization Date
1.				
2.				
3.				
4.				
5.				

Do you require any Special Immunizations needed for this project? yes no
If yes, please list:

If you or your personnel have not received training, you may need to make arrangements to complete the program before beginning the project.

Principal Investigator: _____

Print or type

Signature

Date

Facilities Director: _____

(James G. Spaulding)

Date

IACUC Committee Chairman: _____

Date

V. Per Diem Rates for Animals Housed in the Animal Facilities at Louisiana Tech University

<u>Animal</u>	<u>Code</u>	<u>Housing</u>	<u>Daily Rate</u>
Rat	RW	Wire Bottom Cages	0.20 ea
	RWB	Wire with Bedding	0.25 ea
	RS	Shoebox with Bedding	0.20 ea
	RSH	Special Handling	0.30 ea min
Mouse	MS	1/shoebox w/bedding	0.15 ea
	MB	per Box (2-5 per box)	0.30 ea

Unit cost for animals from University Breeding Colonies

Weanling Rats	WR	\$2.00 ea
250g females	FR250	10.00 ea
250g male	MR250	8.00 ea
Weanling Mice	WM	1.00 ea
20g (45 days)	M20	1.50 ea

APPENDIX B

NEUROCAL SIMULATION TO ILLUSTRATE CROSS CORRELATION TECHNIQUE

The Neurocal simulation performed is a simplified model to demonstrate the reasoning behind the methods used to determine motor activity in the vagus nerve. The vagus nerve is a mixed nerve containing both sensory and motor components. Although the vagus nerve consists of many sensory and motor components, in order to design a simplified model, only two axons were used: one to carry information to the CNS (sensory) and one to carry information from the CNS (motor).

For the simulation, each potential generated in each axon was examined in 0.1 ms fixed steps for 10 ms. Two recording electrodes were placed between the origin of the sensory potential and the origin of the motor potential. The sensory potential originated at 0 and the motor potential originated at 1; there were 60 segments between 0 and 1. The distal recording electrode was placed at segment 30 while the proximal recording electrode was placed at segment 32.

Each electrode, proximal and distal, recorded a voltage at a set time; therefore, for each electrode there was voltage readings at set times. These voltage readings represented compound action potentials (CAP) which consist of motor and sensory potentials passing by the recording electrode. In reality, there are numerous motor and sensory fibers in the vagus nerve which are simultaneously active. However, for simplicity, only two simultaneously active potentials, one motor and one sensory, were used for this simulation.

Plots produced by the simulation showed the propagation of the potential down the axon, but only the forward propagation was shown and not the repolarization of the axon. For this simulation, the sensory potential started 200 μ s before the motor signal. Voltage readings at segments 30 (distal electrode) and 32 (proximal electrode) were taken from 0 to 2.1 ms in 0.1 ms steps. From these values, the CAP was calculated being the average of the

two axons; this produced a CAP for the distal and proximal electrode. The CAP at each electrode was representative of the experimental signal obtained, a combination of multiple signals.

In this study, the motor activity and heart rate are to be correlated. Since the information recorded using the electrodes is a combination of all fibers in the nerve, it would be useful to eliminate information which is not necessary and keep the information which is important. Therefore, if the sensory signal could be eliminated, the remaining signal (motor) would be the useful component. To eliminate the sensory component, a sliding window cross correlation technique introduced by Heetderks can be used [55-56]. A simple example shown below in Figure 43 illustrates the idea behind the process.

For this example, 0 is no information, 1 is sensory, and 2 is motor.	
0 2 0 0 0 1 0 2 0 0 1 2 0	proximal
0 0 2 0 1 0 0 0 2 1 0 0 2	distal
Shift distal forward by number of indices which provides the greatest correlation:	
0 0 0 2 0 1 0 0 0 2 1 0 0 2	shifted distal (0 added to beginning to shift array)
0 2 0 0 0 1 0 2 0 0 1 2 0 0	0 added to proximal to make length of proximal equal to length of distal
Subtract shifted distal from lengthened proximal:	
0 2 0 0 0 1 0 2 0 0 1 2 0 0	
0 0 0 2 0 1 0 0 0 2 1 0 0 2	
0 2 0 2 0 0 0 2 0 2 0 2 0 2	absolute value of remaining signal (no sensory shown)

Figure 43 Example illustrating cross correlation technique

The example in Figure 43 is ideal with all the sensory being removed. However, this example assumes that the exact magnitude signal (exact same CAPs) will pass both electrodes (only 0, 1, or 2 were used). In reality, this is not the case because the nerve is not a static case where all signals are constant. Instead, all fibers in the nerve are carrying information that is constantly changing based on the information provided from the sensory nerve inputs in the body or from the CNS; changing amounts of information will change the CAP. In addition to constantly varying signals, different fibers have different conduction velocities, therefore the CAP passing one recording electrode may not be equal to the CAP passing the next recording electrode. Cross correlation finds the best correlation value and uses that information to determine the shift amount.

Compound action potentials for each electrode are shown in Figure 44; these are the signals which would be acquired by the electrodes. The shifted distal signal is also shown in Figure 44. Figure 45 shows the motor signal at segment 30 (distal), segment 32 (proximal), and the remaining motor signal calculated with the cross correlation method from both recording electrodes. From this plot, motor activity is shown to hit the proximal electrode (segment 32) first which is expected because the proximal electrode is nearest the CNS. The remaining motor signal shows the depolarization and repolarization phases of the action potential. The cross correlation technique was also used to find the sensory information from the CAPs as more evidence of the ability of cross correlation to determine the signal. Figure 46 shows sensory activity at segment 30 (distal), segment 32 (proximal), and the overall sensory activity from both electrodes. Figure 46 shows that sensory activity passes the distal electrode then the proximal electrode, which is expected because the distal electrode is nearest the sensory inputs. Figure 47-48 show the motor and sensory signals which were

calculated with the cross correlation technique which used the CAPs at each electrode. The sensory signal in Figure 47 leads the motor signal; this is expected because for the simulation, a 200 μ s delay was placed on the origination of the motor signal. Therefore, the cross correlation technique agrees with the conditions of the simulation; there is a delay in the motor signal.

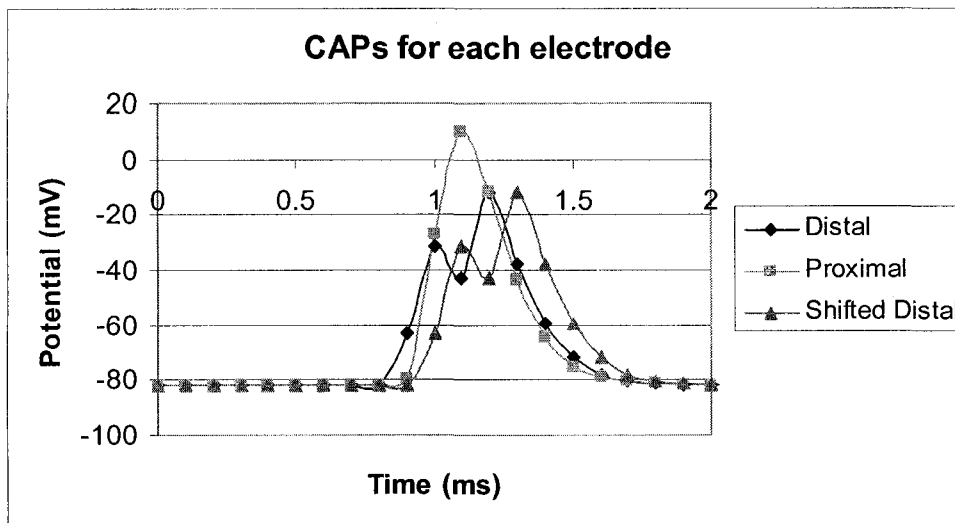


Figure 44 CAPs for each electrode

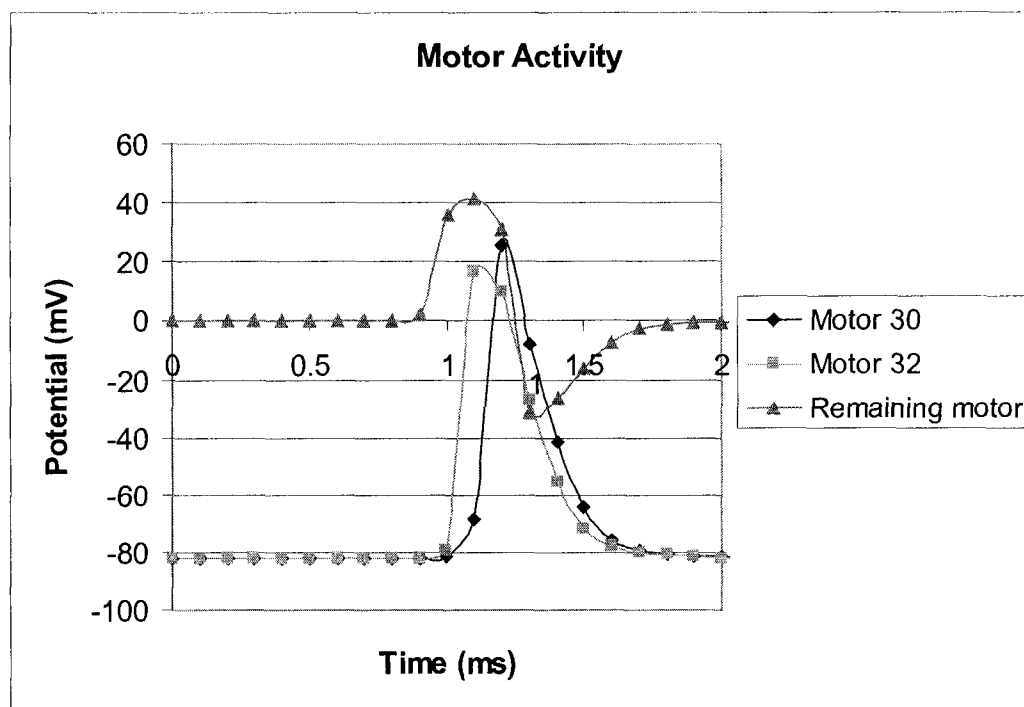


Figure 45 Motor activity at distal electrode, proximal electrode, and overall motor activity from both electrodes

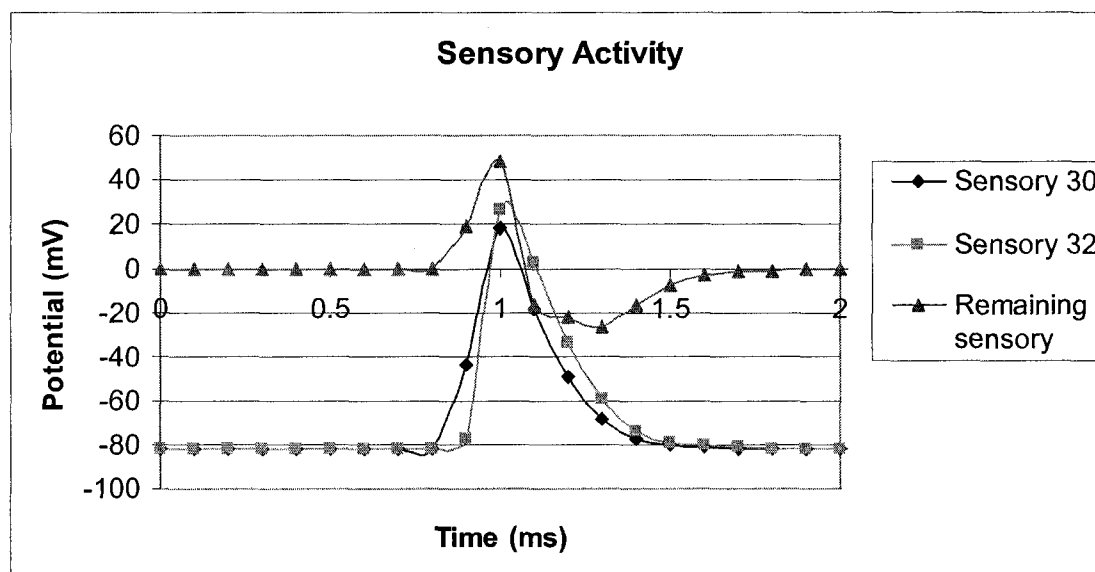


Figure 46 Sensory activity at distal electrode, proximal electrode, and overall sensory activity

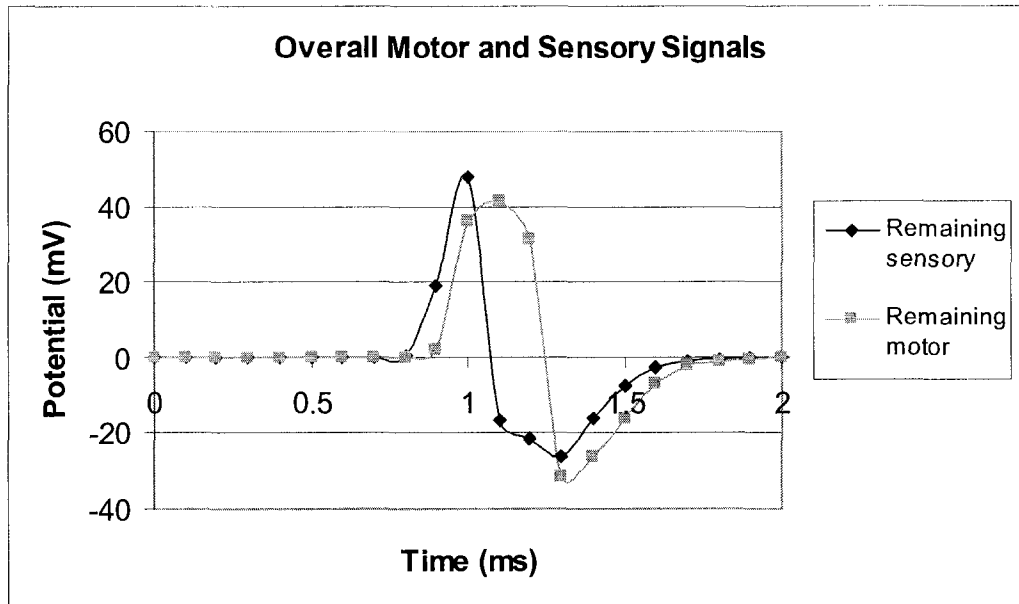


Figure 47 Motor and sensory signals as determined by cross correlation technique

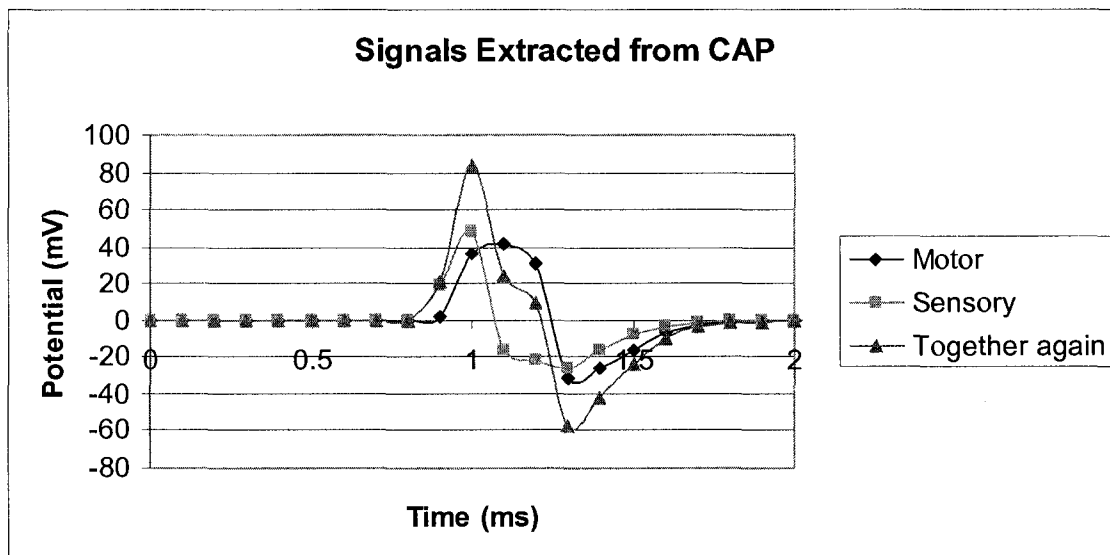


Figure 48 Motor, sensory, and overall CAP determined from the cross correlation technique

In conclusion, the cross correlation technique was able to decipher the motor and sensory signals from the CAPs at each electrode. The motor signal in the simulation was delayed in time compared to the sensory signal, and the cross correlation technique returned

a motor signal which was delayed in time as compared to the sensory signal. In reality, all the sensory activity may not be eliminated because of the continuous flow of information at different conduction velocities, and this can be illustrated by the correlation values used to determine the shift amount. The best correlation value is used; the best correlation value is not 1. However, this technique is useful at removing most of the sensory activity. A better method would be to eliminate sensory activity by using drugs to cause a sensory blockade; however, this would also add to the difficulty of the experiment while introducing extra drugs into the animal. Therefore, this cross correlation technique, while not totally able to eliminate sensory activity, is still very useful in finding the motor signal. Finally, the simulation proved that different recordings would be acquired at different points on the nerve, that the motor signal would hit the proximal contact first, that the sensory signal would hit the distal contact first, and that the cross correlation technique can be used to find the overall motor signal.

APPENDIX C

MATLAB CODE USED FOR SIGNAL ANALYSIS

```

clc
clear

%%%%%%%%% LOOK AT POWER SPECTRUM OF FILE %%%%%%%%%%

% This section calculates the power spectrum of a sampled signal
% between 0 and fsample/2 Hz. The result is a volt/sqrt(HZ) spectrum.

current=load ('DATA_baseline') ;
signal=current(1:75000,1);
signal=signal-mean(signal);
L=max(size(signal));          %samples
fsample=65                    % sampling frequency in KHz
T=1/(fsample*1000);          % sampling period

PP=abs(fft(signal))/L;
% this is a verification that the energy has not changed
energy_freq_of_fft_coef=sqrt(sum(PP.^2))

PPave=zeros(1,fsample*1000);

for i=1:fsample*1000,
    PPave(i)=sqrt(sum( PP(1+round((i-1)*L/(1000*fsample) ) :
round(i*L/(1000*fsample))) .^2));
end

% check if the energy of the signal in time domain is the same
energy_time_signal=sqrt(sum(signal.^2))/sqrt(L)

% check energy again in frequency domain
eneegy_freq_with_coef_per_1Hz=sqrt( sum(PPave.^2) )

PPave= sqrt(2*PPave.^2);          % now each coefficient corresponds to a Hz

figure
plot(PPave)

%%%%%%%%% Hamming window for neural signal %%%%%%%%%%

Fs=65E3;
T=1/Fs;
fn=Fs/2;          %Nyquist frequency
Wn=[1000/fn 5000/fn]; %passband--number b/w 0&1 with 1 being Nyquist frequency
n=1000;          %order of FIR filter
b = fir1(n,Wn) ;      %Hamming window design

```

```

% %%% checking filter %%%
%
% fpoint=(0:0.001:1)*Fs/2;   %50000/.001 points
% omeg=fpoint*2*pi;
% W=omeg*T;
% Hh=freqz(b,1,W);
% figure
% subplot(3,1,1);
% plot(fpoint,abs(Hh))
% grid;
% title('Hamming Window')
% xlabel('f(Hz)');ylabel('Linear Amplitude Response');
% subplot(3,1,2);grid;
% plot(fpoint,20*log10(abs(Hh)))
% grid;
% xlabel('f(Hz)');ylabel('Log Amplitude Response');
% %gtext('more than -46dB attenuation')
% subplot(3,1,3);
% plot(fpoint,unwrap(angle(Hh))/pi)
% grid;
% xlabel('f(Hz)');ylabel('Phase Response');

%%%%%%%%% Hamming window for EKG %%%%%%%%%%

T=1/Fs;
fn=Fs/2;           %Nyquist frequency
Wn1=[.3/fn 100/fn]; %passband--number b/w 0&1 with 1 being Nyquist frequency
n1=500;           %order of FIR filter
b1 = fir1(n1,Wn1) ; %Hamming window design

%%%%%%%%% Using Hamming Window %%%%%%%%%%

filtered_neural1=filter(b,1,current(:,1));

filtered_neural2=filter(b,1,current(:,2));

filtered_EKG=filter(b,1,current(:,3));

%%%%%%%%% Calculating the Heart Rate %%%%%%%%%%
f=1;
g=2*Fs;
h=1;              %iteration
S=[];

```

```

while g<=length(filtered_EKG),
    h                                %iteration number

    HRsignal=filtered_EKG;

    figure;
    plot((f:g),HRsignal(f:g))

    [Samplex Rwave]=ginput;
    close

    Samplex=round(Samplex); %scaling from graph and to make Sample all integer values

    f=g+1;
    g=g+(2*Fs);

    h=h+1;
    S=[S Samplex'];
end

RRinterval=abs(diff(S));

HR=abs(1./RRinterval)*Fs;          %HR per second...1/Sample times Sample/sec
HR_min=HR*60;

save(input('Enter HR_minute filename: '), 'HR_min', 'S')

%%%%%%%%% Finding the motor delay %%%%%%%%%%

subplot(2,1,1); plot(filtered_neural1);
subplot(2,1,2); plot(filtered_neural2);

Fs=65E3;

f=input('Enter f sample value for start of cross correlation: ')
f=eval(f);                          % makes f equal to a number and not a string--input (above) makes
                                     %f a string
g=input('Enter g sample value for end of cross correlation: ')
g=eval(g);

% close all

fsignal=[filtered_neural1(f:g) filtered_neural2(f:g)];
L=length(fsignal);

```

```

COR=zeros(1,round(L/130));
DELAY=zeros(1,round(L/130));
for i=130:130:L-150;          %130 allows for a 2ms length for Fs=65E3;
    cor=zeros(1,41);
    for j=-20:20,            %shift 20 back to 20 forward one shift at a time
        temp=corrcoef(fsignal(i:i+130,1), fsignal(i+j:i+j+130,2));
        cor(j+21)=temp(1,2);
    end
    [I,J]=max(cor);
    COR(i/130)=I;
    if I < 0.5
        DELAY(i/130)=21;
    else
        DELAY(i/130)=J-21;
    end
end

figure;
hist(DELAY,41)

%%%%%%%%% To find largest positive lag correlation value %%%%%%%%%%
for i=1:max(size(COR)),
    if (DELAY(i)>0 & DELAY(i)~=0 & DELAY(i)<6 & COR(i)>=.85), %specifies
        0<Delay<=5 and correlation > 0.85
            corr(i)=COR(i);
            delay(i)=DELAY(i);
        else
            continue
        end
    end
end

[C O R]=find(corr);          %finds location and value of nonzero correlations
[D E L]=find(delay);        %finds location and value of nonzero delays

cordel=[R;L]                %displays correlation in row 1 and delay value in row 2

shift=input('Enter shift value for calculation of motor activity: ');
shift=eval(shift);

c2=[zeros(1,shift) filtered_neural2'];
c1=[filtered_neural1' zeros(1,shift)];
motor=c1-c2;

```

```

%%%%%%%%% 10ms averager for NEURAL SIGNAL %%%%%%%%%
filtered1=abs(motor);          %section of filtered signal
Fs=65E3;
N=Fs*.01;                      % 10 msec averager at freq=15000;
SIZE1=size(filtered1);
length1=max(SIZE1);
ave1=zeros(1,length1);

ave1(1:N-1)=filtered1(1:N-1);
ave1(N)=mean((filtered1(1:N)));

for i=N+1:length1,
    ave1(i)=ave1(i-1)+(filtered1(i)/N)-(filtered1(i-N)/N);
end

%%%%%%%%% integration of motor activity %%%%%%%%%
for j=1:(length(S)-1),          %S is the index value of the Rwave
    f=S(:,j);
    g=S(:,j+1);
    tsum=0;
    area(j)=tsum+sum(ave1(f:g)); %ave1 is the averaged neural signal
end

correlation=corrcoef(HR_min,area)

figure; scatter(area, HR_min)
ylabel('Heart Rate per Minute')
xlabel('Area of Neural Activity before Heart Beat')
title(input('Scatter plot of Heart Rate per Minute and Area of Neural Activity: '))

save(input('Enter area filename: '), 'area')
save(input('Enter rectified averaged motor filename: '), 'ave1')

```

APPENDIX D

**SAS CODE AND OUTPUT FOR TRANSFER
FUNCTION MODEL**

```
1  OPTIONS LS=72;  
2  DATA ONE;  
3  INPUT AREA HR;  
4  AREA1=AREA/1000;  
6  CARDS;
```

NOTE: The data set WORK.ONE has 101 observations and 3 variables.

NOTE: The DATA statement used 0.02 CPU seconds and 2537K.

```
108 ;  
109 PROC PLOT DATA=ONE;  
110 PLOT HR*AREA1='*';
```

NOTE: There were 101 observations read from the data set WORK.ONE.

NOTE: The PROCEDURE PLOT printed page 1.

NOTE: The PROCEDURE PLOT used 0.03 CPU seconds and 2667K.

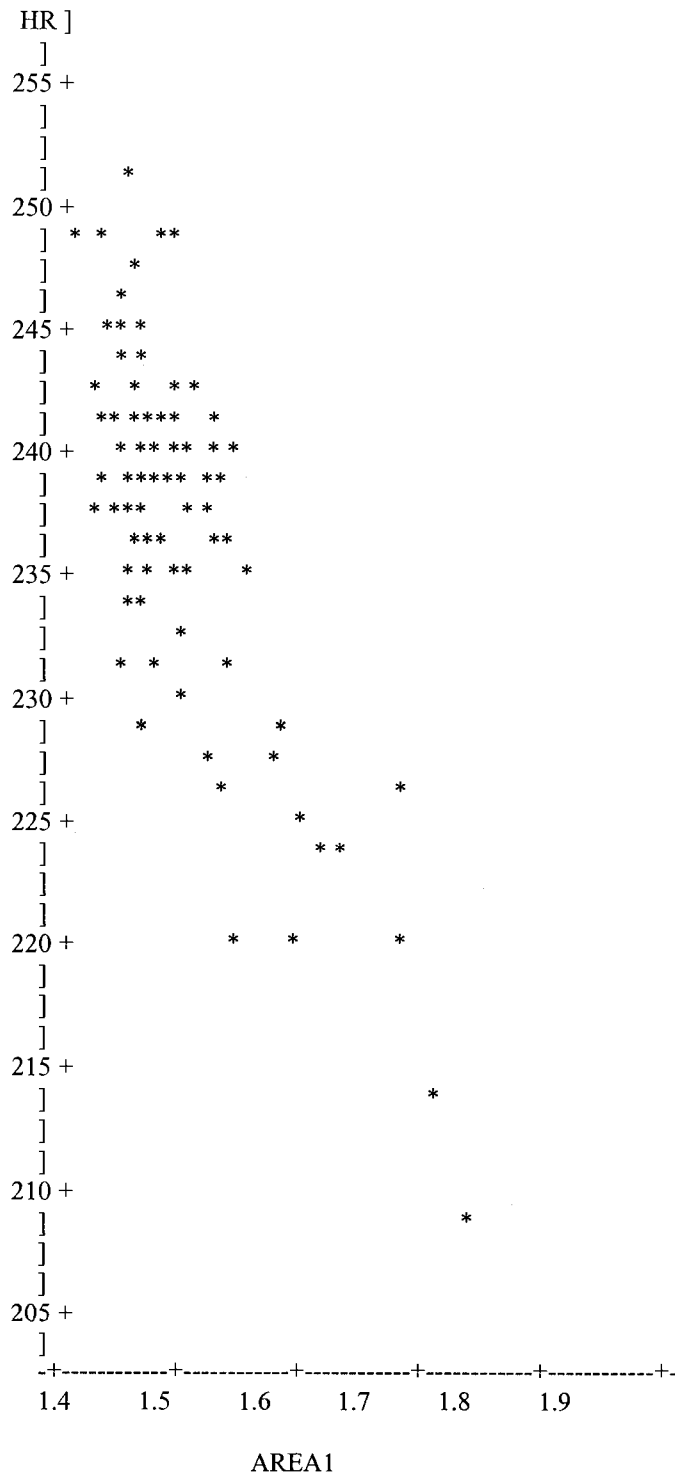
```
111 PROC ARIMA;  
112 IDENTIFY VAR=AREA1 NLAGS=15;  
113 ESTIMATE Q=1 PLOT;  
114 IDENTIFY VAR=HR CROSSCORR=AREA1 NLAGS=15;  
115 ESTIMATE INPUT=(AREA1) PLOT;  
116 ESTIMATE P=2 INPUT=AREA1 PLOT;  
117 FORECAST LEAD=10 PRINTALL;
```

NOTE: The PROCEDURE ARIMA printed pages 2-13.

NOTE: The PROCEDURE ARIMA used 0.15 CPU seconds and 3258K.

NOTE: The SAS session used 0.32 CPU seconds and 3258K.

Plot of HR*AREA1. Symbol used is '*'.



Name of Variable = AREA1

Mean of Working Series 1.522581
 Standard Deviation 0.084701
 Number of Observations 101

Autocorrelations

Lag Covariance Correlation -1 9 8 7 6 5 4 3 2 1 0 1 2 3 4 5 6 7 8 9 1

0	0.0071742	1.00000]	*****]
1	0.0030587	0.42635]	*****]
2	-0.0000828	-0.11154]	.] .]
3	0.00028889	0.04027]	.]* .]
4	0.00054393	0.07582]	.]** .]
5	0.0010612	0.14792]	.]*** .]
6	-0.0002754	-0.03839]	. *] .]
7	-0.0015990	-0.22288]	.****] .]
8	-0.0004241	-0.05912]	. *] .]
9	-0.0000120	-0.00168]	.] .]
10	-0.0001967	-0.02742]	. *] .]
11	-0.0005479	-0.07637]	. **] .]
12	-0.0015599	-0.21743]	.****] .]
13	-0.0006780	-0.09451]	. **] .]
14	0.00073566	0.10254]	.]** .]
15	0.00019675	0.02742]	.]* .]

"." marks two standard errors

Inverse Autocorrelations

Lag Correlation -1 9 8 7 6 5 4 3 2 1 0 1 2 3 4 5 6 7 8 9 1

1	-0.63055]	*****]	.]
2	0.39095]	.]*****]	.]
3	-0.26682]	*****]	.]
4	0.17704]	.]****]	.]
5	-0.14279]	.***]	.]
6	0.04358]	.]* .]	.]
7	0.09268]	.]** .]	.]
8	-0.10336]	. **] .]	.]
9	0.07151]	.]* .]	.]
10	-0.01815]	.] .]	.]

11	-0.01029]	.]	.]
12	0.03109]	.]*	.]
13	0.05399]	.]*	.]
14	-0.07437]	.]*	.]
15	0.02603]	.]*	.]

Partial Autocorrelations

Lag	Correlation	-1	9	8	7	6	5	4	3	2	1	0	1	2	3	4	5	6	7	8	9	1	
1	0.42635]	.]	*****	.]]
2	-0.23626]	*****]]
3	0.19038]	.]	****]
4	-0.04334]	.]	*]
5	0.18707]	.]	****]
6	-0.26295]	*****]]
7	-0.05269]	.]	*]
8	0.05771]	.]	*]
9	-0.07317]	.]	*]
10	0.02965]	.]	*]
11	-0.08637]	.]	**]
12	-0.13230]	.]	***]
13	0.05352]	.]	*]
14	0.07589]	.]	**]
15	-0.04748]	.]	*]

Autocorrelation Check for White Noise

To	Chi-Square	DF	Pr >	ChiSq	-----	Autocorrelations	-----		
6	22.24	6	0.0011	0.426	-0.012	0.040	0.076	0.148	-0.038
12	34.42	12	0.0006	-0.223	-0.059	-0.002	-0.027	-0.076	-0.217

Conditional Least Squares Estimation

Parameter	Standard Estimate	Error	Approx t Value	Pr > t	Lag
-----------	-------------------	-------	----------------	---------	-----

MU	1.52258	0.01196	127.26	<.0001	0
MA1,1	-0.66595	0.07517	-8.86	<.0001	1

Constant Estimate 1.522575
Variance Estimate 0.005294
Std Error Estimate 0.072757
AIC -240.762
SBC -235.531
Number of Residuals 101

* AIC and SBC do not include log determinant.

Correlations of Parameter Estimates

Parameter	MU	MA1,1
MU	1.000	-0.000
MA1,1	-0.000	1.000

Autocorrelation Check of Residuals

To Lag	Chi-Square	Pr > DF	ChiSq	-----Autocorrelations-----						
6	2.89	5	0.7162	-0.045	-0.016	0.057	-0.018	0.145	0.010	
12	14.84	11	0.1897	-0.247	0.065	-0.015	-0.036	0.033	-0.195	
18	19.29	17	0.3124	-0.061	0.129	-0.007	-0.058	0.081	-0.079	
24	29.58	23	0.1620	0.243	-0.105	-0.030	-0.005	0.093	-0.027	

Autocorrelation Plot of Residuals

Lag Covariance Correlation -1 9 8 7 6 5 4 3 2 1 0 1 2 3 4 5 6 7 8 9 1

0	0.0052936	1.00000]	*****]						
1	-0.0002402	-.04538]	.	*	.	.]		
2	-0.0000851	-.01607]	.]	.	.]		
3	0.00029992	0.05666]	.]	*	.]		
4	-0.0000952	-.01798]	.]	.	.]		
5	0.00076577	0.14466]	.]	***.	.]		
6	0.00005171	0.00977]	.]	.	.]		
7	-0.0013076	-.24702]	*****]	.	.	.]		

9	-0.01349]	.]	.]
10	-0.03420]	.]*	.]
11	0.02258]	.]	.]
12	-0.13279]	.	***]	.]
13	-0.08607]	.	**]	.]
14	0.07666]	.]**	.]
15	0.05301]	.]*	.]

Model for variable AREA1

Estimated Mean 1.522575

Moving Average Factors

Factor 1: 1 + 0.66595 B**(1)

Name of Variable = HR

Mean of Working Series 236.932

Standard Deviation 7.679309

Number of Observations 91

Autocorrelations

Lag Covariance Correlation -1 9 8 7 6 5 4 3 2 1 0 1 2 3 4 5 6 7 8 9 1

0	58.971781	1.00000]	*****]
1	17.494027	0.29665]	.]*****]
2	-0.825453	-0.01400]	.] .]
3	3.403952	0.05772]	.] * .]
4	3.736130	0.06335]	.] * .]
5	4.642815	0.07873]	.] ** .]
6	0.660869	0.01121]	.] .]
7	-7.226701	-.12255]	.] **]
8	-2.679936	-.04544]	.] *]
9	-9.941714	-.16858]	.] ***]
10	-9.487840	-.16089]	.] ***]
11	1.705209	0.02892]	.] * .]
12	-8.233952	-.13963]	.] ***]
13	-9.579390	-.16244]	.] ***]
14	-3.784288	-.06417]	.] * .]
15	5.085805	0.08624]	.] ** .]

"," marks two standard errors

Inverse Autocorrelations

Lag	Correlation	-1	9	8	7	6	5	4	3	2	1	0	1	2	3	4	5	6	7	8	9	1		
1	-0.38684]]	
2	0.17413]]
3	-0.06044]]
4	-0.03648]]
5	0.03798]]
6	-0.14457]]
7	0.18403]]
8	-0.12975]]
9	0.07382]]
10	0.13881]]
11	-0.16688]]
12	0.17347]]
13	-0.05281]]
14	0.10427]]
15	-0.11618]]

Partial Autocorrelations

Lag	Correlation	-1	9	8	7	6	5	4	3	2	1	0	1	2	3	4	5	6	7	8	9	1		
1	0.29665]]
2	-0.11184]]
3	0.10606]]
4	0.01136]]
5	0.07143]]
6	-0.03810]]
7	-0.12230]]
8	0.02451]]
9	-0.21247]]
10	-0.03556]]
11	0.08504]]
12	-0.18977]]
13	-0.02047]]
14	-0.02902]]
15	0.15527]]

Autocorrelation Check for White Noise

To	Chi-Square	Pr >	DF	ChiSq	-----Autocorrelations-----				
6	9.63	0.1413	0.297	-0.014	0.058	0.063	0.079	0.011	
12	19.17	0.0846	-0.123	-0.045	-0.169	-0.161	0.029	-0.140	

Correlation of HR and AREA1

Number of Observations	91
Variance of transformed series HR	58.76547
Variance of transformed series AREA1	0.005481

Both series have been prewhitened.

Crosscorrelations

Lag Covariance Correlation -1 9 8 7 6 5 4 3 2 1 0 1 2 3 4 5 6 7 8 9 1

-15	-0.074324	-.13095]	.***]	.]
-14	-0.026648	-.04695]	. *]	.]
-13	0.015312	0.02698]	.]*	.]
-12	0.062150	0.10950]	.]**	.]
-11	-0.077932	-.13731]	.***]	.]
-10	0.035810	0.06309]	.]*	.]
-9	0.050169	0.08839]	.]**	.]
-8	-0.0002110	-.00037]	.]	.]
-7	0.085753	0.15109]	.]***	.]
-6	-0.036311	-.06398]	. *]	.]
-5	-0.029164	-.05139]	. *]	.]
-4	-0.0026763	-.00472]	.]	.]
-3	-0.013956	-.02459]	.]	.]
-2	-0.031974	-.05634]	. *]	.]
-1	0.079334	0.13978]	.]***	.]
0	-0.462578	-.81503]	*****]	.]
1	0.113720	0.20037]	.]****	.]
2	-0.074322	-.13095]	.***]	.]
3	-0.0066592	-.01173]	.]	.]
4	-0.0007745	-.00136]	.]	.]
5	-0.011561	-.02037]	.]	.]
6	-0.052539	-.09257]	. **]	.]
7	0.090672	0.15976]	.]***	.]
8	-0.090538	-.15952]	.***]	.]

9	0.064319	0.11333]	.]**.]
10	0.068194	0.12015]	.]**.]
11	-0.031781	-.05600]	.]*.]
12	0.111924	0.19720]	.]****]
13	0.026702	0.04705]	.]*.]
14	0.018019	0.03175]	.]*.]
15	0.0044741	0.00788]	.] .]

"," marks two standard errors

Crosscorrelation Check Between Series

To	Chi-	Pr >	-----Crosscorrelations-----						
Lag	Square	DF	ChiSq						
5	65.71	6	<.0001	-0.815	0.200	-0.131	-0.012	-0.001	-0.020
11	73.90	12	<.0001	-0.093	0.160	-0.160	0.113	0.120	-0.056

Both variables have been prewhitened by the following filter:

Prewhitening Filter

Moving Average Factors

Factor 1: $1 + 0.66595 B^{**}(1)$

Conditional Least Squares Estimation

Parameter	Standard Estimate	Approx Error t	Value	Pr >]t]	Lag	Variable	Shift
MU	345.84400	8.52305	40.58	<.0001	0	HR	0
NUM1	-71.59717	5.59393	-12.80	<.0001	0	AREA1	0

Constant Estimate	345.844
Variance Estimate	21.22657
Std Error Estimate	4.60723
AIC	538.2526
SBC	543.2743
Number of Residuals	91

* AIC and SBC do not include log determinant.

Correlations of Parameter Estimates

Variable		HR	AREA1
Parameter		MU	NUM1
HR	MU	1.000	-0.998
AREA1	NUM1	-0.998	1.000

Autocorrelation Check of Residuals

To	Chi-	Pr >	-----Autocorrelations-----							
Lag	Square	DF	ChiSq							
6	14.22	6	0.0273	0.265	-0.168	-0.092	0.139	0.078	-0.128	
12	23.60	12	0.0231	-0.245	-0.026	0.132	0.058	0.058	-0.085	
18	34.07	18	0.0124	-0.047	-0.041	-0.068	-0.203	-0.203	-0.038	
24	38.91	24	0.0279	0.097	-0.036	-0.074	0.049	0.136	0.052	

Autocorrelation Plot of Residuals

Lag Covariance Correlation -1 9 8 7 6 5 4 3 2 1 0 1 2 3 4 5 6 7 8 9 1

0	21.226570	1.00000]	*****]
1	5.616723	0.26461]	*****]
2	-3.572588	-.16831]	***]
3	-1.958422	-.09226]	**]
4	2.951048	0.13903]	***]
5	1.660385	0.07822]	**]
6	-2.724074	-.12833]	***]
7	-5.191518	-.24458]	*****]
8	-0.547423	-.02579]	*]
9	2.799895	0.13191]	***]

10	1.238087	0.05833]	.]*	.]
11	1.241565	0.05849]	.]*	.]
12	-1.800964	-.08484]	.	**]	.]
13	-1.005331	-.04736]	.	*]	.]
14	-0.866724	-.04083]	.	*]	.]
15	-1.449128	-.06827]	.	*]	.]

"." marks two standard errors

Inverse Autocorrelations

Lag	Correlation	-1	9	8	7	6	5	4	3	2	1	0	1	2	3	4	5	6	7	8	9	1	
1	-0.35518]								*****]	.]
2	0.17594]								.]	****]
3	0.00365]								.]	.]
4	-0.16766]								.	***]	.]
5	0.10403]								.]**	.]
6	-0.05537]								.	*]	.]
7	0.20247]								.]	****]
8	-0.00899]								.]	.]
9	-0.09368]								.	**]	.]
10	0.11999]								.]**	.]
11	-0.21711]								.	****]	.]
12	0.15452]								.]**	.]
13	-0.02302]								.]	.]
14	0.05000]								.]*	.]
15	0.05073]								.]*	.]

Partial Autocorrelations

Lag	Correlation	-1	9	8	7	6	5	4	3	2	1	0	1	2	3	4	5	6	7	8	9	1
-----	-------------	----	---	---	---	---	---	---	---	---	---	---	---	---	---	---	---	---	---	---	---	---

1	0.26461]	.]*****]	
2	-0.25627]	*****]	.]	
3	0.03625]	.]*	.]
4	0.13345]	.]***.]	
5	-0.03162]	.	*]	.]
6	-0.10754]	.	**]	.]
7	-0.16798]	.	***]	.]
8	0.05057]	.]*	.]
9	0.04434]	.]*	.]
10	0.01493]	.]	.]
11	0.15183]	.]***.]	
12	-0.16294]	.	***]	.]
13	-0.00715]	.]	.]
14	-0.11373]	.	**]	.]
15	-0.06813]	.	*]	.]

Crosscorrelation Check of Residuals with Input AREA1

To	Chi-	Pr >									
Lag	Square	DF	ChiSq	-----Crosscorrelations-----							
5	4.73	6	0.5786	-0.097	0.146	-0.042	-0.089	-0.010	0.107		
11	17.67	12	0.1260	-0.038	-0.083	-0.204	0.039	0.296	0.056		
17	31.60	18	0.0245	0.069	0.076	0.251	0.144	-0.097	-0.222		
23	35.22	24	0.0651	0.129	0.033	-0.027	-0.090	-0.052	0.103		

Model for variable HR

Estimated Intercept 345.844

Input Number 1

Input Variable AREA1
Overall Regression Factor -71.5972

Conditional Least Squares Estimation

Standard Approx

3	-0.00512]	.]	.]
4	0.10792]	.]**	.]
5	-0.01540]	.]	.]
6	-0.07261]	.	*]]
7	-0.17906]	****]	.]
8	-0.02065]	.]	.]
9	0.17159]	.]**	.]
10	-0.02844]	.	*]]
11	0.16508]	.]**	.]
12	-0.13066]	.]**]]
13	-0.10662]	.	**]]
14	-0.08461]	.	**]]
15	-0.06620]	.	*]]

Crosscorrelation Check of Residuals with Input AREA1

To	Chi-	Pr >								
Lag	Square	DF	ChiSq	-----	Crosscorrelations	-----				
5	8.44	6	0.2079	-0.060	0.252	-0.122	-0.008	0.013	0.101	
11	18.20	12	0.1098	-0.078	-0.076	-0.192	0.106	0.214	-0.041	
17	29.18	18	0.0462	0.117	0.083	0.254	0.079	-0.086	-0.147	
23	34.99	24	0.0685	0.200	-0.070	-0.008	-0.072	-0.033	0.112	

Model for variable HR

Estimated Intercept 355.9442

Autoregressive Factors

Factor 1: $1 - 0.40129 B^{**}(1) + 0.30897 B^{**}(2)$

Input Number 1

Input Variable AREA1
Overall Regression Factor -78.2341

Forecasts for variable HR

Obs	Forecast	Std Error	95% Confidence Limits		Actual
1	236.2950	4.2810	227.9043	244.6857	238.1860
2	237.0538	4.2810	228.6632	245.4445	238.1860
3	241.3695	4.2810	232.9789	249.7602	237.3689
4	240.0360	4.2810	231.6453	248.4267	241.5711
5	243.1250	4.2810	234.7343	251.5157	239.0318
6	242.0063	4.2810	233.6156	250.3970	240.1366
7	241.7105	4.2810	233.3199	250.1012	235.4249
8	239.4306	4.2810	231.0399	247.8212	235.3351
9	238.9842	4.2810	230.5935	247.3749	238.6020
10	240.3879	4.2810	231.9972	248.7786	238.7020
11	232.3316	4.2810	223.9409	240.7223	230.7414
12	236.6270	4.2810	228.2363	245.0177	248.7477
13	245.6211	4.2810	237.2304	254.0118	237.9403
14	235.2661	4.2810	226.8754	243.6568	233.2308
15	240.2430	4.2810	231.8524	248.6337	239.3416
16	242.2157	4.2810	233.8250	250.6064	240.3232
17	240.9066	4.2810	232.5159	249.2973	237.2925
18	239.5534	4.2810	231.1628	247.9441	238.0004
19	242.4681	4.2810	234.0774	250.8588	236.9152
20	220.8737	4.2810	212.4830	229.2644	224.3702
21	218.3496	4.2810	209.9590	226.7403	226.6467
22	236.1454	4.2810	227.7547	244.5361	227.8636
23	234.6732	4.2810	226.2825	243.0639	238.1597
24	242.4049	4.2810	234.0142	250.7956	241.3947
25	236.2822	4.2810	227.8915	244.6728	241.6917
26	235.8354	4.2810	227.4448	244.2261	236.0744
27	234.3598	4.2810	225.9691	242.7505	231.9986
28	236.2848	4.2810	227.8941	244.6755	228.2527
29	237.0816	4.2810	228.6909	245.4723	230.7924
30	242.2863	4.2810	233.8956	250.6770	249.1043
31	245.1573	4.2810	236.7666	253.5480	241.8909
32	243.0566	4.2810	234.6659	251.4473	244.9305
33	239.6580	4.2810	231.2673	248.0487	241.4730
34	238.0606	4.2810	229.6699	246.4513	248.6756
35	239.4082	4.2810	231.0175	247.7989	242.6200
36	239.8501	4.2810	231.4594	248.2408	243.1485
37	238.4732	4.2810	230.0825	246.8639	240.3983
38	238.5932	4.2810	230.2025	246.9839	243.4254
39	238.0175	4.2810	229.6269	246.4082	237.4396
40	238.2878	4.2810	229.8972	246.6785	235.2517
41	238.2509	4.2810	229.8602	246.6416	237.4908
42	236.7531	4.2810	228.3625	245.1438	236.9030

43	221.9039	4.2810	213.5132	230.2946	223.2263
44	219.5013	4.2810	211.1106	227.8920	219.4701
45	233.5788	4.2810	225.1881	241.9695	235.0360
46	238.3928	4.2810	230.0021	246.7835	235.8648
47	236.4055	4.2810	228.0148	244.7962	230.4999
48	229.3823	4.2810	220.9916	237.7729	226.1506
49	235.5436	4.2810	227.1530	243.9343	238.1093
50	244.3174	4.2810	235.9268	252.7081	239.5101

Forecasts for
variable HR

Obs Residual

1	1.8910
2	1.1322
3	-4.0006
4	1.5351
5	-4.0932
6	-1.8697
7	-6.2857
8	-4.0955
9	-0.3822
10	-1.6859
11	-1.5902
12	12.1207
13	-7.6808
14	-2.0353
15	-0.9014
16	-1.8924
17	-3.6141
18	-1.5531
19	-5.5529
20	3.4965
21	8.2971
22	-8.2818
23	3.4865
24	-1.0102
25	5.4095
26	0.2389
27	-2.3612
28	-8.0321
29	-6.2892
30	6.8180
31	-3.2664
32	1.8739

33	1.8149
34	10.6149
35	3.2118
36	3.2984
37	1.9251
38	4.8322
39	-0.5780
40	-3.0361
41	-0.7601
42	0.1499
43	1.3224
44	-0.0313
45	1.4572
46	-2.5280
47	-5.9056
48	-3.2317
49	2.5657
50	-4.8073

Forecasts for variable HR

Obs	Forecast	Std Error	95% Confidence Limits		Actual
51	236.6121	4.2810	228.2214	245.0028	230.9324
52	225.7487	4.2810	217.3580	234.1393	220.1122
53	239.4910	4.2810	231.1003	247.8817	241.7283
54	242.0841	4.2810	233.6934	250.4748	240.3721
55	244.6914	4.2810	236.3007	253.0821	248.9851
56	244.7276	4.2810	236.3370	253.1183	244.4905
57	225.8691	4.2810	217.4784	234.2598	228.8818
58	227.4620	4.2810	219.0713	235.8527	227.5225
59	226.7191	4.2810	218.3284	235.1098	227.3111
60	226.7215	4.2810	218.3308	235.1122	225.3027
61	242.1948	4.2810	233.8042	250.5855	248.6514
62	214.7094	4.2810	206.3187	223.1001	214.2396
63	208.3563	4.2810	199.9657	216.7470	209.2812
64	239.2263	4.2810	230.8356	247.6170	241.3260
65	238.6177	4.2810	230.2270	247.0084	239.1012
66	239.0467	4.2810	230.6560	247.4374	241.7756
67	239.6783	4.2810	231.2876	248.0690	241.7623
68	239.1191	4.2810	230.7284	247.5098	240.8264
69	241.6217	4.2810	233.2310	250.0124	240.9671
70	240.5138	4.2810	232.1231	248.9045	241.4375
71	236.9542	4.2810	228.5635	245.3448	242.3807
72	241.1687	4.2810	232.7780	249.5593	247.4541
73	242.0175	4.2810	233.6269	250.4082	243.3798

74	238.0215	4.2810	229.6308	246.4121	236.2150
75	239.1387	4.2810	230.7480	247.5294	237.7259
76	236.7463	4.2810	228.3556	245.1369	239.4997
77	237.8821	4.2810	229.4914	246.2727	239.3592
78	242.7482	4.2810	234.3575	251.1389	238.4208
79	230.0683	4.2810	221.6777	238.4590	220.0389
80	232.4793	4.2810	224.0886	240.8700	239.4282
81	245.4208	4.2810	237.0301	253.8115	246.7388
82	244.4442	4.2810	236.0535	252.8349	242.7918
83	238.5910	4.2810	230.2004	246.9817	238.1623
84	237.4319	4.2810	229.0412	245.8226	235.2687
85	241.9277	4.2810	233.5370	250.3184	244.4980
86	241.1369	4.2810	232.7462	249.5276	235.7069
87	236.8433	4.2810	228.4526	245.2340	233.2455
88	237.3647	4.2810	228.9740	245.7553	236.6691
89	239.4291	4.2810	231.0384	247.8198	238.7078
90	234.5710	4.2810	226.1803	242.9617	235.6814
91	240.2188	4.2810	231.8281	248.6095	251.4886
92	244.6471	7.1223	230.6877	258.6066	.
93	234.8427	8.2491	218.6748	251.0106	.
94	234.7269	8.2734	218.5114	250.9424	.
95	236.5972	8.3105	220.3089	252.8856	.
96	237.3835	8.3114	221.0936	253.6735	.
97	237.1212	8.3136	220.8267	253.4157	.
98	236.7730	8.3144	220.4770	253.0690	.
99	236.7143	8.3145	220.4183	253.0103	.
100	236.7983	8.3146	220.5021	253.0946	.

Forecasts for
variable HR

Obs	Residual
51	-5.6797
52	-5.6365
53	2.2373
54	-1.7121
55	4.2937
56	-0.2371
57	3.0127
58	0.0605
59	0.5920
60	-1.4188
61	6.4566
62	-0.4698
63	0.9248
64	2.0997

65	0.4835
66	2.7288
67	2.0839
68	1.7073
69	-0.6546
70	0.9238
71	5.4266
72	6.2854
73	1.3623
74	-1.8065
75	-1.4128
76	2.7534
77	1.4772
78	-4.3274
79	-10.0294
80	6.9488
81	1.3179
82	-1.6525
83	-0.4287
84	-2.1632
85	2.5703
86	-5.4301
87	-3.5978
88	-0.6955
89	-0.7213
90	1.1104
91	11.2698
92	.
93	.
94	.
95	.
96	.
97	.
98	.
99	.
100	.

Forecasts for variable HR

Obs	Forecast	Std Error	95% Confidence Limits		Actual
101	236.8502	8.3146	220.5540	253.1465	.

Forecasts for
variable HR

Obs	Residual
-----	----------

101	.
-----	---

REFERENCES

- [1] J. G. Webster, *Design of Cardiac Pacemakers*. Piscataway, NJ: IEEE Press, 1995, pp. 10-12, 290-304.
- [2] D. Dubin, M.D., *Rapid Interpretation of EKG's*, 5th ed., Tampa, Florida: Cover Publishing Company, 2000, pp. 13, 16, 19-20.
- [3] Mission Internal Medical Group, "Electrical conduction system," October 2007, http://www.mimg.com/cardiology_electricalconduction.html.
- [4] American Heart Association, "Heart Disease and Stroke Statistics," April 2006, www.americanheart.org.
- [5] Center for Disease Control, "The Burden of Chronic Diseases as Causes of Death, United States," October 2007, <http://www.cdc.gov/nccdphp/burdenbook2004/Section01/tables.htm>.
- [6] Medtronic, Inc., "Rate responsive pacing systems," October 2007, http://www.medtronic.com/servlet/ContentServer?pagename=Medtronic/Website/StageArticle&ConditionName=Bradycardia&Stage=Treatment&Article=brady_art_rate_responsive.
- [7] K. A. Ellenbogen, M.D., *Practical Cardiac Diagnosis: Cardiac Pacing*, Blackwell Science, 1996, pp. 97-106.
- [8] M. P. R. Hexamer, M. Meine, A. Kloppe, and J. Werner, "Rate-responsive pacing based on the atrio-ventricular conduction time," *IEEE Transactions on Biomedical Engineering*, vol. 49, pp. 185-195, March 2002.
- [9] J. Werner, M. Hexamer, M. Meine, and B. Lemke, "Restoration of cardio-circulatory regulation by rate-adaptive pacemaker systems: The bioengineering view of a clinical problem," *IEEE Transactions on Biomedical Engineering*, vol. 46, pp. 1057-1064, September 1999.
- [10] M. N. Levy, T. Iano, and H. Zieske, "Effects of repetitive bursts of vagal activity on heart rate," *Circulation Research*, vol. 30, pp. 286-295, 1972.
- [11] M. Schaldach, *Electrotherapy of the heart*, New York: Springer-Verlag, 1992.

- [12] R. Berger, S. Akselrod, D. Gordon, and R. Cohen, "An efficient algorithm for spectral analysis of heart rate variability," *IEEE Transactions on Biomedical Engineering*, vol. 33, pp. 900-904, September 1986.
- [13] M. V. Kamath, A. R. M. Upton, A. Talalla, and E. L. Fallen, "Effect of vagal nerve electrostimulation on the power spectrum of heart rate variability in man," *Pacing and Clinical Electrophysiology: Pace*, vol. 15, pp. 235-243, February 1992.
- [14] S. Akselrod, et al., "Hemodynamic regulation: Investigation by spectral analysis," *American Journal of Physiology*, vol. 249, pp. H867-H875, 1985.
- [15] S. Akselrod, et al., "Power spectrum analysis of heart rate fluctuation: A quantitative probe of beat-to-beat cardiovascular control," *Science*, vol. 213, no. 10, pp. 220-222, 1981.
- [16] A. Malliani, M. Pagani, F. Lombardi, and S. Cerutti, "Cardiovascular neural regulation explored in the frequency domain," *Circulation*, vol. 84, pp. 482-492, 1991.
- [17] B. Pomeranz, et al., "Assessment of autonomic function in humans by heart rate spectral analysis," *American Journal of Physiology*, vol. 248, pp. H151-H153, 1985.
- [18] M. Pagani, et al., "Power spectral analysis of heart rate and arterial pressure variabilities as a marker of sympatho-vagal interaction in man and conscious dog," *Circulation Research*, vol. 59, pp. 178-193, 1986.
- [19] AK Ahmed, AJ Mearns, and JB Harness, "Posture entrainment," *Automedica*, vol. 4, pp. 193-196, 1983.
- [20] M. Pagani, et al., "Simultaneous analysis of beat to beat systemic arterial pressure and heart rate variabilities in ambulatory patients," *Journal of Hypertension*, vol. 3 (suppl. 3), pp. S83-S85, 1985.
- [21] S. Guzzetti, et al., "Sympathetic predominance in essential hypertension: A study employing spectral analysis of heart rate variability," *Journal of Hypertension*, vol. 6, pp. 711-717, 1988.
- [22] E. L. Fallen, et al., "Spectral analysis of heart rate variability following human heart transplantation: Evidence for functional reinnervation," *Journal of the Autonomic Nervous System*, vol. 23, pp. 199-206, 1988.
- [23] P. G. Katona and J. I. H. Felix, "Respiratory sinus arrhythmia: Noninvasive measure of parasympathetic cardiac control," *Journal of Applied Physiology*, vol. 5, pp. 801-805, 1975.

- [24] M. Appel, et al., "Beat to beat variability in cardiovascular variables: Noise or music?," *Journal of the American College of Cardiology*, vol. 14, pp. 1139-1148, 1989.
- [25] G. B. Stanley, K. Poola, and R. A. Siegel, "Threshold modeling of autonomic control of heart rate variability," *IEEE Transactions on Biomedical Engineering*, vol. 47, pp. 1147 - 1153, September 2000.
- [26] J. T. Bigger, Jr., et al., "Correlations among time and frequency domain measures of heart rate variability two weeks after acute myocardial infarction," *American Journal of Cardiology*, vol. 69, pp. 891-898, 1992.
- [27] M. N. Levy and P. J. Schwartz, *Vagal control of the Heart: Experimental Basis and Clinical Implications*, New York: Futura Publishing Co., Inc., pp. 485-486, 1994.
- [28] A. C. Guyton and J. E. Hall, *Textbook of Medical Physiology*, 10th ed., Philadelphia: W. B. Saunders Co., pp. 697-703, 2000.
- [29] M. F. Bear, B. W. Connors, and M. A. Paradiso, *Neuroscience: Exploring the Brain*, 2nd ed., Baltimore, Maryland: Lippincott Williams and Wilkins, pp. 505-511, 2001.
- [30] D. B. Popovic' et al., "Sensory nerve recording for closed-loop control to restore motor functions," *IEEE Transactions on Biomedical Engineering*, vol. 40, pp. 1024-1031, October 1993.
- [31] J. A. Hoffer, M. Haugland, and T. Li, "Obtaining skin contact force information from implanted nerve cuff recording electrodes," in *Proceedings of the Eleventh Annual International Conference of IEEE EMBS*, 1989, pp. 928-929.
- [32] J. A. Hoffer and M. Haugland, "Signals from tactile sensors in glabrous skin: Recording, processing, and applications for restoring motor functions in paralyzed humans," *Neural Prostheses: Replacing Motor function after Disease or Disability*, R. B. Stein, H. P. Peckham, and D. B. Popovic, New York: Oxford University, 1992, pp. 99-125.
- [33] T. D. Coates, Jr., L. J. Larson-Prior, S. Wolpert, and F. Prior, "Classification of simple stimuli based on detected nerve activity," *IEEE Engineering in Medicine and Biology Magazine*, pp.64-76 January/February 2003.
- [34] Y. Ikeda, et al., "Explorations into development of a neurally regulated cardiac pacemaker," *American Journal of Physiology*, vol. 269, pp. H2141-H2146, 1995.
- [35] T. Suzuki, et al., "Analysis of chronically recorded autonomic nerve signals for the control of artificial heart systems," in *Proceedings of the Second Joint EMBS/BMES Conference*, October 23-26, 2002, pp. 1577-1578.

- [36] K. Mabuchi, et al., "Attempt to control an artificial heart system using sympathetic nervous signals," in *Proceedings-20th Annual International Conference-IEEE/EMBS*, 1998, pp. 458-461.
- [37] M. Sugimachi and K. Sunagawa, "Bionic cardiovascular medicine," *IEEE Engineering in Medicine and Biology Magazine*, pp. 24-31, July/August 2005.
- [38] T. Yambe, et al., "Vagal nerve activity recording in the awake condition for control of an artificial heart system," *Artificial Organs*, vol. 23, pp. 529-531, June 1999.
- [39] T. Yambe, et al., "Recording vagal nerve activity for the control of an artificial heart system," *ASAIO Journal*, vol. 49, no. 6, pp. 698-700, 2003.
- [40] T. Yambe, et al., "A future prediction type artificial heart system," *Artificial Organs*, vol. 23, no. 3, pp. 268-273, 1999.
- [41] T. Yambe, et al., "Continuous monitoring of autonomic nerve information for the control of an artificial heart," *ASAIO Journal*, vol. 44, pp. M696-M699, 1998.
- [42] M. N. Levy and H. Zieske, "Autonomic control of cardiac pacemaker activity and atrioventricular transmission," *Journal of Applied Physiology*, vol. 27, pp. 465-470, October 1969.
- [43] M. N. Levy, "Cardiac sympathetic-parasympathetic interactions," *Federation Proceedings*, vol. 43, pp. 2598-2602, August 1984.
- [44] M. N. Levy, "Autonomic interactions in cardiac control," *Annals of the New York Academy of Sciences*, vol. 601, pp.209-221, 1990.
- [45] J. Philip Saul, "Beat to beat variations of heart rate reflect modulation of cardiac autonomic outflow," *News in Physiological Sciences: An international journal of physiology produced jointly by the International Union of Physiological Sciences and the American Physiological Society*, vol. 5, pp. 32-37, February 1990.
- [46] J. F. Thayer and G. J. Siegle, "Neurovisceral integration in cardiac and emotional regulation," *IEEE Engineering in Medicine and Biology Magazine*, pp 24-29, July/August 2002.
- [47] M. N. Levy, T. Yang, and D. W. Wallick, "Assessment of beat by beat control of heart rate by the autonomic nervous system: Molecular biology techniques are necessary, but not sufficient," *Journal of Cardiovascular Electrophysiology*, vol. 4, pp. 183-193, April 1993.
- [48] S. E. Mace and M. N. Levy, "Autonomic nervous control of heart rate: Sympathetic-parasympathetic interactions and age related differences," *Cardiovascular Research*, vol. 17, pp. 547-552, 1983.

- [49] J. M. Lash, E. Haase, and A. A. Shoukas, "Systemic responses to carotid occlusion in the anesthetized rat," *Journal of Applied Physiology*, vol. 72, pp.1247-1254, April 1992.
- [50] J. G. Moss, et al., "Vascular occlusion with a balloon-expandable stent occluder," *Radiology*, vol. 191, pp. 483-486, May 1994.
- [51] H. Dallmer, M. Derks, P. Bucher, and W. Meesmann, "Construction and function of a new hydraulic cuff occluder," *Pflugers Archiv: European Journal of Physiology*, vol. 380, pp. 99-100, May 1979.
- [52] R. F. Spetzler and W. R. Selman, "New design of an implantable vessel occluder," *Surgical Neurology*, vol. 13, pp.317-319, April 1980.
- [53] E. M. Krieger, "Carotid occlusion in the rat: Circulatory and respiratory effects," *Acta Physiologica Latino Americana*, vol. 13, pp. 350-357, 1963.
- [54] E. M. Krieger, "Neurogenic hypertension in the rat," *Circulation Research: a journal of the American Heart Association*, vol. 15, pp. 511-521, 1964.
- [55] W. J. Heetderks and W. J. Willams. "Partition of gross peripheral nerve activity into single unit responses by correlation techniques," *Science*, vol. 188, pp. 373-375, April 1975.
- [56] L. Fiore, L. Geppetti, D. Ricci, and B. Di Vizio, "Cross-correlation-based evaluations of the impulse transmission in a nerve: Simulation and experimental studies," *Journal of Neuroscience Methods*, vol. 27, pp. 235-243, April 1989.
- [57] W. W. S. Wei, *Time Series Analysis: Univariate and Multivariate Methods*, Redwood City, California: Addison-Wesley Inc., 1994, pp. 20, 293-294.
- [58] S. de Waele, R. Booiij, P.M.T. Broersen, W.S.J. Uijttewaal, "The application of time series analysis to laser-doppler anemometry data," in *Proceedings of the Eighth International EALA Conference on 'Laser Anemometry, Advances and Applications'*, 1999 pp.191-198.
- [59] S. de Waele, P.M.T. Broersen, "A time domain error measure for resampled irregular data," in *Proceedings of IEEE Instrumentation and Measurement Technology Conference*, 1999, pp.751-756.
- [60] R. V. Edwards, "Report of the special panel on statistical particle bias problems in laser anemometry," *Journal of Fluids Engineering*, vol. 109, pp. 89-93, June 1987.

- [61] P. M. T. Broersen and R. Bos, "Estimating time series models from irregularly sampled data," in *Proceedings of the IEEE Instrumentation and Measurement Technology Conference*, May 2005, pp. 1723–1728.
- [62] R. J. Adrian and C. S. Yao, "Power spectra of fluid velocities measured by laser doppler velocimetry," *Experiments in Fluids*, vol. 5, pp. 17-28, 1987.
- [63] H. E. Evans, *Miller's Anatomy of the Dog*, Philadelphia: W. B. Saunders, 1993.
- [64] E. C. Greene, "Gross Anatomy," in *The Rat in Laboratory Investigation*, E. J. Farris and J. Q. Griffith, Jr., Eds. New York: Hafner Publishing Company, 1962, pp. 31, 43.